Thermo-Elastic Analysis of a Spiral Dish Antenna Reflector In Space

Master Thesis

Nathan J. van der Wielen

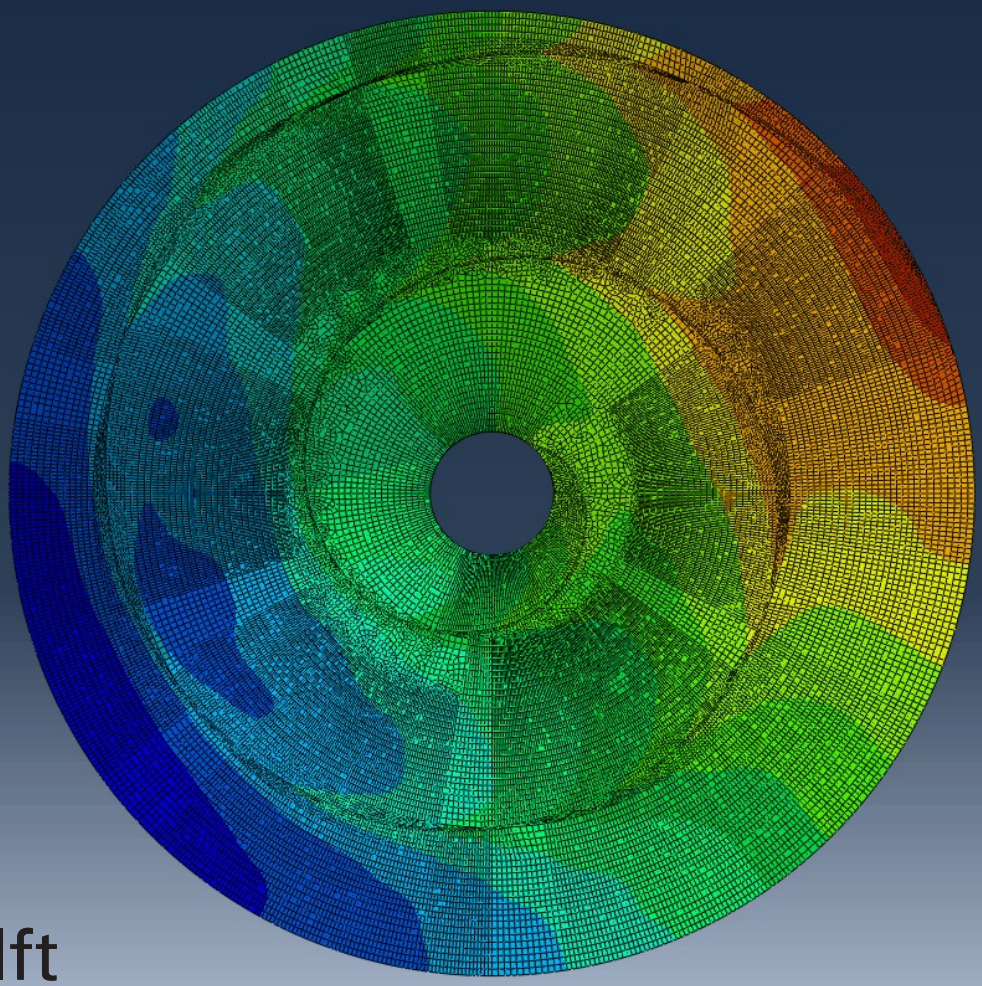

TU Delft

Thermo-Elastic Analysis of a Spiral Dish Antenna Reflector In Space

Master Thesis

by

Nathan J. van der Wielen

to obtain the degree of Master of Science
at the Delft University of Technology,
to be defended publicly on Monday October 3rd, 2022 at 14:00 PM.

Student number:	4938135	
Project duration:	July 12th, 2021 – October 3rd, 2022	
Thesis committee:	Assistant Prof. dr. J. Guo,	TU Delft, supervisor and chair
	I. Uriol Balbin,	TU Delft, co-supervisor
	Associate Prof. Dr. Ir. J. van Campen,	TU Delft, external examiner
	Researcher Dr. Ir. J. Bouwmeester,	TU Delft, external examiner

An electronic version of this thesis is available at `http://repository.tudelft.nl/`.

TU Delft

Acknowledgements

This work was conducted at the Delft University of Technology in the Netherlands. The literature study and analyses were conducted remotely as result of the Covid 19 pandemic. This led to difficulties in communicating with faculty and in exchanging ideas with my peers. I would like to thank Ines Balbin, who served as my daily supervisor, for her help on the Finite Element Modelling aspects of the work and her unwavering support on other issues. Without her I may have never had the strength to push through during times of isolation. I want to thank Jian Guo, who served as my supervisor, for his patience throughout this experience. He gave me the time and space to recover from personal issues, and allowed me to explore and learn new engineering skills. I want to thank Alden Yellowhorse, Just Herder, and Lorenzo Lannini, the original writers of "SELF-ASSEMBLING KIRIGAMI STRUCTURES", on which this thesis is based, for each giving me personal time and guidance in my research. I would like to thank Pablo Solano who offered his expertise in the space thermal analysis aspects and always guided me in the right direction to solve issues that arose when trying to model the reflector. Without him I would never have been able to gain confidence in my thermal analyses. I wish to extend my thanks to Tom Boxtel, Fabio Hu, and Henri (from ESATAN-TMS) who each helped me solve large road blocks faced through my thesis. Lastly, I would like to thank my parents, my friends, and the Da Vinci Satellite team who all supported me throughout this project.

Nathan van der Wielen
June, 2022

Contents

List of Figures

List of Tables

Abstract

At the Technical University of Delft(TU Delft), a Kirigami inspired method of spirally deploying a coiled up band into a parabolic reflector is being studied for its use in space.

This thesis performs a thermo-elastic analysis on the spiral dish Antenna (SDA) using a combination of ESATAN-TMS, Abaqus, and python scripting. After analysing a reflector for different low earth orbital cases in ESATAN, the heat fluxes are transferred to Abaqus to perform a second thermal analysis. A base SDA is modelled with an Aluminum zipper and Carbon-fiber-reinforced polymers (CFRP) band. The SDA is shown to experience temperatures ranging from 175K to 375K with temperature changes of 100K in less than 100s. The reflector can experiences maximum temperature deltas of 93K across the reflector at a single moment during orbit. These temperature changes cause the SDA to have a maximum displacement of 20mm with a maximum root mean square (RMS) of 6mm. This thesis also shows the creation of a cross pattern on the SDA most likely created by the coefficient of thermal expansion (CTE) mismatch between the zipper and band material. An improved SDA is modelled after an initial parametrization, showing an improvement to the displacement field with the max RMS being around 1mm.

This thesis shows how the base model of the SDA deforms into an cross pattern and experience high displacement regions near the end of the spiral interface. This version of the SDA is shown to not be able to perform in space. A short parametrization analysis with regards to materials choice, spiral geometry, and thickness does show a path in which the SDA can perform similarly to a normal reflector with the same design parameters.

Acronyms and Abbreviations

CAD - Computer Aided Design

CFRP - Carbon-Fiber-Reinforced Polymers

CTE - Coefficient of Thermal Expansion

FDM - Finite Difference Method

FEM - Finite Element Method

GMM - Geometrical Mathematical Model

JWST - James Webb Space Telescope

LPM - Lumped Parameter Method

LSS - Large Space Structure

MLI - Multi-Layer Insulation

NASA - National Aeronautics and Space Administration

RF - Radio Frequency

RMS - Root Mean Square

SAR - Synthetic Aperture Radar

SDA - Spiral Dish Antenna

TMM - Thermal Mathematical Model

TUD - Technical University of Delft

1

Introduction

Large space structures have always been of interest to the aerospace industry due to their potential in improving space exploration, communication satellites, and high precision instruments. Just recently, the James Webb Space Telescope has successfully launched and been placed in orbit. It is set to revolutionise the study of the universe thanks to its 6.5m diameter gold-coated beryllium reflector (see Figure 1.1). Large space structures (LSS) have often faced criticism for the difficulty required in placing them in orbit. In the case of the JWST, a complex origami deployment mechanism was used to deploy the reflector. Due to the complexity of the system, it took over 20 years from initial proposal to launch. This has led to a large effort in finding ways of improving methods for creating large space structures. Between building them piece by piece in orbit or having complex deployment mechanisms, many new and interesting technologies have been invented to make large space structures a more viable option for future space missions.

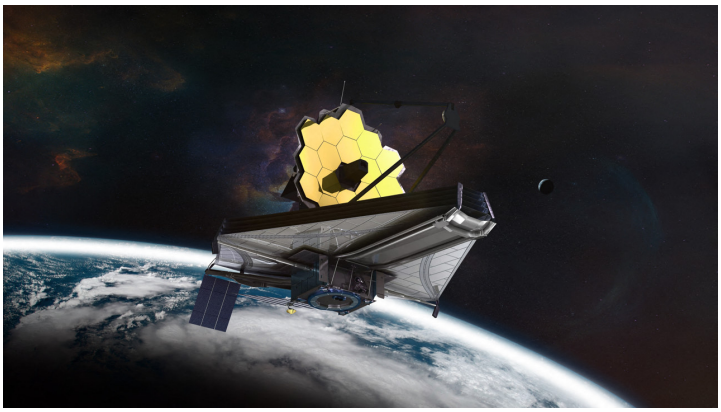

Figure 1.1: Artistic rendering of the James Webb Space Telescope [1]

At the Delft university of technology, a new method of deploying a parabolic antenna reflector is being studied. Through the lens of Kirigami Engineering, researchers are looking to spirally deploy a band out into a paraboloid. This method, first described in "Self-assembly Kirigami Structures" by Yellowhorse[2], is still at a conceptual phase. With its capability of deploying a solid band from a compact stowed position, to a large surface area, this technique is being considered, for this thesis, for its use as a large space reflector. This thesis looks to further the concept, by analysing the impact on performance of a large spiral dish antenna (SDA) in the thermal environment of space.

Parabolic reflectors have always been a important part of communication and instrument systems for satellites. When looking to have a large reflector for a space mission, it is often difficult to design them to fit in the size provided by the launcher. This is true for large satellites that use up the entire fairing, and small satellites that are often launched with several other missions. The current approach for large reflectors has been to often use mesh reflectors that offer a lightweight and deployable solution. The problem is that the mesh reflectors don't offer the same performance parameters than solid reflectors, see Figure 1.2. The SDA could offer an optimal solution: a solid reflector that can be stored in a tight space. This would open the door for new reflector technologies that use the SDA concept.

Parabolic reflectors offer a passive means to either concentrate signals to a receiver or direct an emitter's signal to a specific region. To properly function they must be able to keep their shape so as not distort the signal being reflected. Therefore, minimizing and understanding the distortions experienced by a reflector is important for reflector design. In space, one of the largest cause of reflector distortion is caused by the cyclical temperature variations experienced by entering and exiting eclipse. Reflectors can experience temperature variations from 208K to 368K [4], which can cause thermal strain across the reflector. Understanding how these thermal strains are formed with respect to the orbit, helps in the design consideration of a reflector. As a novel concept, the SDA has yet to have been studied as a reflector experiencing orbital temperature variations.

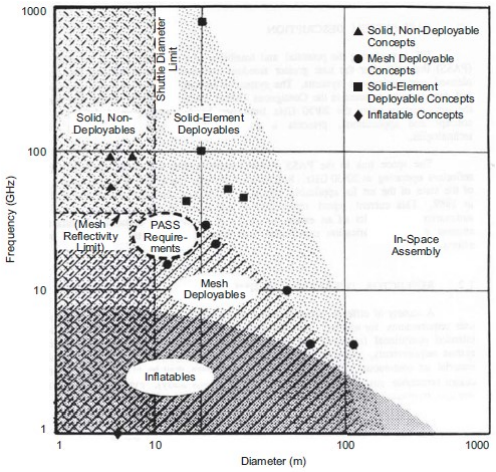

Figure 1.2: Mechanical Constraints for Reflectors[3]

Methodology

In this section, the method used in the analysis of the SDA is outlined. The background of the research performed by the author can be found in a detailed literature review [5], in which Origami Engineering, Space Thermal Environment, the SDA, Antennas, Reflectors, and Space Modelling are all studied in preparation of the following research.

The approach taken for this thesis is to perform a similar process as outlined in Boyer [6] except for a simplification made for the study of the RF effects, see Figure 1.3. For the radio frequency (RF) analysis, Ruze [7] is used to compare the performance of the SDA. Because of this, the work is split in three different categories: thermal analysis, thermo-elastic analysis, and radio frequency analysis. For the base design of the model, Park [8] and Sharp [9] are used to build the model of an SDA and standard shaped reflector without the spiral interface. Both Sharp and Park are described in more detail in Chapter 2. This standard reflector will help in pointing out the effects of the spiral interface on the temperature field and the displacement.

For this thesis, the thermal analysis is performed for the entire period of a few different orbits. Two standard low earth polar orbits with a 45° inclination, with one describing a Summer case, and the other a Winter case. The third orbit studied is an equatorial low earth orbit where the reflector is nadir pointing during the entire period. This allows for a larger view of different temperature fields that could impact the reflector and therefore shows the potential impact of the spiral interface with different load cases. ESATAN-TMS is used to perform the different thermal analyses due to it being built specifically to perform thermal analyses for space. A combination of several Python Scripts [10], and Abaqus is used to perform the thermo-elastic analysis. With Abaqus, a separate thermal analysis is needed, with the ESATAN results as load cases, to then perform the thermo-elastic analysis. Lastly, another

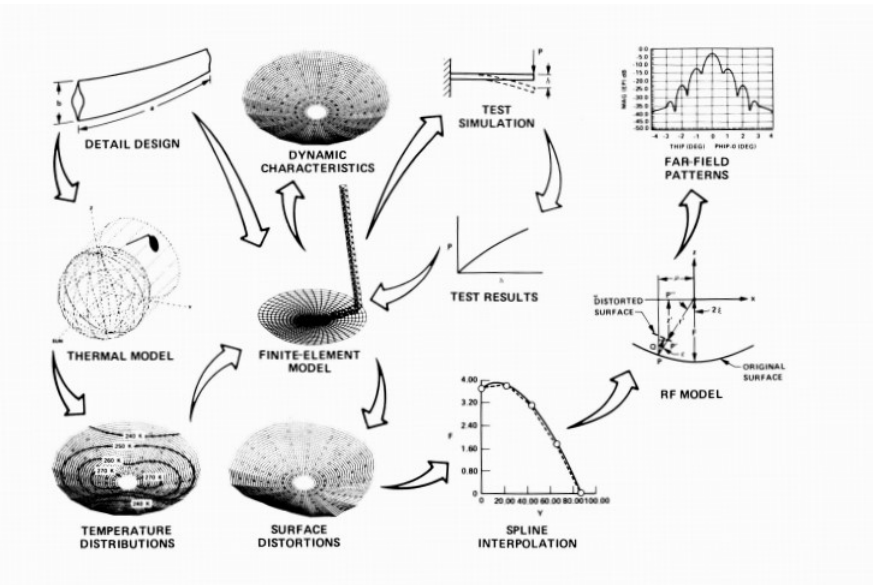

Figure 1.3: Thermo-Elastic analysis Process[6]

Python Script is used to perform a surface RMS analysis and to out put a variety of different plots and information with regards to the analysis of the SDA.

Thesis Outline

This section gives the outline of the thesis report. Chapter 1 introduces the thesis and outlines the work performed. Chapter 2 is a shortened literature review of the one previously made [5] in which the SDA is explained in more detail, the thermal environment, and two main papers used throughout the thesis are introduced. Chapter 3 is split in between two main parts. Firstly Section 3.3.3, where the thermal analysis performed with ESATAN TMS. In this section a detailed description of the methods used and the results obtained is given. Secondly Section 3.3.4, where the thermal Analysis performed in Abaqus with another description of the methods used and the results obtained. Chapter 4 presents the process used for the thermo-elastic analysis and the results obtaines. Chapter 5 is a parametrization analysis to improve and study the effects of different parameters on the SDA. Chapter 6 presents the results of the Radio frequency analysis through the means of a surface RMS analysis. Chapter 7 discusses the results, the limitations of the analysis, and further research that can be performed. It also looks to answer the research questions. Lastly, **??** concludes on the thesis. Figure 1.4 outlines the main analysis process of the thesis with the different software suits used and their respective Chapters.

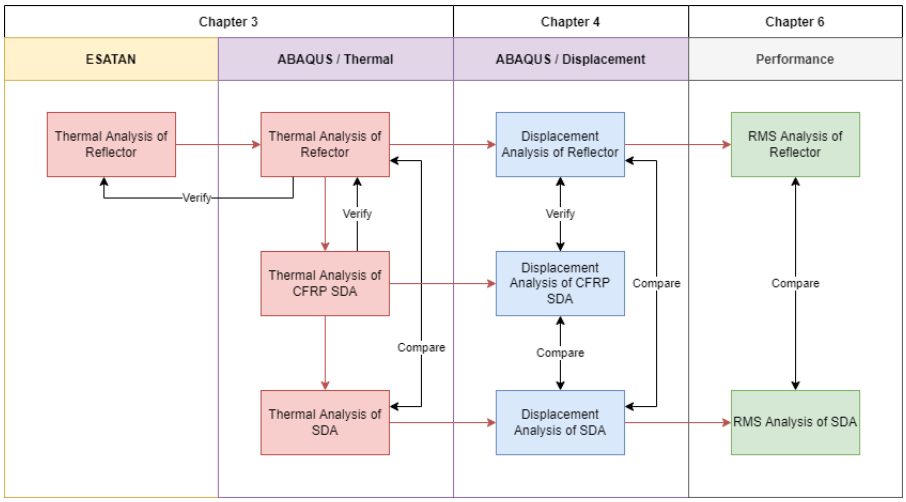

Figure 1.4: Thermo-elastic analysis process and software suit

2

Literature Review

This chapter provides some background information for this thesis. As the source of this thesis stems from Yellowhorse [2], a detailed summary about the concept of the SDA and the research surrounding it is provided. This allows for a strong base to understand the benefits provided by the SDA as a means if deployment for a reflector. This is followed by an introduction to the thermal environment to give background information on the temperatures that can be expected and the effects it may have on an orbiting structure. As guides for the rest of the thesis, two papers with thermo-elastic analyses for spaceborne reflectors are introduced. Lastly, looking at the gap in the literature and the SDA, research questions are formulated.

2.1. The Spiral Dish Antenna

Alden Yellowhorse, Just Herder, and Lorenzo Lannini have been working on a novel concept that could be used for an parabolic antenna reflector. This structure is discussed in "Self-assembling Kirigami Structures"[2]. It is important to point out that their research is, at off the writing of this thesis, still pending publication. Yellowhorse has been working on Origami-inspired engineering. His interests lie in deployment mechanisms, robotics, precision devices, and compliant mechanism. Lannini is a remote sensing expert whose research interest include interferometric and tomographic processing of synthetic aperture radar imagery. Lastly, Herder is a interactive mechanism and mechatronics expert. Together, they have come up with a novel method for the storage and assembly of curved-crease Kirigami structures. Their method, inspired by the previously mentioned research and projects, could deploy a band in a spiral that could end in a large parabolic surface, see Figure 2.1a. This surface could be used for a variety of different things but due to its high deployed-to-stowed ratio, it was considered to be interesting to use it for a parabolic reflector for a satellite antenna.

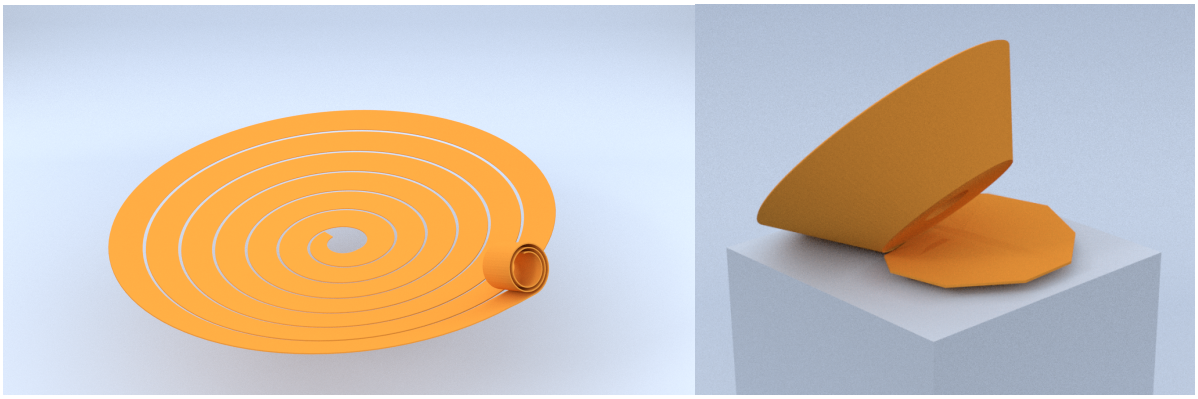

(a) SDA deployed [2]

(b) SDA stowed [2]

Figure 2.1: Deployed and Stowed concepts for the Spiral Dish Antenna

Yellowhorse points to three challenges of using Origami and compliant mechanisms (flexible mechanisms that achieve force and motion transmission through elastic body deformation[11]): preventing unwanted motion in the deployed state, self-intersection during motion, and ensuring sufficiently compact storage.

To answer the issue of compact storage, Yellowhorse proposes taking a large structure and dissembling it into strips. These strips can then be tightly rolled up to form a compact roll. If cut into a single strip, the process has just to be reversed to deploy the structure. Yellowhorse points out that this has the benefit of being a single degree of freedom mechanism: rolling and unrolling. An example of this process can be seen in Figure 2.1b. Note this idea can be used on other shapes than parabolic surfaces, such as spherical, and disks. The advantages of this technique are that it can fold a doubly curved, non developable geometry. Developable surfaces are defined as smooth surfaces with zero Gaussian curvature[12]. Therefore, a non-developable surface is one that can not be flattened onto a plane without distortion. It is often very tough for traditional Origami to fold non developable surfaces. The process of mapping a doubly curved surface is very tough as overlapping parts can occur. To prevent this problem, Yellowhorse uses a spiral shape as it simplifies the path. Being able to form a doubly-curved surface is advantageous as it increases both stiffness and precision. This is due to the introduction of an out-of-plane component to the geometry. To be able to gain the advantages of a doubly-curved surface, the seams of the spiral need to be connected. The spiral simplifies the connection process as the assembly can be done along a single smooth seam. The last advantage, is that the assembly method does not require any complicated robot with multiple components and degrees of freedom. Currently, a simple technique of a zipper with a central key is used.

Yellowhorse list several steps to efficiently use the method:

1. Identify desired shape. Here the parabola is considered
2. Find the cut crease geometry of the surface
3. Find the flat shape and mechanical strains
4. Estimate the size and geometry of the stowed state
5. Select a simple, single-seam assembly process

Yellowhorse describes the formulas describing the Kirigami shape and the geometry of the flat state, to facilitate 2D fabrication. The formulas describing the storage efficiency are found and a prototype is finally made to validate the design method.

The parabolic strip discretization is described in Equation 2.1:

$$\vec{x}_{ps} = (1-\xi)\vec{x}_p(\theta - 2\pi) + \xi\vec{x}_p(\theta) = \begin{matrix} w\xi cos(\theta) + \frac{\theta w cos(\theta)}{2\pi} - wcos(\theta) \\ w\xi sin(\theta) + \frac{\theta w sin(\theta)}{2\pi} - wsin(\theta) \\ \frac{\theta^2 w^2}{16\pi^2 f} + \frac{\theta w^2 \xi}{4\pi f} - \frac{\theta w^2}{4\pi f} - \frac{w^2\xi}{4f} + \frac{w^2}{4f} \end{matrix} \tag{2.1}$$

where ξ is the parameter controlling position on the width of a strip, θ is the azimuth angle of a point on a surface, w is the width of the strip, and f is the focal length of a parabolic reflector.

The different radii of the stowed version is found using Equation 2.2:

$$1 + \frac{w}{R_b} = \frac{R_c}{R_s} \tag{2.2}$$

where R_b is the radius of curvature at the inner edge in its deployed state, R_s is the radius of curvature of the frustrum upper edge in the rolled state, R_c is the radius of curvature of the frustrum base. An image showing the different radius variables can be seen in Figure 2.2

The length of the strip can be found using Equation 2.3:

$$S_{total} = \frac{\pi D^2}{4w} \tag{2.3}$$

where D is the reflector Diameter.

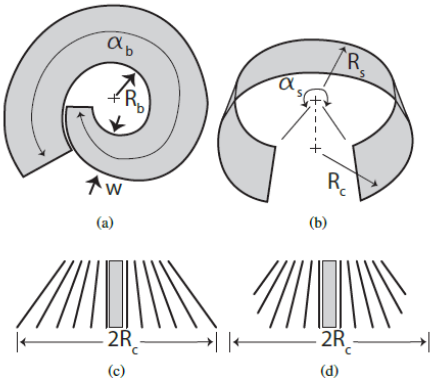

Figure 2.2: (a) Variables describing a deployed spiral strip, (b) its rolled form, (c) a cross section of its rolled state and (d) a cross section where the outer layers are narrower [2]

A prototype has been made and an image of the deployed prototypes can be seen in Figure 2.3. This has shown that a parabolic shape could be formed using this method.

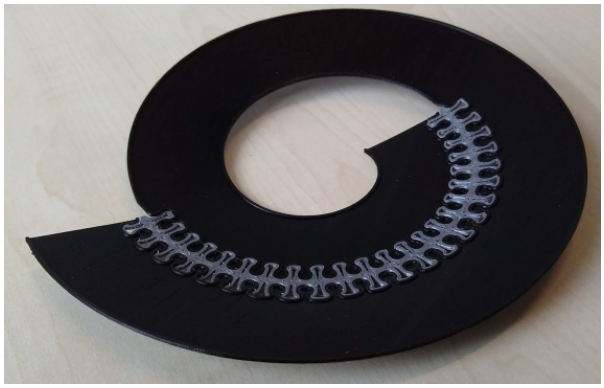

Figure 2.3: Zipper with the Key [2]

Lannini, later in the paper, takes steps to validate the use of this method for an antenna reflector. Using photogrammetry, Lannini studied the surface accuracy of the paraboloid. The results of his study and the parameters used can be seen in Table 2.1

Table 2.1: A list of the parameters describing the spiral antenna prototype and test results.[2]

Parameters	Value	Unit
Diameter	19	cm
Focal Length	9	cm
Spiral Width	2.5	cm
Hole Diameter	2.5	cm
Ideal RMS Error	0.133	mm
Real RMS Error	0.946	mm

With Yellowhorse improving the assembly method of the antenna, and Lannini working on the electromagnetic aspect of the antenna, there is another important aspect of creating a mechanism for space that has yet to be tackled. How well would a SDA tackle the obstacles created by the space environment? This will be discussed in the next section.

2.2. Thermal Environment

When travelling in Earth Orbit, a spacecraft may receive radiant thermal energy from three sources: incoming solar radiation, reflected solar energy (albedo), and outgoing long-wave radiation emitted by the Earth (infra-red). These fluxes are shown in Figure 2.4. Radiation is the primary form of heat exchange with the satellite and the space environment due to the high vacuum in space. On the internal side of the satellite, radiation and conduction are possible with internal heat being created by means of waste heat and circulating heat. When studying the external temperature of the satellite, internal temperature change can often be ignored[13].

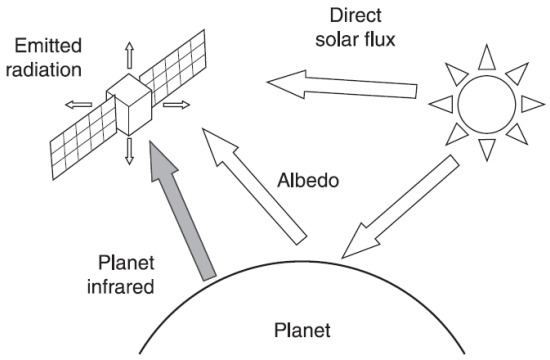

Figure 2.4: Environmental heat fluxes for a planet-orbiting spacecraft[4]

As the satellite orbits periodically around the Earth, the satellite will experience occlusions where the Earth will block the view of the sun. This is one of the reasons, the external surface of the satellite will experience a cyclic variation of heat[14]. Another reason for temperature variation is that the albedo effect is a function of the angle between satellite, Earth, and the Sun. As the satellite passes in view of the Sun, the amount of energy reflected will grow till the satellite intersects the line connecting Earth and the Sun. From there on, the amount of reflected sun will diminish until the satellite passes behind the Earth again. The Infra-red effect is more stable but still varies with the temperature of the ground. Both Infra-red and Albedo effects are also affected by cloud coverage and by the properties of the ground reflecting or emitting heat. Due to these many parameters that can affect Infra-red and Albedo effects, simulating them can be very complicated and many simplifications must be made. These simplifications can be found throughout many different research papers [15][16].

With heat being introduced by the external factor and heat being drown out by the black environment, satellites can experience large temperature changes. These changes vary depending on the orbit of the satellite. Examples of this can be seen in Figure 2.5a and Figure 2.5b which show temperature variations on an exterior point of a satellite for LEO and GEO orbits. As a consequence, the in-orbit spacecraft experiences large temperature difference and gradient, leading to thermal deformation, and bringing about anomalies like signal errors therewith. As a rule of thumb for LEO, the temperatures experienced by the spacecraft can range from -120 and 120°C[17]. To properly prepare a spacecraft for this environment, it is important to consider the following parameters: orbit parameters, thermo-optical properties (solar absorptivity, IR emissivity, transmissivity), Sun incidence, and radiative and conductive couplings with the surround parts of the spacecraft. With the help of ground experiments and simulations[18], thermal control measures can help counter act dramatic temperature changes and stop any damage from occurring. Passive measures must be taken including reasonable arrangement, adoption of appropriate materials and hardware. Active measures should be applied as well, including adaptive adjustment of heat exchange parameters and temperature compensation[19][20].

2.3. Similar Research

As shown in section 2.2.2 a spacecraft can experience large changes in temperature. These changes in temperature can often cause deformations for large space structures. With a reflector being a large but thin structure, they are often prone to deformation. For these reasons, many projects involving reflectors perform thermoelastic analyses to make sure the deformations do not seriously affect the reflectors performance. The following two research papers are used throughout the thesis as a guide, therefore a summary of both papers is given.

Thermal Distortion Analysis of Antennas in Space

In "Reflector Surface Distortion Analysis Techniques (Thermal Distortion Analysis of Antennas in Space)"[9] by R.Sharp a prediction of the far-field pattern in the thermal environment is performed for an Advance Communication Technology Satellite (ACTS) Reflector.

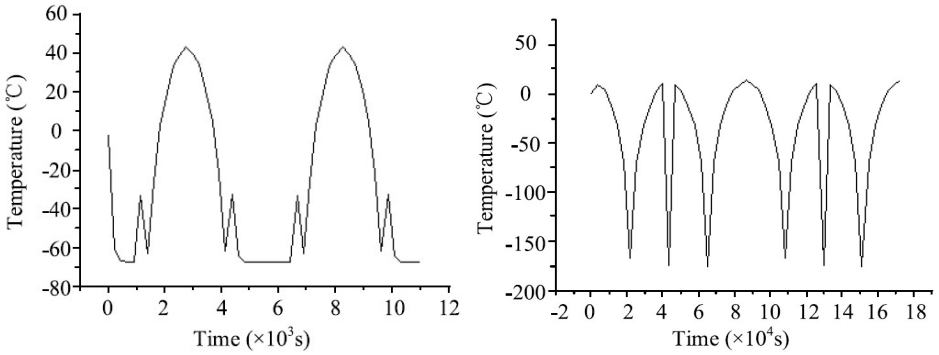

(a) The temperature change of a feature point in an antenna in LEO[21]

(b) The temperature change of a feature point in an antenna in GEO[21]

Figure 2.5: Temperature Profiles for feature points

A suite of large computer programs (TRASYS/SINDA, NASTRAN, and RF ANALYSIS) are used to perform a thermal, thermo-elastic, and far-field pattern analysis respectively. The order of usage of these programs is shown in Figure 2.6. To facilitate the transfer of results between the different programs, new smaller interface programs are used (SNIP and SPLINE II). SNIP allows for the transfer of the thermal results to NASTRAN which can then perform a thermo-elastic analysis. SPLINE II takes the displacement values to interpolate and smooth out the data to allow for the far-field analysis in RF ANALYSIS. The combination of these programs forms a linear process, that can easily be repeated to predict the far field pattern. By repeating the analysis for different radiation loads case which represent different orbital positions the far-field pattern can be predicted across the entire orbit. This lays the foundation of a process that can be used for the thesis to study the effects of the thermal environment on the SDA.

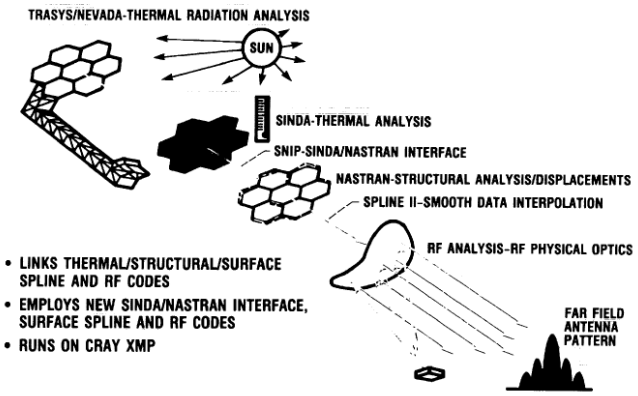

Figure 2.6: Computer Programs used for ACTS reflector analysis [9]

With a process outlined, Sharp has the advantage of a detailed design for the ACTS Reflector to perform his analysis. Not only does Sharp have a reflector with a complex cross-section to model but also has predefined optical parameters to use in his analysis. This allows him to also integrate the effects of the satellite body in his thermal analysis. Thanks to this detailed model design, Sharp does not spend any time questioning the effects of the reflector's geometry, physical and optical properties on the deformation of the reflector. It is clear that the focus of the paper is to predict the far-field pattern and not redesign the architecture or design of the reflector.

Sharp finds throughout his analysis of the ACTS reflector, that for the specific mission case and design, the hottest case temperatures of 231K to 271K occur at the orbit time of 13h, the coldest case temperatures varie from 177K to 191K at the orbit time of 24h. This is shown in Figure 2.7a. No color image was found as the NASA archives are in black and white. These temperatures then translate to deflections of 0.53 to 0.76mm in the hot case and 0.76 to 1.143mm in the cold case as shown in Figure 2.7b.

Thermal Analysis of Unfurlable CFRP Skin-Based Parabolic Reflector

In "Thermal Design and Analysis of Unfurlable CFRP Skin-Based Parabolic Reflector for Spaceborne SAR Antenna" by T.Park[8], a thermal analysis is performed on a new kind of SAR reflector. In this paper, Park works off of a design first proposed by C.Wiley [22]. This reflector is unique in that it has separate petals

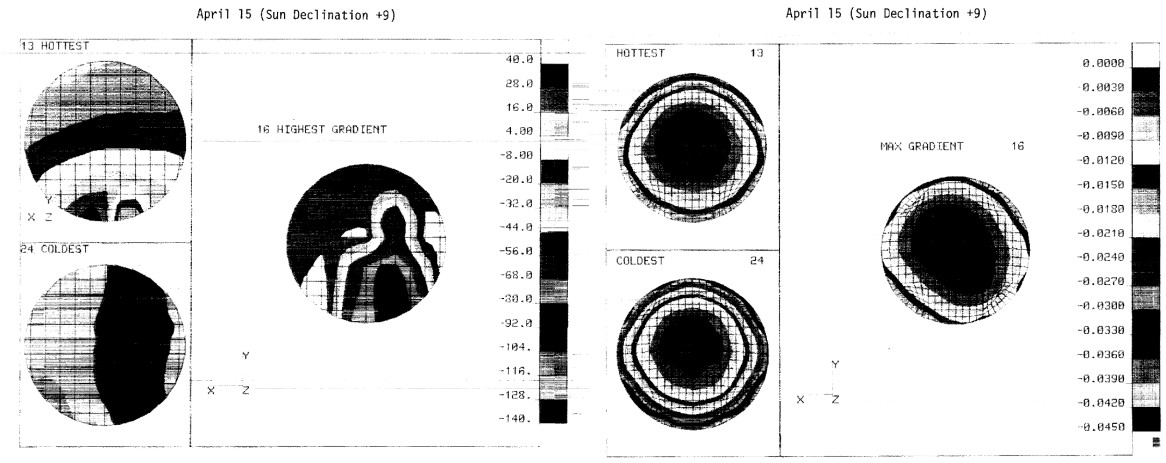

(a) ACTS temperature summary

(b) ACTS displacement summary

Figure 2.7: Temperature and displacement maps for the ACTS at hottest, coldest, and max gradient moments [9]

that end up forming a parabolic reflector. See Figure 2.8 for an image of the three dimensional model of the reflector. Due to these separate petals, Park is interested in seeing how they could affect the temperature and displacement fields of the reflector as it orbits.

Using Thermal desktop and SINDA, a similar process as Sharp [9] is used to find the deformations in the reflector. In this case, Thermal desktop is used to build a TMM which can be used to perform the thermal analysis. Park studies the reflector for a polar orbit during the summer and winter season at different moments during the orbital period. Due to its intended use as a SAR (synthetic aperture radar) reflector, Park adds "imaging" periods in the orbit where the satellites rotates to point towards the earth. Otherwise, for the rest of the orbital period, the satellite points away from the Sun. This adds an additional moment, different to the eclipse, of rapid change to the thermal loads. Unlike Sharp, Park not only includes the shadowing effects of the satellite body, but also includes the effect of the secondary reflector and the solar panels. This can be done because of a strong confidence in the reflector design but also because these are of interest to the rest of the satellite design. Similarly to the primary reflector, predicting the effects of deformation on the smaller secondary refelctor, helps to quantify the performance of the system as a whole. It is for this same reason that the solar cells are studied as depending on their configuration, these could heavily impact the thermal loads on the reflector. As Park looks to already optimize the setup of the SAR antenna with a petal reflector, he additionally studies a few different coating cases on the primary and secondary reflector. This allows a further optimization of the reflector and therefore furthers the confidence that the results will reflect the effects on a final design of the petal reflector.

In his research, Park concludes that the thermal design based on SiO2 coating and MLI is feasible for minimization of the thermal gradient of the reflector assembly. Figure 2.9 shows the results of the deformation analysis with the maximum deformation being 1.405mm. In addition, the effect of deployed solar panels on the thermal gradient of the reflector indicate that a reduction of the solar panel length while increasing the number of panels is one way to minimize the increase of the thermal gradient.

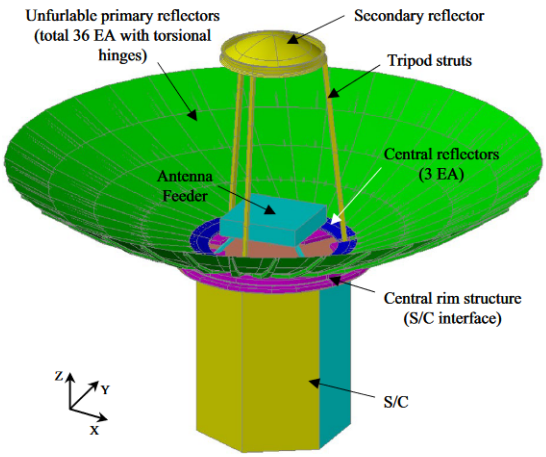

Figure 2.8: Thermal mathematical model of SAR antenna based on CFRP skin-based reflector assembly[8]

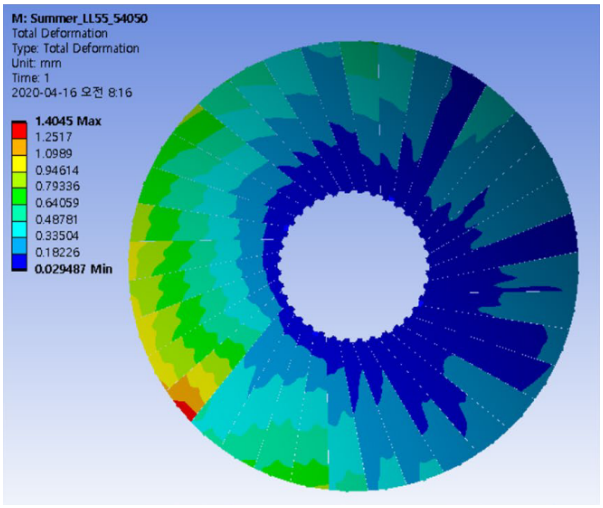

Figure 2.9: SAR antenna reflector deformation analysis[8]

2.4. Gap in Literature and Research Questions

Yellowhorse describes the concept of the SDA mathematically and approaches the idea of using it for space due to the benefits it could provide. A few different steps have been taken to analyse the SDA and prove the concept could work as a real deployment technique: building a prototype and performing a photogrammetry analysis of the reflector surface with the zipper. To further the validation of this concept, this thesis looks to study the SDA in the thermal environment of space and see how it is affected. The reason this is of interest is due to the unique geometry and assembly method of the SDA. This research for the SDA currently does not exist and many researchers related to the project have formulated interest in exploring it. From the author's point of view, the thermal environment poses a potential danger to the performance of the SDA and therefore needs study. The following research question was formulated:

RQ: Would an asymmetric spiral band parabolic reflector with a spiral inter-band interface properly perform with regards to the space thermal environment?

The first aspect to look at in the research question is to properly define the thermal environment of space. Looking at the literature outlined in the previous section, understanding the thermal environment of space is always of interest for space missions. As outlined by Xeng [21] and by Meseguer [4], many different parameters affect the thermal behaviour of satellites and of reflectors in space. The literature around the fluxes impacting satellites is well developed but is heavily impacted by the design of satellites. As much as general temperature ranges can be given for different systems of a satellite, getting a proper temperature field requires specific analysis. To perform a thermal analysis for the SDA, it is noted that many parameters have yet to have been decided for the SDA. It is therefore important to properly outline the assumptions made to make sure that the thermal loads placed on the SDA reflect a correct temperature field. This therefore shows that for the analysis of the SDA, a baseline model is needed to compare both to literature and to the SDA. Therefore the following sub-question was formulated to make sure that the thermal environment used in the study of the SDA is correct:

SQ1: What temperature fields may be expected on a reflector orbiting Earth?

With the thermal environment properly defined, the interest of this thesis still lies with the SDA. As it is new, there is no information on how the temperature field on a reflector may differ for an SDA because of how the spiral interface that could change the way heat flows through the reflector. For this reason, as a joint question to the first sub-question, the following sub question rounds out the thermal analysis aspects for the SDA:

SQ2: How does the zipper interface impact the temperature field on the reflector?

To next step in looking at the effects of the thermal environment on the performance is to study the deformation of the reflector. The thermo-elastic study for satellites differ slightly from normal thermo-elastic analyses as the thermal loads often come from a software specifically made for space. Both Sharp [9] and Park [8] show the process and methods used for the study of the deformation and performance of a reflector for space. Their methods are of use, and many of the assumptions or designs can be used as guides for research, but their answers will not be able to answer the research question posed. As the first sub question poses a general question on the temperature field experienced by a reflector, the baseline concept needs to be continued with regards to the deformations. The following sub-question is therefore formulated:

SQ3: How does the temperature field experienced by a reflector affect the deformation of the SDA?

As much as Park [8] performs a thermal analysis for a reflector that shares cuts in its design, it does not equate to the SDA which has its cut spiral around the reflector. With a baseline modelled which does not have the cut, the next question to be asked is how does the spiral interface of the SDA impact the deformation. This question builds off of the second sub-question similarly as sub-question 3 builds off of sub-question 1.

SQ4: How does the zipper interface impact the deformation of the reflector?

With the thermal and thermo-elastic aspects of the research question answered by the four first sub-questions, the next aspect is to judge the performance of the reflector. Similarly to the thermo-elastic analysis, Park and Sharp offer methods used to judge reflector performance. With the analysis of the SDA being consistently compared to a baseline model which can be compared to the literature, the last step for the analysis is look at the performance of the SDA. Seeing how the temperature field and the deformations of the reflector are affected by the spiral interface are interesting to know what thermally and mechanically is happening to the SDA but doesn't answer if the SDA can still be used. To therefore cover the final aspect of the research question, the final sub-question ask is:

SQ5: How does the deformation of the SDA impact its performance?

By looking to answer these sub-questions in the order that they are provided, the thesis will look to be able to formulate an answer to the main research question.

3

Thermal Analysis

This chapter explains the approach adopted in performing the thermal analysis of the SDA and the subsequent results. In Section 3.1.1, the basic theory of thermal transfer is outlined to point out the many variables that affect the thermal loading of a system in space. Section 3.3.2 introduces the method used in performing the thermal analysis of the SDA. Section 3.3.3 explains how ESATAN is used to define and analyse a reflector in different orbits over Earth. Section 3.3.4 explain how Abaqus is used to automate, define, and perform the thermal analysis for the Reflector and SDA models.

3.1. Thermal Analysis-An Explanation

3.1.1. Heat Transfer

Due to space being a vacuum, convection can be neglected and therefore radiation and conduction are the primary means of heat transfer. To properly understand the amount and type of energy hitting the antenna it is important to quickly go over the fundamentals [23] and see the different types of heat transfers.

Heat Transfer Fundamentals The amount of energy impacting a surface is often referred as heat flux q (J/(s-m^2). This heat flux is a function of the heat transfer rate Q (J/s or W) and the surface area A being hit.

$$q = \frac{Q}{A} \tag{3.1}$$

This heat flux stems from the first law of thermodynamic which states that for a closed system you get the following relationship:

$$Q = \frac{dE}{dt} + W \tag{3.2}$$

where $\frac{dE}{dt}$ is the change of energy within the system and W is the the sum of all the heat and work transfer interaction experienced by the closed system.

Solar Radiation The first radiative heat transfer to look at is the amount of radiation emitted by the Sun onto the antenna or spacecraft. This is described by the following equation [24] of the solar heat flux:

$$q_s = \alpha F_S S \cos\psi \tag{3.3}$$

where S is the incident Solar flux, α is the absorptivity of the surface (material or coating property describing the fraction of energy absorbed), F_S is the view factor of the solar radiation, and ψ is the angle between the direction of the solar heat flux and the normal of the structural component's surface.

The view factor is defined as the fraction of the radiant energy which leaves surface i and strike surface j. This is defined by the following equation:

$$F_{ij} = \frac{1}{A_i} \int_{A_j} \int_{A_i} \frac{cos\beta_i cos\beta_j}{\pi r^2} dA_i dA_j \tag{3.4}$$

where A_i is the area of surface i, r is the distance from the element of surface dA_i to the element of surface dA_j.β_i is the angle between the normal to dA_i and the straight line joining dA_i and dA_j, and β_j is the analogous angle for dA_j.

Earth/IR Radiation The Earth in itself radiates energy which can also impact the satellite if it is flying close to the Earth. The further the satellite is the less of an impact the earth radiation also known as infra-red radiation (as other celestial bodies will also exhibit similar radiations) will have on the spacecraft. The infra-red heat flux is described using the following equation which stems from Stefan-Boltzman law of black body radiation:

$$q_{ir} = \alpha F_{ir} \sigma T_{ir}^4 \cos\theta \tag{3.5}$$

where F_{ir} is the view factor of the spacecraft to the emitting body, T_{ir} is the temperature of the emitting body, σ is the Stephan-Boltzman's constant, and θ is the angle between the direction to the emitting body and the normal of the surface being hit.

Earth Albedo Radiation Similarly to the IR radiation, when a spacecraft orbits close to a celestial body, there is an amount of solar energy that is reflected off of the surface of that body that will hit the space craft as well. This flux is described by the following equation.

$$q_r = \alpha F_E \rho S \cos\theta \tag{3.6}$$

where ρ is the solar radiation reflected off the surface of the Earth.

Radiated Energy As much as the spacecraft receives heat from these different sources, it also does radiates heat back out into space. This dissipated flux is described by:

$$q_{rad} = R_{ij}(T_j^4 - T_i^4) \tag{3.7}$$

where T_i and T_j are the temperatures at point i and j, R_{ij} is the radiation conductance defined by the following equation:

$$R_{ij} = \sigma \epsilon_i A_i B_{ij} \tag{3.8}$$

where σ is the Stefan-Boltzmann constant, ϵ_i is the surface emissivity, A_i is the surface area, B_{ij} is the Gebhart factor. B_{ij} is defined as the rate of energy absorbed at surface j which originated as emission from surface i, divided by the total rate of energy radiated by surface j [25]. B_{ij} is also defined by the following equation:

$$B_{ij} = \epsilon_j F_{ij} + \sum_{k=1}^{N} (1 - \epsilon_k) F_{ik} B_{kj}, \quad i = 1, 2, ..., N \tag{3.9}$$

Conduction The conduction describes the heat transfer through material contact or inside the material itself if the surface is discretized. The heat flux due to conduction can be described by the following:

$$q_{cond} = K_{ij}(T_j - T_i) \tag{3.10}$$

where T_i and T_j are the temperatures at point i and j, K_{ij} is the linear conductance defined by the following equation:

$$K_{ij} = \frac{\kappa A}{L} \tag{3.11}$$

where κ is the material thermal conductivity, A is cross section area, L is the distance between the two points.

Heat Balance Equation According to the principle of energy conservation, the sum of energy absorbed by the spacecraft and the energy generated by the spacecraft equal the sum of the heat radiated to space and the internal energy variation:

$$q_i + q_d = q_S + q_r + q_{ir} \tag{3.12}$$

where q_i is the internal energy variation.

3.1.2. Thermal Analysis

The aim of most thermal analysis for a spacecraft is to figure out the temperature ranges experienced by different components of the spacecraft, so as to iteratively design methods of keeping the components within a required temperature range. Due to the extreme environment of space and the complex designs of a spacecraft, this process is performed throughout the design phase and can often be a leading vector for design changes. Because of its importance to overall mission success, being able to model and simulate the system using software has allowed for better thermal control designs.

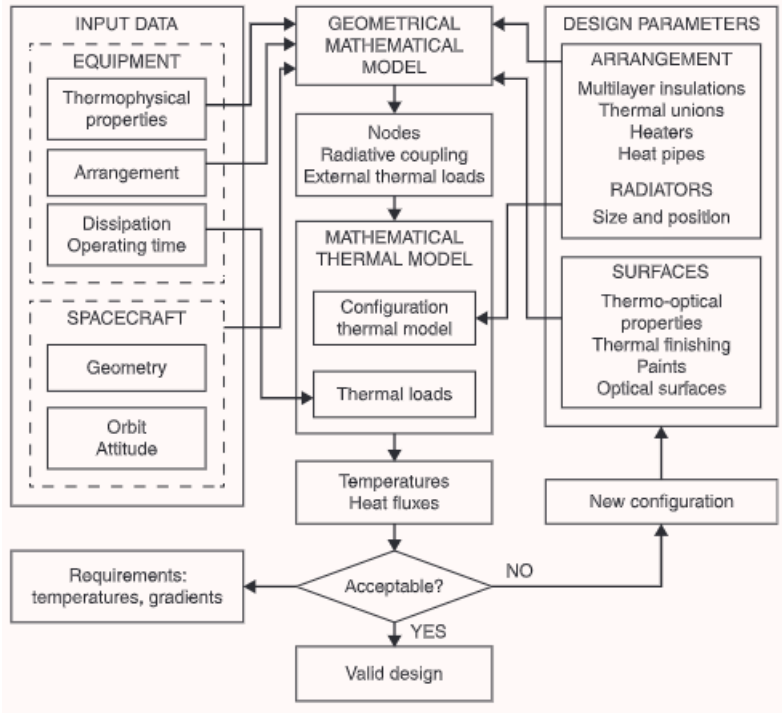

Figure 3.1: Thermal Analysis Process [4]

The main thermal analysis methods used in the space industry follow a similar process. Figure 3.1 shows the design process for the thermal control of a space craft. The "INPUT DATA" box shows the parameters with direct influence on thermal behaviour. The "SPACECRAFT" group has the satellite geometry, its orbit, and its attitude. This will define the external thermal loads, and the exchange of radiation between different surfaces. The "EQUIPMENT" group are the equipment characteristics and power distribution. These properties of the components (mass, shape and thermal capacity) have a major influence on the thermal behaviour of the spacecraft. The "Design Parameter" box are the parameters for the thermal control system, they can usually be modified or appropriately selected for thermal reasons (i.e. the selection of coatings). The solar absorptance, α, and the infra-red emissivity, ϵ, govern the radiation exchanges, either with the environment or between spacecraft surfaces. Another important parameter for thermal design is related to the thermal behaviour of the mechanical joints. Hence, the design of the mounting concepts.

Once the appropriate thermal hardware has been selected, a geometrical mathematical model (GMM) and a thermal mathematical model (TMM) are set up to analyse the design and to determine the temperatures

[4]. As shown in Figure 3.1 the GMM outputs for each discretized node of the system, the radiative coupling and the external loads experienced by the node. This is often done by discretizing the geometry of the system into a network of isothermal elements, characterized by its temperature and capacitance. This numerical approach is called the "lumped parameter network" and due to conservation of energy implies that the temperature of the ith node must evolve in time according to Equation 3.13 [26]:

$$C_i \frac{dT_i}{dt} = \dot{Q}_{sun,i} + \dot{Q}_{alb,i} + \dot{Q}_{planet,i} + \dot{Q}_{dis,i} + \sum_{j=i}^{n} K_{ij}(T_j - T_i) + \sum_{j=0}^{n} R_{ij}(T_j^4 - T_i^4) \tag{3.13}$$

where C_i and T_i are the thermal capacitance and temperature. $\dot{Q}_{sun,i}$, $\dot{Q}_{alb,i}$, $\dot{Q}_{planet,i}$, and $\dot{Q}_{dis,i}$ are the solar, albedo, planetary infra-red, and dissipated thermal loads. K_{ij} and R_{ij} are the conductive and radiative couplings between different nodes of the system.

Once the GMM has set up Equation 3.13 for each node, the TMM consists of a system of ordinary differential equations (ODE). This system of equations is solved using an ODE solver and outputs the temperature of the nodes over time.

$$C_i = \rho_i c_i V_i \tag{3.14}$$

where ρ_i is the density of the material, c_i is the constant pressure heat capacity, and V_i is the node volume.

3.2. Method Selection

As shown in Figure 3.1 the thermal analysis process is iterative and performed throughout the design cycle of a spacecraft. For the purpose of studying the SDA, the idea of the thermal analysis differs slightly. When one normally runs a thermal analysis to converge to an optimal design, the thermal analysis performed for the SDA has the goal of exploring how reflectors in space heat up and how those temperature affect the shape of the reflector. To perform this, a simple model of a paraboloid is required with a dense mesh to get a better idea of temperature differences across the reflector. If a lesser dense mesh is used, the overall temperature differences would be known but the more minute temperature effects might be missed out. Because of this need of denser mesh, a thermal analysis software is of major importance.

The Aerospace Industry uses a variety of different thermal analysis options: ESATAN-TMS, SINDA, Thermal Desktop, Thermica, and Ansys [4]. For the purpose of this project ESATAN-TMS is selected as the software package that will be used due to ease of access and its built in capability of being able to easily manipulate orbital parameters.

3.3. ESATAN Thermal

ESATAN-TMS is a software made by ITP Engines UK Ltd. under the European Space Agency contract 4791/81/NL/DK(SC)[27]. ESATAN is, at its core, a program for obtaining solutions to lumped parameter thermal models. These models must be generated by the user, though extensions to ESATAN. In the case of this project the Workbench extensions is utilized as it allows for the generation of three-dimensional thin-shell models, automatic calculation of radiative and solid conductors for models and output in the form of an ESATAN input deck. Workbench also has the advantage of a comprehensive three-dimensional visualisation capability[28].

3.3.1. Model Definition

Workbench provides a single environment for performing all of the phases of modelling and analysis for the reflector. The phases of the modelling and analysis are:

- Geometry – to create the model itself.
- Radiative – for radiative analysis specification and calculations.
- Reporting – to report details of the model and the results of the calculations.
- Thermal – to generate, manage and run thermal analyser models.
- Administration/Library – administration of the Workbench model database, model import/export and library properties.

- Visualisation – can be used at any time, in parallel with the other phases, to visualise the geometric model, the model in orbit and the results of calculations.

Figure 3.2 shows the general flow of performing an analysis through Workbench. In the next few sections, the Geometry, Radiative, and Thermal modules will be explained in further detail and the definition of the reflector will be described.

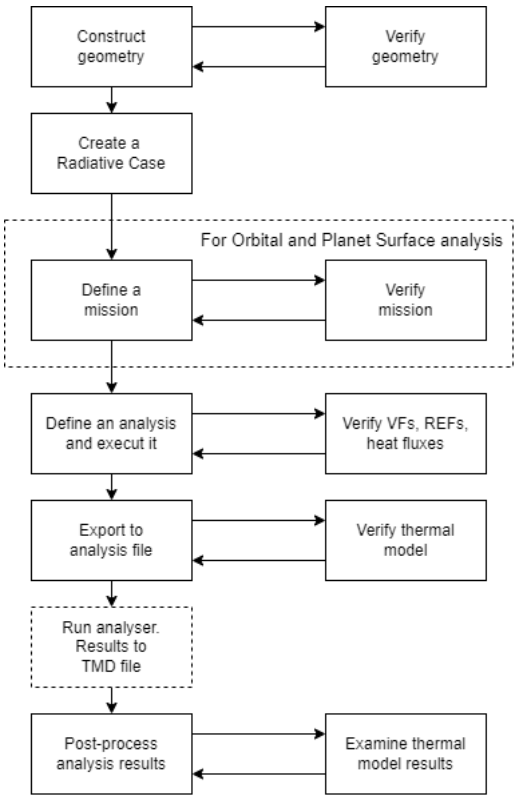

Figure 3.2: Flowchart of Workbench activities [28]

Assumptions

The following assumptions are made to perform the thermal analysis of the SDA:

AT1 - The reflector is simplified to the shape of a paraboloid.

AT2 - Each side of the reflector will be coated by a singular coating.

AT3 - The material of the reflector will be considered isotropic.

AT4 - The reflector will point in the same direction during orbit and no reflector movement will be considered.

AT5 - No active thermal control method will be considered in the analysis.

AT6 - The SDA will be fully deployed during the analysis.

AT7 - No thermal effect caused by the bending of the material will be considered.

AT8 - The SDA zipper will be made out of a single material.

AT9 - No satellite body will be modelled in the analysis of the reflector

Geometric Module

The Geometry module is used to create the geometry and properties of the model in a three-stage approach:

- Defining primitive geometry
- Creating assemblies with relative movement between components
- Assigning thermo-optical properties to components

Geometry

Defining the geometry of the ESATAN model for the analysis of the SDA is simplified to the basic shape of a paraboloid. ESATAN facilitates the design of a parabolic reflector by defining a parabolic reflector using just 3 parameters (flength, hmax, and angmax). 'flength' is the focal length, defined as the distance between the centre of the paraboloid and the focal point. 'hmax' is the height of the reflector, and 'angmax' is the angle of revolution of the reflector. These Attributes can be seen in 3.3.

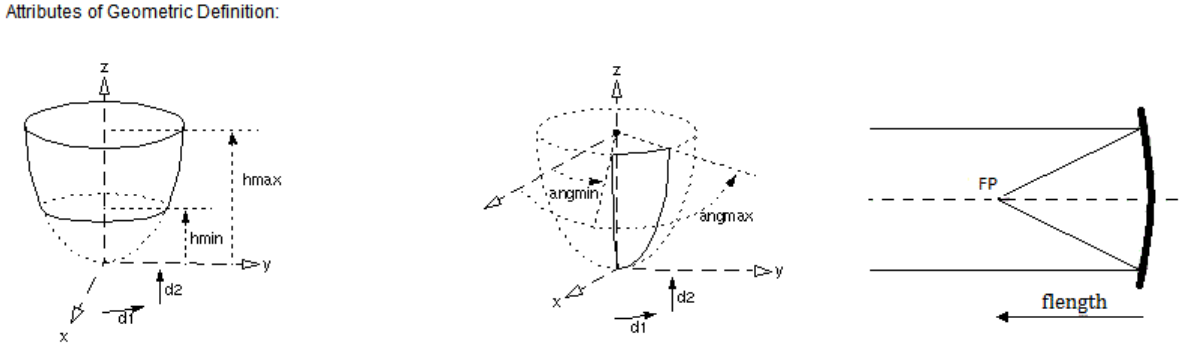

Figure 3.3: ESATAN Parabolic Geomteric Attributes

At this stage, a simple model of a paraboloid can be obtained and can be manipulated using the equation of a parabola . The problem that arises is what geometry to chose? Because the SDA is still a concept, no given geometry or design has been defined. This is most likely due to the fact that reflector designs are closely tied to the mission parameters (orbit, pointing direction, communication/instrument needs). The SDA is tied to no mission, meaning these parameters can not be derived by design requirements. As much as a it would be possible to parametrically analyse the SDA, it is mostly deemed out of the scope of this thesis. It is decided that the geometry of the SDA model would be derived from the literature. At this stage, Sharp's analysis of a reflector distortion [9] is used to help define the reflector. In Sharpe's analysis, the ACTS 3m reflector is simulated and analysed to study the distortion effects on the radiation patterns of the reflector. It is decided that the geometrical properties ACTS reflector would be the basis of the SDA model for further analysis. These parameters are outlined in Table 3.1.

Table 3.1: SDA Model Parameters

Diameter (m)	Focal Distance (m)	Height (m)	θ_0 (deg)	Frequency (GHz)	f/d
3.0	1.654	0.34	48.77	20	0.55

Even with all these parameters obtained from Sharp's analysis, there is still a big problem that arises. By nature the ACTS reflector and the SDA differ greatly by there means of deployment. The ACTS reflector is a rigid reflector that deploys only through the means of swinging out from a stored position where it is pushed against the spacecraft bus. The reflector itself does not change shape through the deployment. As shown in section 2.2.1 the SDA will spiral out and form the parabolic shape only once fully deployed. Because of this deployment mechanism, the design of the bands of the reflector need to be flexible enough for its stored position while also being able to keep its doubly curved shape once deployed. To simplify the approach of the design of the band, the decision is made to simulate it as a uniform monolithic structure. This is widely different than the ACTS cross section which, as shown in Figure 3.4, is comprised of supporting ribs, a honeycomb core, Multi-Layer Insulation, and Fiberglass-epoxy sheets. Not only does this mean that comparing

the results from Sharp's ACTS reflector analysis to the SDA results to be very hard, but also means that the thickness of the SDA cannot be derived from the ACTS.

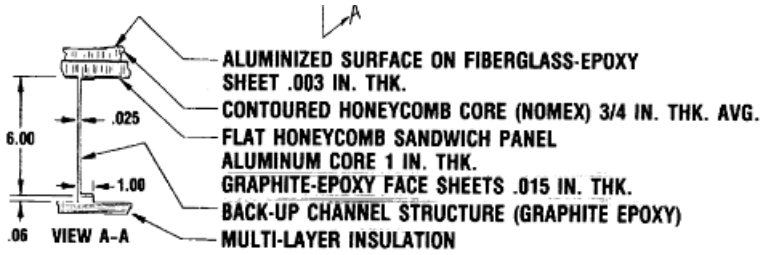

Figure 3.4: Cross Section of ACTS reflector [9]

To remedy this, more literature had to be found for a deployable reflector. It is important to note that there are no reflectors like the SDA in existence, in which a spiral shaped interface spirals around a parabolic shape. The closest form of reflector this could be compared to is the petal shaped reflector shown in appendix B. In Park's "Thermal Design and Analysis of Unfurlable CFRP Skin-Based Parabolic Reflector for Spaceborn SAR Antenna" [8], a thermal analysis is performed on a petal shaped reflector proposed by C.Wiley [22]. As shown in Figure 2.8, the reflector is comprised of a thin CFRP sheet with ribs for support. It is decided that the thickness of 0.4mm would be used to describe the SDA band an that the thermo and physical properties adopted for the petal reflector would also be used for the SDA thermal analysis.

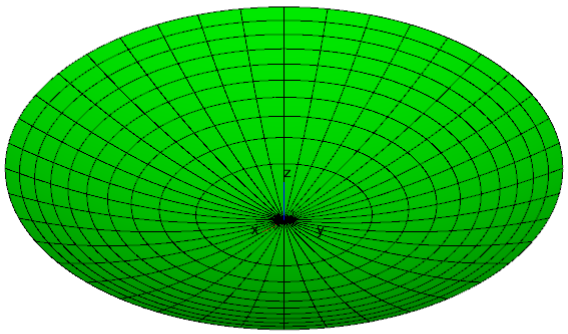

Figure 3.5: ESATAN Parabolic Reflector

With all these geometrical parameters, Figure 3.5 shows the reflector geometrical model created in ESATAN. At this stage of the analysis the spiral zipper has not been taken into account. This is due to three reasons.

Firstly, ESATAN has some interesting capabilities to be able to build complex models, but does not have the capability to design a complex three dimensional spiral based paraboloid. Though the ESATAN-TMS suit does come with its own CAD software "CAD bench", it is only used to import CAD models from other an software, which can then be simplified for ESATAN workbench. A consideration is made to define the conductors between the different nodes of the reflector to recreate the effect of the spiral zipper. This is feasible for a paraboloid with a limited amount of faces as the ESATAN input file could manually be edited. A problem arose for the case where we the number of nodes is very high as the manual edits would take a lot longer and would be prone to high error due to human input.

Secondly, the plan is to transfer the thermal results from ESATAN to an dedicated FEM software, ABAQUS in this case, in which the thermo-elastic analysis can be performed. Therefore it is decided to limit switching back and forth between software suits and make the analysis path as linear as possible.

Thirdly, is based on the method of result transfer from ESATAN to the Abaqus. As discussed in section 3.1.2 ESATAN will output temperature and heat fluxes for each node. The first option for result transfer is to get the temperature field from ESATAN and transfer these temperature fields to the Abaqus thermo-elastic model to see the deformations. As much as this idea is viable for a steady state analysis due to being able to assign a predefined temperature field in Abaqus, this is not feasible for a transient analysis. The bigger issue with this is that by transferring the temperature from a reflector that does not have the spiral zipper models, the zipper's effect on temperature will not be shown. The second option, and the only way that is found to have a both spatial and time varying thermal field in ABAQUS, is to transfer the heat fluxes from ESATAN to ABAQUS. This can be done because Abaqus allows for the definition of surface heat loads with varying amplitude over time. Due to only transferring the heat flux, the presence or not of a spiral zipper in the ESATAN model will not affect the results. This does mean that Abaqus will consist of two models: thermal and thermo-elastic. This method of performing a thermo-elastic analysis in Abaqus is outlined as the Sequentially coupled thermal-stress analysis [29]. For all these reasons the Geometry of the ESATAN model only need to consists of a parabolic reflector.

Meshing

In continuation of the reasoning of result transfer between ESATAN and ABAQUS, when given the option between performing the ESATAN analysis using the Lumped Parameter (LPM) or finite element (FEM) mathematical model formulation, the LPM method is selected. In the FEM formulation, the geometry is meshed into a set of small elements over which the temperature is assumed to vary linearly in all direction (see Figure 3.7). The solution determines the temperature at each node or every element. The nodes of the model are strictly point-like and therefore have zero extent. In the LPM formulation, the model is divided into a number of pieces represented as a point with physical properties lumped together (heat capacity, heat dissipation, heat inputs, heat losses, conductances to other nodes, exchanges to nodes, and temperature) . A network is then created connecting each point, also named nodes, together using conductive and radiative couplings (see Figure 3.6). Lumping of the temperature has an important consequence: the material of the node is treated as being isothermal. Both methods would tend towards the same result but LPM has the advantage of being viewed as dealing with pieces. These nodes can be matched to faces in Abaqus and can make the transfer of heat fluxes easier for the user.

Assembly

Once the Geometry of the reflector is completed, it needs to be assigned to an assembly. This means connecting the reflector with any other major component in the analysis. A full thermal analysis in space often requires a spacecraft bus as the bus will often impact the temperature field on the reflector due to the shadow it will project onto the reflector. In the case where the reflector is being illuminated by the sun but that the spacecraft bus is in between a section of the reflector and the Sun, the drop in temperature on the reflector will be greater due to the shadow causing that section of the reflector to be colder. As shown in Park [8] the main bus is omitted but the effects of the solar panels are calculated as their configuration and size may cause the reflector to distort more. In Sharp's analysis [9], the bus is included but is modelled as a large cube. This is an important aspect in thermal analyses for a space mission but seeing that the SDA is a proof of concept phase, this is not a priority in the analysis of the SDA's performance to space's thermal environment. The main focus is to understand how the spiral zipper impacts the temperature field and not how does the bus impact it. By taking this approach the spacecraft bus and the feed are omitted from any further analysis.

Another point to note in the assembly of the model is effects of the attachment mechanisms. The attachment mechanism can be considered as a path for heat to pass through. This would mean that the attachment mechanism would affect the overall temperature distribution on the reflector. To remedy this, a passive thermal control mechanism is often used to minimize its effect. This is often done using titanium due to it high strength and low thermal conductivity. Other means of thermal control may also be used. In the case of the SDA, this would only be present at the base of the reflector as this would be the point from which the reflector would deploy. By following the concept of the SDA, there shouldn't be the need of any other attachment point

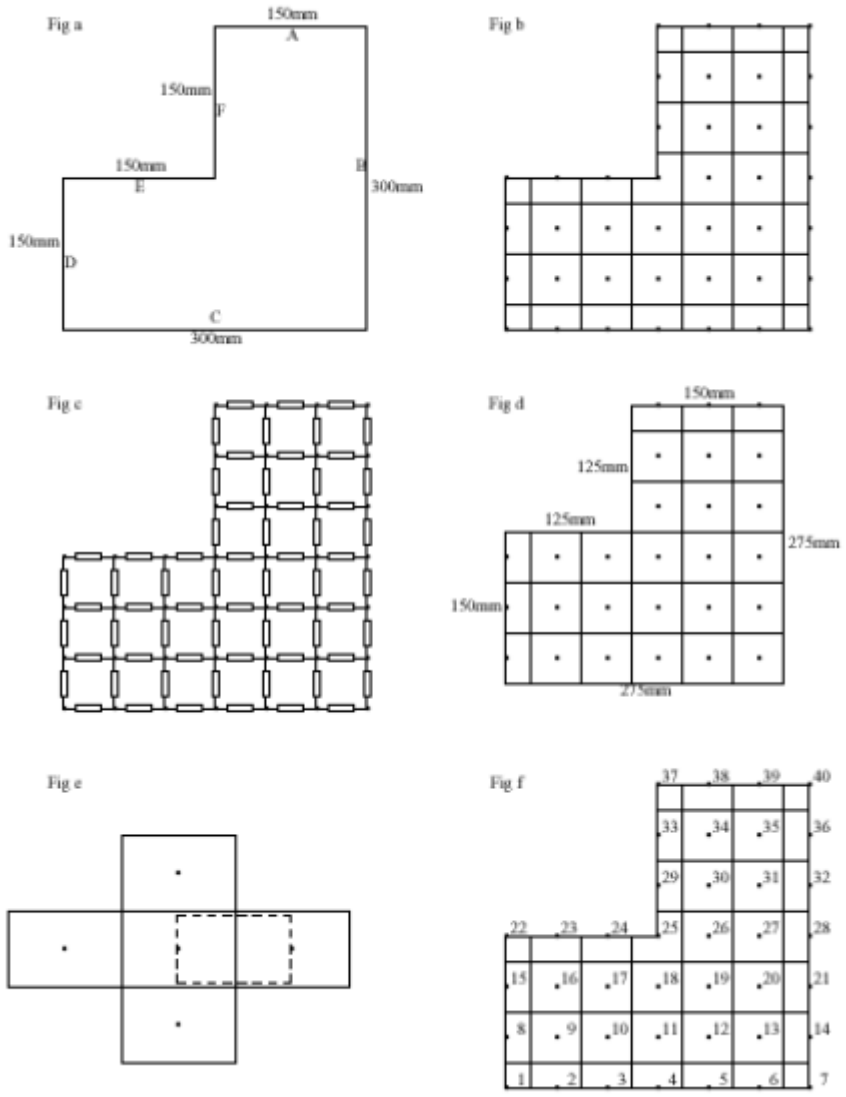

Figure 3.6: Lumped Parameter Discretization [28]

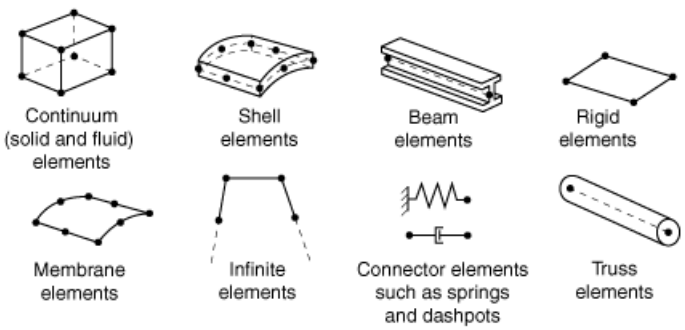

Figure 3.7: Finite Element Discretization

due to its doubly curved nature. This is extraneous to the analysis as there is no clear mechanism in mind yet for how the reflector will be connected to the spacecraft bus and therefore seen as outside the scope of this thesis.

Properties

As discussed on the geometry section, Park's analysis on the petal reflector has provided physical and optical parameters that can be used to perform the analysis of the SDA. A thin CFRP(M55J) is used for the band while a Aerospace grade Aluminum 6063-T6 is used for the Zipper. Note that this does not mean that these materials are best suited for the construction of the SDA but will be used for it analysis. The properties of these materials are listed out in Table 3.2

Table 3.2: Thermo-physical properties utilized for thermal analysis. [8]

Material	Density (kg/m^3)	Conductivity (W/m/K)	Specific heat (J/kg/K)
CFRP (M55J)	1623	46.97	827.05
Aluminum 6063-T6	2700	200	900

When it comes to the selection of the optical properties of the reflector, Park's [8] is used once again as a guide. The first case to look at consist of a fully CFRP optical property based reflector. This means that both the top and bottom of the reflector have the CFRP optical property. A second case is studied where Silicon Dioxide (SiO_2) is used as a coating on both sides. Note is Table 3.3 that the silicon dioxide coating differs by having a much lower absorptivity and emissivity than the CFRP properties. This means, it can be expected to absorb but also emit less energy. The last case consists of having a Silicon Dioxide coating on the top of the reflector and a coating of white paint on the back.

Table 3.3: Thermo-optical properties utilized for thermal analysis. [8]

Optical property	Absorptivity (α)	Emissivity (ϵ)	Specularity	α/ϵ
CFRP (M55J)	0.92	0.8	-	1.150
White Paint	0.2	0.9	-	0.222
SiO_2	0.14	0.12	0.5(solar)/0.5(IR)	1.167

Radiative Module

The Radiative module is used to calculate the view factors (VFs), radiative exchange factors (REFs), and Direct and absorbed heat fluxes (HFs) of the Geometric model. In this module, the orbital parameters are defined for the different analysis cases. Following Park's analysis, Hot and Cold cases are defined as orbits during the Winter and Summer Solstice respectively. These are realistic orbits that could be expected for a Low Earth Orbit (LEO) satellite. For a worst case scenario, a LEO equatorial circular orbit is also analysed and shown in Figure 3.8. As shown in Table 3.5 the LEO orbit spends the most time in eclipse and therefore offers the more time for the reflector to tend to a colder temperature creating a bigger difference in temperature over an entire orbit. This is also compared with a similar orbit but at Geosynchronous Orbit (GEO) altitudes. Each of these orbits are being simulated for Earth as the SDA would first have to prove to work in Earth orbit before being used for any exploration missions. Lastly, the pointing direction direction differs between the LEO/GEO and Summer/Winter cases. Following Park's analysis, the Summer and Winter cases point away from the sun to limit the amount of heat that would reflect inside the reflector. Unlike Park's analysis, no satellite movement is added to this thesis analysis to allow for a short window of pointing the reflector to earth for sensing.

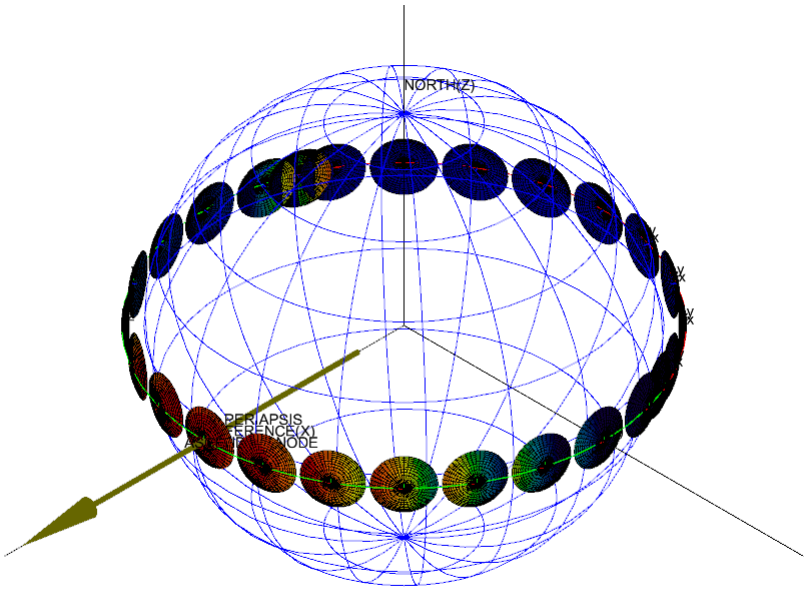

im

Figure 3.8: LEO orbit and Solar Flux absorbed

Table 3.4: Orbital parameters and environmental fluxes for thermal analysis

Item	Summer	Winter	LEO
Altitude (km)	550	550	550
Orbital Inclination (deg)	45	45	0.0
Orbital Period (s)	5736.63	5736.63	5736.63
Season	Summer Solstice	Winter Solstice	-
Solar β angle (deg)	-21.2	-68.1	0.0
Sun Initial Right Ascension (deg)	89.59	-90.42	0.0
Solar Declination (deg)	23.45	-23.45	0.0
Right ascension of ascending node (RAAN, deg)	7.8	190	0.0
Solar Constant (W/m^2)	1287	1420	Calculated in Orbit
Albedo coefficient	0.3	0.35	0.306
Earth IR flux (W/m^2)	227	249	254.3
Primary Pointing Vector	[0.0, 0.0, 1.0]	[0.0, 0.0, 1.0]	[0.0, 0.0, 1.0]
Primary Pointing Direction	ANTI TRUE SUN	ANTI TRUE SUN	NADIR
Secondary Pointing Vector	[0.0, 1.0, 0.0]	[0.0, 1.0, 0.0]	[0.0, 1.0, 0.0]
Secondary Pointing Direction	NORMAL TO ORBIT	NORMAL TO ORBIT	NORMAL TO ORBIT

Table 3.5: Eclipse Timing.

Item	Summer	Winter	LEO
Eclipse Entry (deg)	196.68	238.36	112.99
Eclipse Exit (deg)	327.16	251.76	247.01
Percent time in Eclipse (%)	36.24	3.72	37.23
Percent time Sunlit (%)	63.76	96.28	62.77

Thermal Module

The thermal module is used to generate and control the thermal analyser models. Once ESTAN Workbench has calculated all the radiative coupling between the different faces, the complete thermal analysis can be performed. In this case ESATAN offers us a few fully thermal solvers that can be used to compute the temperatures of each node on the reflector:

- SLCRNC Crank-Nicolson forward-backward transient solver
- SLFRTF Frequency response transfer function solver
- SLFRWD Forward differencing transient solver
- SLFWBK Crank-Nicolson forward-backward transient solver
- SLGEAR Gear-formulation transient solver (matrix)
- SLGRDJ Gear-formulation transient solver (iteration)
- SLMODE All modes modal analysis solution routine
- SOLVFM Full matrix steady state solver
- SOLVIT Iterative steady state solver
- SOLVCG Conjugate gradient steady state solver

Following the ESATAN Thermal User Manual [27] SLCRNC is primarily used to perform the Transient Analyses. This solver is defined by the following equation:

$$\frac{u_i^{n+1}-u_i^n}{\Delta t}=\frac{1}{2}\left[F_i^{n+1}\left(u,x,t,\frac{\partial u}{\partial x},\frac{\partial^2 u}{\partial x^2}\right)+F_i^n\left(u,x,t,\frac{\partial u}{\partial x},\frac{\partial^2 u}{\partial x^2}\right)\right] \qquad \text{(Crank–Nicolson).} \tag{3.15}$$

The choice of the input time step is made by finding the minimum ratio of capacitance to sum of conductances. ESATAN gives this equation by using the CSGMIN function but is also defined using the following equation:

$$\delta_t = min_{allnodes} \frac{C}{\sum G} \tag{3.16}$$

Where δ_t is the time step, C represents thermal capacitance, and G conductance

With the input time step calculated and the solver selected, a cyclic meta solver (SOLCYC) is also used to output a result only once periodic temperature oscillation matches over several periods. This is needed because without the cyclic meta solver, the thermal inertia of the model would cause a general rising slope over several periods of orbits before the total radiated heat from the reflector to space during an orbital period matched the total external received by the reflector over that period. Note that the environment temperature is set to 3K as a rounded up value of the Cosmic Microwave Background Radiation Temperature [30].

3.3.2. ESATAN Thermal Results

This section will show the results of the different cases outlined above and will compare the different results to each other. At first the LEO, Winter, and Summer cases with CFRP coating will be analysed to confirm that the temperature profiles are what can be expected for these kind of orbits. Following this, a comparison of the different coating cases for the LEO orbit is studied to see how coating may affect the temperature profile. The results obtained in this section are important as they will be the input for the thermo-elastic analysis and it is therefore important to make sure they are correct.

LEO Case

In the case of the reflector being in LEO the following temperature profile are obtained and shown in Figure 3.9a. Note that for this orbit, the satellites starts at a right ascension of 0.0° with an orbital inclination of 0.0°. In Figure 3.9d this starting location of the orbit is represented by the reflector intersecting the yellow arrow pointing to the direction of the sun.

At its starting position, the reflector is shown to experience temperatures ranging from 366K to 376K with the mean temperature being 371K. This temperature range is the highest experienced by the reflector in LEO. This is shown by looking at Figure 3.9a where the temperature only tends back up to this temperature range as the reflector completes its orbit to come back to its original position.

During the rest of the orbit, the temperature overall drops and tends to 204K, with a maximum of 206K and a minimum of 202K, before rising back to 371K. This low temperature range is experienced around 3900s, which corresponds to the end of the eclipse phase. During the eclipse, the only heat source impacting the reflector, is the IR heat from the earth impacting the top of the reflector. For simplicity the top of the reflector is defined as the concave side of the reflector. It is for this reason that the temperature quickly tends to a steady state in which the amount on energy impacting the reflector is equal to the amount of energy being dissipated back into space.

Interestingly, two areas of the plot seem to break the overall trend of the temperature during orbit. These regions are the two spikes in temperature at the 1720s and 4245s mark. The first spike in temperature has the mean temperature go from 255K to 264K, while the second spike goes from 204K to 251K and back down to 247K. These spikes in temperature are even more pronounced for the maximum temperatures on the reflector, with the first spike experiencing temperatures drop to 284K up to 298K, while the second spike rises from 206K to 297K back down to 277K. These two regions also correspond closely to the before entry into and after exit of the eclipse. These regions correspond to the moment the top of the reflector catches a glimpse of the Sun and therefore receives some solar heat flux. Looking at Figure 3.9b, one can see the jump in temperature correspond to the same moments there is a spike in the Top QS plot. This can also be visually seen in Figure 3.9d, where when reaching the 100° position, the top of the reflector is heated up and turns red. The main difference between these two spikes is that the change in temperature of the first spike is slower than that of the second spike. This is explained by the fact that the reflector is already warm in the case of the first spike and therefore closer to the steady state temperature of the entry into eclipse case. The reflector is much colder in the second case and therefore the change in temperature is much more faster.

When looking at the overall trend of the temperature, one can see how the drop and rises in temperature are not linear for most of the orbit. When looking at the start of the orbit, the reflector experiences heat flux loading from Top QA, Top QE, and Bottom QS. The bottom QS and Top QA both drop as the reflector orbits into an eclipsed position. In the case of the albedo, the load drops as the amount of sun reflecting of the earth back to the reflector lowers. For the solar heat flux hitting the bottom of the reflector, the pointing angle of the reflector relative to the sun changes during the orbit. Therefore the cross sectional area of solar flux hitting the bottom of the reflector shrinks and tends to zero. This trend in the heat fluxes is mirrored once the reflector exits eclipse.

Figure 3.9c shows the temperature difference on the reflector at an time. In this figure, the largest temperature delta are not found at the spike but actually at the moments of large temperature change as the reflector orbits. The largest temperature delta on the reflector is 92K at around 4704s.

Overall, the temperature profiles on the reflector make sense as they match what is expected from the literature[21]. The range of temperature also matches what is expected for an antenna dish from Meseguer [4] where the temperature range is expected to be 208K to 368K. The resulting temperature for the LEO case only differ by a difference of 8K.

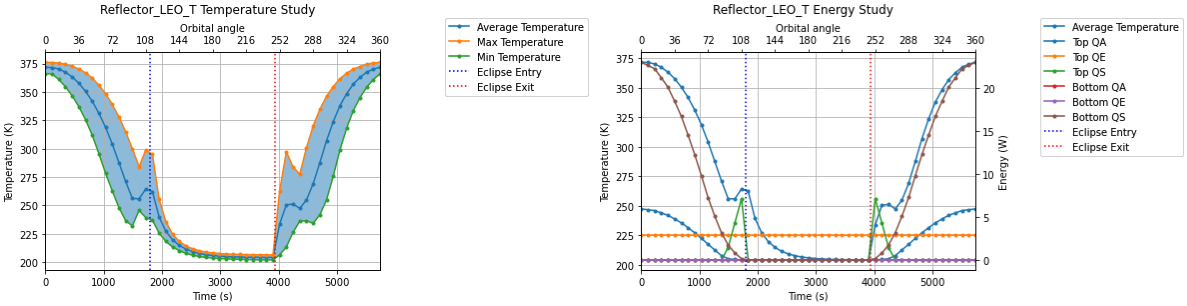

(a) LEO Temperature Profile

(b) LEO Heat Profile

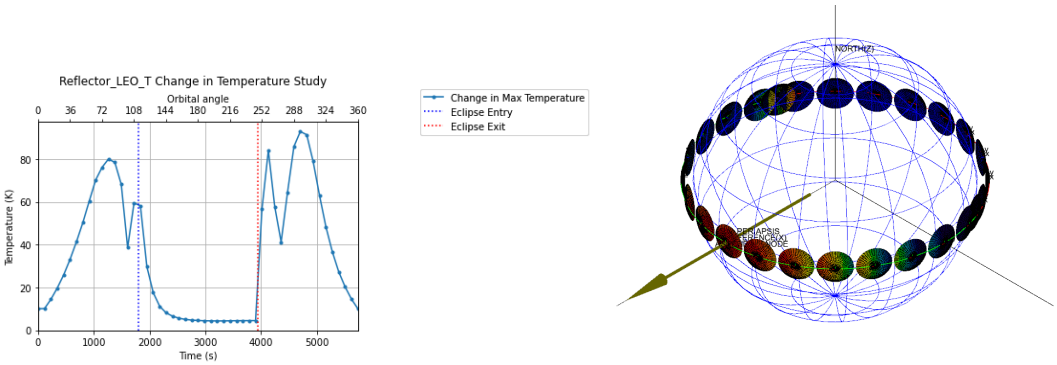

(c) LEO Temperature Delta Profile

(d) LEO Orbit

Figure 3.9: LEO Case

Summer Case

In the case of the reflector being in Summer the following temperature profile are obtained and shown in Figure 3.10a. It is important to remember that the contrary to the LEO case where the reflector always pointed to the Earth, the Summer case has a reflector always pointing away from the Sun.

At its starting position, the reflector is shown to experience temperatures ranging from 338K to 345K with the mean temperature being 341K. During the rest of the orbit, the temperature slightly rises up to form a sort of bump, before exponentially dropping during the eclipse. During the bump, the temperature across the reflector has a maximum of 362K and a minimum of 351K. Figure 3.10c also shows how the difference in

temperature across the reflector grows during this bump. Looking at Figure 3.10b, the slight rise in temperature is explained by the slight rise in the albedo and IR energy (Top QA and Top QE) received by the reflector. This coincides with the moment the top of the reflector comes into view of the Earth.

One can also see that when entering and exiting the eclipse, the spikes observed in the LEO case are not present. This is explained due to the pointing of the reflector being ANTI TRUE SUN and therefore always pointing away from the sun. Due to this, the spike in temperature due to the reflector suddenly catching a glimpse of the sun does not happen. In addition the cross sectional area of the reflector with regards to the sun is always the same, and seeing that the solar flux is by far the largest input of heat, the temperature on the reflector is mostly driven by the solar flux. This is seen by the step function characteristic of the temperature, which follows the step function characteristic of the solar flux hitting the bottom of the reflector (Bottom QS).

Lastly, one can see that the drop in temperature during eclipse first stabilises around 178K before finally dropping to a mean of 170K. This is actually driven by the slight rise of the earth IR flux (Bottom QE) hitting the bottom of the reflector. Looking at Figure 3.10b, one can see how to final dip in temperature happens when the Bottom QE starts dipping. At this moment the maximum temperature is 178K and the minimum temperature is 163K. Looking at Figure 3.10c, one can see that the maximum delta of 14K across the reflector, can also be found at this low temperature case.

Overall, the temperature profile for the summer orbit is more stable and behaves more like a step function of hot and cold cases. This is much more different than the LEO orbit which had a more curved temperature profile with two spikes of rapid temperature change.

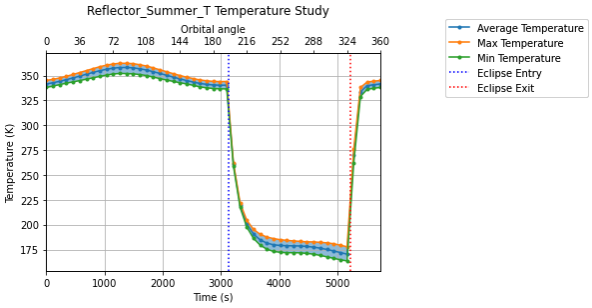

(a) Summer Temperature Profile

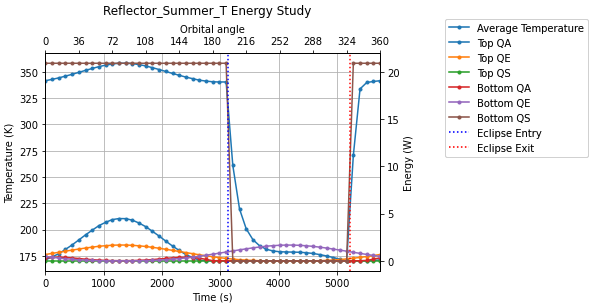

(b) Summer Heat Profile

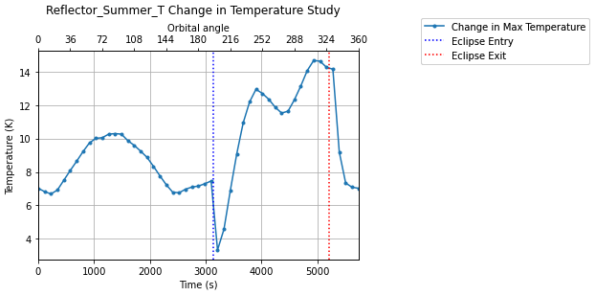

(c) Summer Temperature Delta Profile

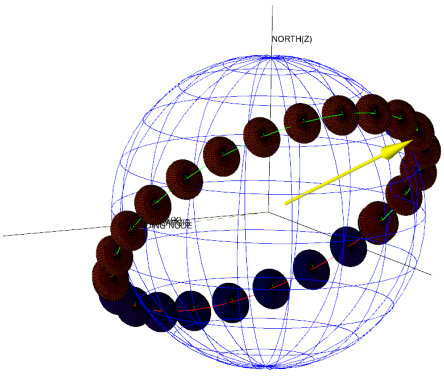

(d) Summer Orbit

Figure 3.10: Summer Case

Winter Case

In the case of the reflector being in Winter the following temperature profile are obtained and shown in Figure 3.11a. It is important to remember that the contrary to the LEO case where the reflector always pointed to the Earth, the Winter case has a reflector always pointing away from the Sun.

At its starting position, the reflector is shown to experience temperatures ranging from 348K to 355K with the mean temperature being 352K. During the rest of the orbit, the temperature slightly rises up to form a sort of bump, similarly to the Summer case. The temperature then experiences a rapid drop before rising back to its original temperature range. During the bump, the temperature across the reflector has a maximum of 356K and a minimum of 352K. At the drop, the reflector temperature drops to 227K. Looking at Figure 3.11c, the largest delta on the reflector is 9.5K and can be found at 4130s.

Similarly to the Summer case, the reflector does not experience any spike at the entry and exit of the eclipse. One can see that due to the very short eclipse of 3.72% of the orbit, the temperature drop is very short and does not have time to reach a similarly low temperature as in the Summer case.

Overall, the temperature profile for the Winter orbit resembles that of the Summer orbit in the fact that they have the same bumps at the start of the orbit and then tend to a lower temperature without any spikes. The main difference is caused by the length of the eclipse allowing for the temperature drop to last longer in the Summer case compared to the Winter case.

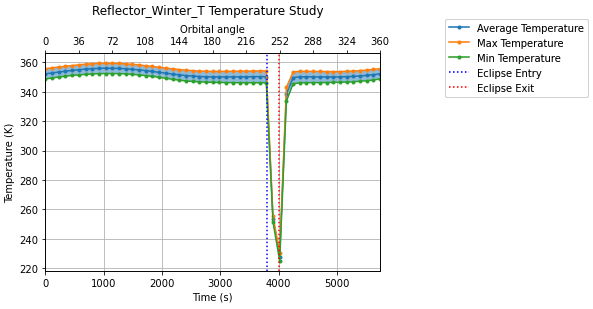

(a) Winter Temperature Profile

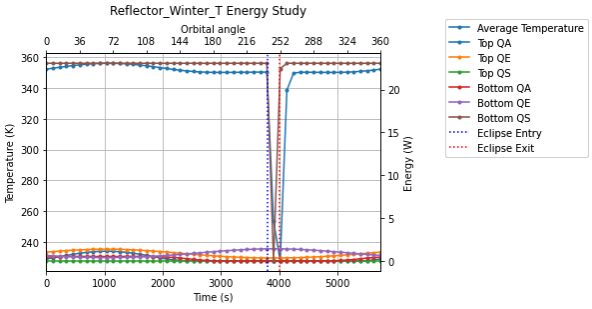

(b) Winter Heat Profile

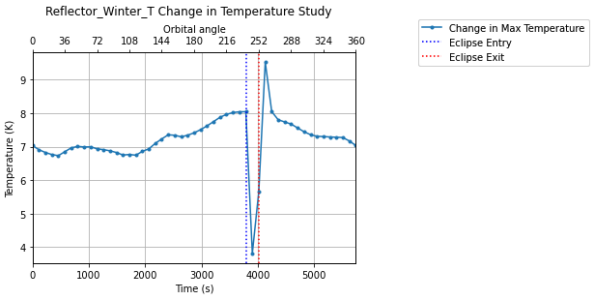

(c) Winter Temperature Delta Profile

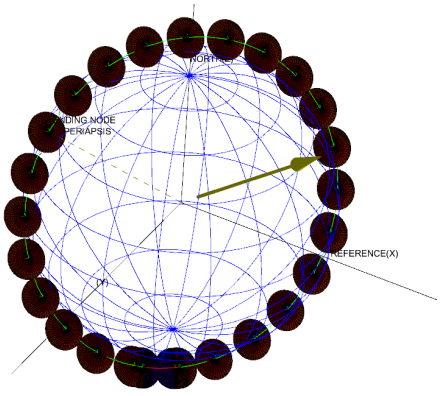

(d) Winter Orbit

Figure 3.11: Winter Case

Coating effect

As thermal control method used for many reflectors, coatings are often used to try and control how much heat is absorbed and emitted from the reflector. Figure 3.12 shows the three different cases of coating similar to the analysis performed in Park's analysis of a petal reflector. In this figure the temperature ranges are described, with the edges of the bands describing the min and max temperatures on the reflector.

Table 3.6: Optical Cases

	CFRP Case (α/ϵ)	SiO_2 Case (α/ϵ)	White Paint Case (α/ϵ)
Reflector Top	CFRP (0.92/0.8)	SiO_2 (0.14/0.12)	SiO_2 (0.14/0.12)
Reflector Bottom	CFRP (0.92/0.8)	SiO_2 (0.14/0.12)	White Paint (0.2/0.9)

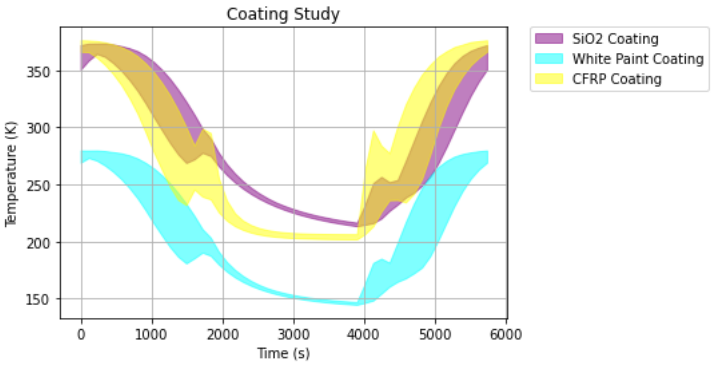

Figure 3.12: Coating Study

The CFRP coating offers a high emissivity and absorptivity which makes the reflector very reactive to changes in the heat flux. It is for this reason that the CFRP coated reflector temperature quickly tends to a steady state temperature when the eclipse starts. The Silicon Dioxide coating, has the opposite, with a low emissivity and absorptivity. This is why the profile seems to take more time to react to temperature changes. The reason the range of temperatures is similar to the CFRP coated reflector can be explained because of the ratio of emissivity and absorptivity which are similar. This shows that both of these cases have the same capacity of absorption to emission but differ in the time it takes for the temperatures to reach steady states.

When adding white paint to the back of the second case, the emissivity is very high with a low absorptivity. Here the reflector is able to emit more energy out compared to the Silicon Dioxide case. It is for this reason that the range of temperature is lower than the Silicon Dioxide case. As much as it is favourable to have lower temperatures for the reflector as one could expect less material expansion and therefore less displacement, white paint coating adds a heavy layer to reflectors. Because of this, the white paint is not favourable for deployable reflectors like the SDA. The Silicon Dioxide coating does show a better promise as it take more time to react. In the case of the Winter orbit, the reflector would not have the time to drop in temperature so much. What it also shows is that the delta in temperature is slightly smaller overall than the CFRP coating.

Looking at the different orbital cases it is clear that the Summer and Winter orbits are favourable due the smaller delta in temperature. These orbital cases describe the mission selected by Park and therefore do describe a realistic orbit. The only problem with this, is that Park is already using a thermal control method of having the reflector always point away from the sun. This is an acceptable case for the situation where the reflector is only needed for a short time but in the case where the reflector needs to be used consistently, the LEO case depicts a more diverse temperature profile which would allow for a better overall analysis of the reflector. It is for this reason that the LEO case will be used as the base model for further analysis. This does not mean that the Summer and Winter cases are omitted as they are in their own way important to be

studied. When looking at the worst case for all these scenarios, we can expect the results to be similar as the displacements will react to the extreme temperatures and all three case share similar limits.

The temperature profile for the LEO case has been verified by the literature in both Xeng[21] and Mesenguer[4]. By understand what happens in this case, the Summer and Winter case are also verified with the backing up of Park[8]. Lastly, the conclusion of the coating study are similar to those in Park and help in showing that the model being used is giving good results. With this combination of literature and study of results, the data obtained is deemed to be a good input to use for study of the effect of the thermal environment on the SDA.

3.4. Abaqus Thermal

ESATAN results match what can be expected from literature as shown in [21][8] and additionally the results make sense when compared with the heat flux's being absorbed by the reflector and compared with the times it enters and exits eclipse. The next step in the thermal analysis of the SDA is to correctly transfer the results to ABAQUS. As previously mentioned in the plan, ABAQUS will consist of 2 designs: a normal parabolic reflector, and a parabolic reflector with the spiral included.

3.4.1. Automation

Initially, the transfer of data from ESATAN to Abaqus is done by hand. This is still at the stage where the meshing in ESATAN is not very detailed. To be able to do this, ThermXL (another program offered in the ESATAN suite) had to be use to extract the data from ESATAN to be sent to an Excel sheet. As the meshing grew smaller a decision is made to start automating the process (see Figure3.13). Abaqus offers a scripting library in Python which allows for the modelling of the Abaqus model to be fully scripted. The advantages of having the Abaqus models scripted are :

- Allow for more data to be transferred between ESATAN and ABAQUS consistently without human interaction.
- Test out different methods of transferring data between ESATAN and ABAQUS.
- Iterate different building methods for the reflector.
- Facilitate Troubleshooting.
- Facilitate running and keeping track of different Cases
- Remove human error.

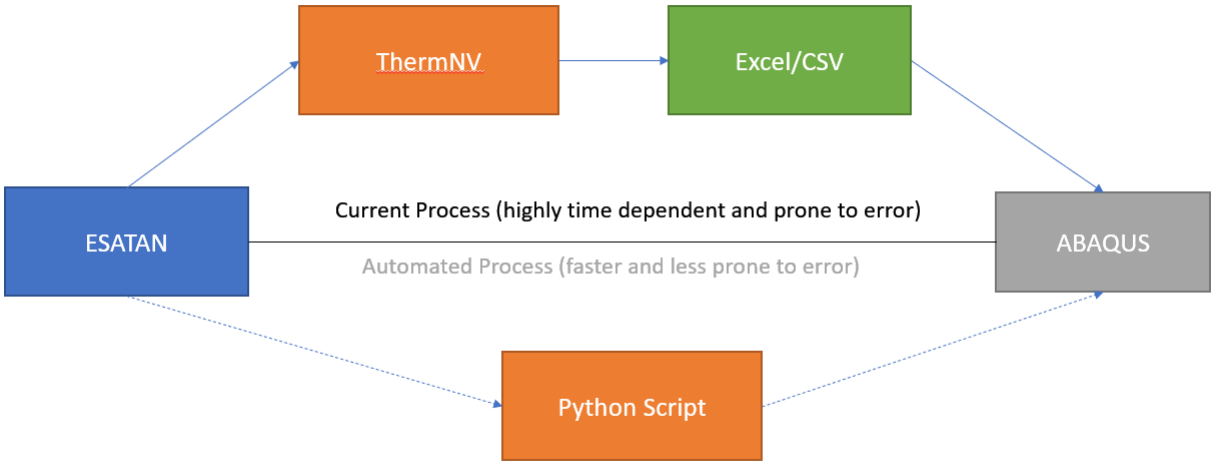

Figure 3.13: Automation Overview

3.4.2. Reflector Model Definition

Unlike ESATAN, Abaqus does not offer a paraboloid tool to construct the reflector. To be able to design a paraboloid, a half parabolic spline has to be created and then rotated around a central axis. It is important to make sure that the parabolic curve matches that of the paraboloid in ESATAN. Using Equation of a parabola, a number of points can be created to define the path of the spline. By placing more points to guide the spline, the better the resolution of the spline and therefore the more it will match the reflector defined in ESATAN. This process is automated using the `Create_Reflector_Sketch` function the python Script [10].

Once the sketch of the half parabola is created, a 3 dimensional part is defined the parabolic sketch is revolved as a shell. A shell is used over a solid due to the thin nature of the reflector sheet. The part is then

assigned a section which assigns properties to the part. For the shell, there are 5 different options: Homogeneous shell sections, Composite shell sections, Membrane sections, Surface sections, General shell stiffness sections. To have bending stiffness and did not over complicate the model definition, the homogeneous shell section is used with generalized material properties when feasible. During the creation of the shell, the thickness of 0.4 millimetres can be assigned.

At this stage, the geometry of the reflector is created but loads can't be applied yet. As previously mentioned, when thinking of how to transfer the ESATAN results to ABAQUS, two choices are offered: temperature and heat fluxes. Due to limitations in the Abaqus model definition option, heat transfer is selected as the method for transferring data. This is done by first having ESATAN output the 6 different heat loads into CSV files. This is done by controlling the output calls by inserting the following line for each different heat load.

```
CALL PRNCSV(' ', 'QS', Top, 'NODE', 'Top_QS.csv')
```

This line of code simply tells ESATAN to print the solar heat energy absorbed (QS) for the Top of the reflector, for each Node into a CSV file called "`Top_QS.csv`". The heat for the top and bottom can then be added together and can be input as an amplitude. This means that for an ESATAN reflector with 400 Nodes, 800 amplitudes define the top and bottom heat loads. These loads can be input into Abaqus as surface fluxes loads. These loads are input into Abaqus using python due to the high number of amplitudes. These are done using numpy genfromtxt() functions which read the CSV files and made 2 dimensional numpy arrays from them. This is shown in the "Get Data From CSV File" section of the code [10].At the end of the section, the different heat loads (solar, albedo, and infra-red) are added together to have the top and bottom total heat loads.

To be able to input these loads onto the Abaqus model, a partition has to be created to match the mesh of the ESATAN model. To be able to do this a new sketch has to be created on which a similar web pattern is created and then projected onto the part. It is very important to make sure the 2 web patterns match by checking a few points on each different model and make sure they are at the same place relative to their local coordinate system (See function `Create_Partition`). With this web pattern projected on the part, the 800 different heat amplitudes can be assigned to their respective surfaces. As shown in Figure 3.14 ESATAN numbers its node starting on the right of the center and going counter clockwise while alternating between the top and the bottom of the reflector. The first step to make the amplitude to surface assignment correct is to have split the top and bottom heat loads output. This allows to only have to assign loads to one side of the reflector at a time. The second step is to have Abaqus give a list of all the face objects in the model with a coordinate point corresponding to these faces. These points are then sorted using the `surf_sort` function which output a list of the points in the same order as the ESATAN meshing. These points are then used to get a list of the faces in the same order as the ESATAN meshing which can then be assigned a load and a corresponding amplitude.

To start resembling the SDA, a circular cut is extruded out of the base of the reflector to represent the section of the SDA from which it will deploy. This is simply done using the `Create_Center_Cut` function. As much as this section is not necessarily needed for the reflector model and is more important for the SDA model, it is added to better compare the 2 different models without having to worry about the impact of the center cut. Because of this, the surface loads must be defined a little differently. At this stage the surface loads are defined as the total Energy for each surface. To remedy this, the surface areas from ESATAN are output in a similar way as for the `Top_QS` and the heat load are divided by the surface areas to give the heat flux for each surface. This is performed at the previously mentioned assigning of the loads and amplitude section of the code [10]. This means that no matter the geometry inside the web mesh, the surface loads will correspond to the same as ESATAN.

3.4.3. SDA Model Definition

A normal reflector model has been created and can be used to create an SDA model. For the SDA, two approaches are taken: creating a split part separating at the zipper location, or creating a resistance model where a partition will be defined as the zipper. The first method is attempted where the reflector is split by taking a strip in the shape of a spiral off of the reflector. The opposite is then performed to just have the spiral strip of material. The two different parts are then added to the same assembly and one edge of the spiral band is tied down to the reflector section. The issue with this method arose with the connection between the edge

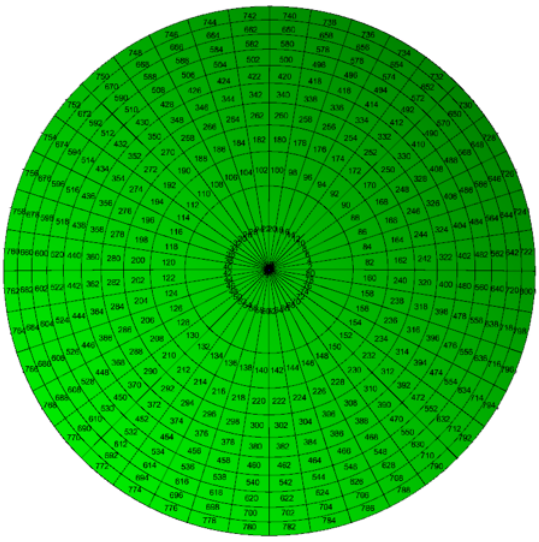

Figure 3.14: ESATAN Node Numbering Scheme

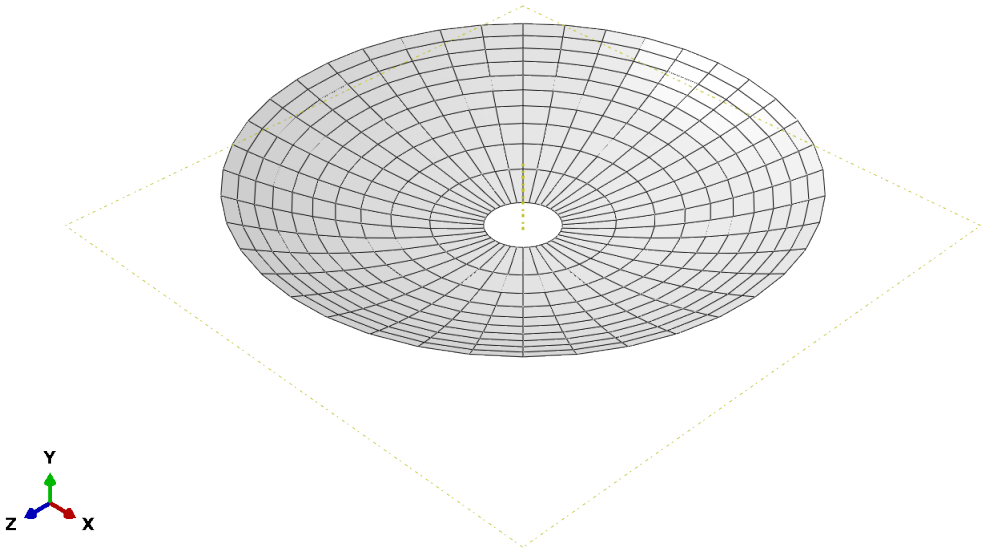

Figure 3.15: ABAQUS Reflector Model

of the untied down section of the spiral part and the reflector part. There is no method to properly connect the zipper edges and have it stay connected and behave as a zipper. For this reason a second method is used. In this method a spiral strip is also created but it is used to partition the reflector. By partitioning the surface with a spiral, it allows for the surface to be defined with another material. This means that structurally the model is seen as one part but the change in material will affect the reflector just as the presence of a zipper would. This does mean that the model is exactly reflecting a zipper but more like evaluating the effects of a spiral shaped mechanisms on the reflector.

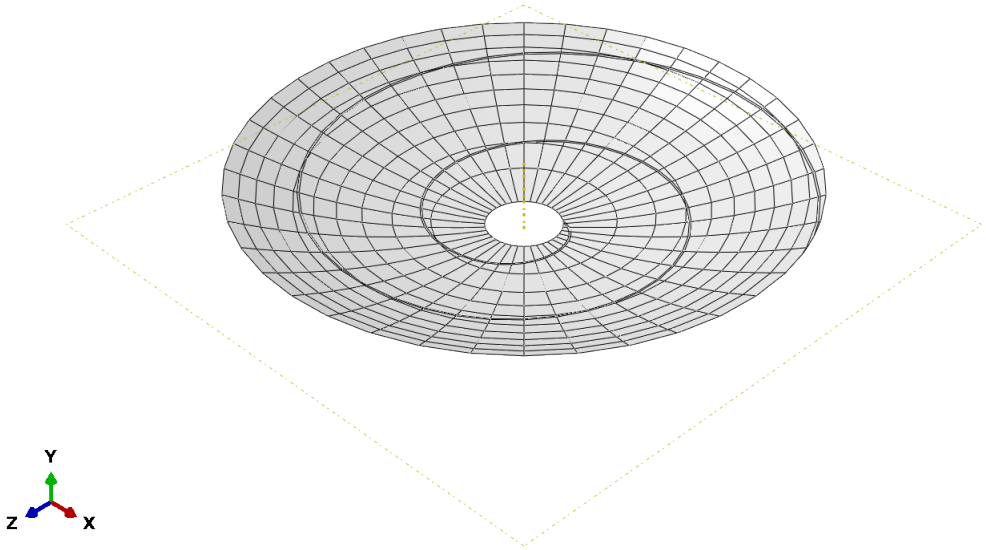

Figure 3.16: ABAQUS SDA Model

Adding the spiral partition is done using the `Create_Spiral_Partition` function in the SDA python script [10]. The reason the reflector script and SDA script are separate, even though they share a lot of similarities, is to allow for the models to be ran separately. Even thought the spiral partition is the simplest way of simulating the SDA, it create its own problems. The previously mentioned `surf_sort` is actually extended because of the addition of the spiral. With the spiral partition and the web partition, there are now many more faces to match with than the ESATAN model has. It is for this reason that the `surf_sort` actually outputs the IDs of all the faces corresponding to an ESATAN surface while also making sure it is in the correct order. This allows for the proper assignment of amplitudes and loads to the correct surfaces. The next complication arose with the selection of the surfaces within the spiral. It is possible to have ABAQUS give a list of all the edges created by the projection of the spiral onto the reflector but there is no easy way to have ABAQUS return all the faces in between those edges. To be able to find these specific surfaces, the `Find_Spiral_Surfaces` function is used to cycled through all the faces on the reflector and stored all the faces that are in contact with two spiral edges. The function then gathered all the edges on the selected faces and recycled through all the reflector faces taking into account the new edges. This function seems to be able to successfully find the spiral faces when the web meshing is not too big. It is important to note for anyone using this model to double check that the reflector is correctly selecting all the spiral faces.

Material and Coating

The assigning of the materials is done in the same way for the reflector and the SDA models. The only difference is that the SDA assigns a different material for the section corresponding to the spiral. To be able to properly perform the thermal analysis, the density, specific heat capacity, and conductivity of the material need to be defined. For the analysis, CFRP (M55J) is used for the reflector sheet of both the reflector and the SDA. For the SDA, the Zipper will be made using a simple Aluminum 6063-T6. For the coating of the reflector and the SDA, the same coating is used for the entirety of the top or the bottom. It is important to note though

that the absorptivity of a Coating must be changed in ESATAN as the the heat loads are calculated with the absorptivity in mind.

Radiation

For both of the ABAQUS models, radiation has to be considered. Unlike ESATAN which automatically has its model radiate energy out into space, this feature needs to be specifically implemented in ABAQUS. This is done in 2 different ways: using the cavity radiation tool and the surface radiation tool. The optimal set-up for the model is to set the cavity radiation to the top of the reflector and make sure to set "to ambient" to allow for the model to radiate to itself but also to an outside point. It is also important to make sure the no blocking option is selected to improve analysis time. This is feasible for simple meshed parts but grows more complicated for complex meshed surfaces as there is a software limit of 16000 nodes. In case of the model having more than 16000 the backup is to define the top surface as only having surface radiation to ambient. The difference between the 2 will be compared to make sure the assumption does not fundamentally change the results. For both surface radiation and cavity radiation the emissivity of the selected coating and the ambient temperature need to be given. The outside point defined in the surface radiation tool acts as space and therefore also need to be given a ambient temperature. In this case 3 K is used, similarly to the way it is used for ESATAN.

Step

For the thermal analysis of both the reflector and the SDA, there is only one heat transfer analysis offered within Abaqus. For the purpose of the analysis of the SDA and the Reflector, this step is defined as a transient analysis with the same time period as an orbital period. Abaqus utilizes the backward Euler method to solve the system of ODEs describing the models. The backward Euler method is described by the following equation:

$$\frac{u_i^{n+1} - u_i^n}{\Delta t} = F_i^{n+1}\left(u, x, t, \frac{\partial u}{\partial x}, \frac{\partial^2 u}{\partial x^2}\right) \qquad \text{(backward Euler)}, \tag{3.17}$$

Mesh

For the heat transfer step, DS4 and DS3 elements are used. These elements are suitable for both the Reflector and the SDA models. The meshing of the Reflector model is not complicated due to symmetry in the model which allowed for well formed elements across the entire reflector. Figure 3.17 shows the meshing created by setting the reflector to quad dominated with a general seed size of 0.1. The reflector mesh shows no sign of distorted elements and the verify mesh tool highlights no error or warning from the mesh.

When meshing for the SDA, things are more complicated. As shown in Figure 3.18, the mesh for the SDA is not as organized as the Reflector model and gives way to regions where the mesh is chaotic. Due to the thermal test being performed as a precursor to a stress test and due to the presence of the spiral zipper, a finer mesh is used to catch the intricacies of the effect of the zipper on the overall thermal and stress analysis.

To try and provide more flexibility in the way meshing is done, the edges on the reflector are splits into 3 different sets. The first set are the edges comprising the sides of the zipper region. The second set consisted of the edges inside of the zipper region. The last set consisted of all the other edges on the reflector, which consisted of all the edges in the reflector sheet region without the edges that are part of the zipper. Even though this gives more precision in the way the edges are seeded, a problem caused by the overlapping nature of the web partition and the zipper partition arose.

As shown in Figure 3.20 the spiral zipper, in its nature, breaks any symmetry in the reflector due to the fact that it spirals around the reflector. As shown from Figure 3.17, meshing with the reflector being partitioned with the web partition causes a mesh that propagates outwards from the center of the reflector. It shows the elements growing bigger gradually as one radially moves out from the center but it also shows that Abaqus looks to keep the same number of elements angularly. This shows how the partition guides the meshing process. When adding the zipper region, the zipper partition interferes with the mesh generators ability to keep the same number of elements angularly with a slightly growing element radially. As the zipper spirals around the reflector, the edges of the zipper region intersect the web partition edges and cause many smaller edges

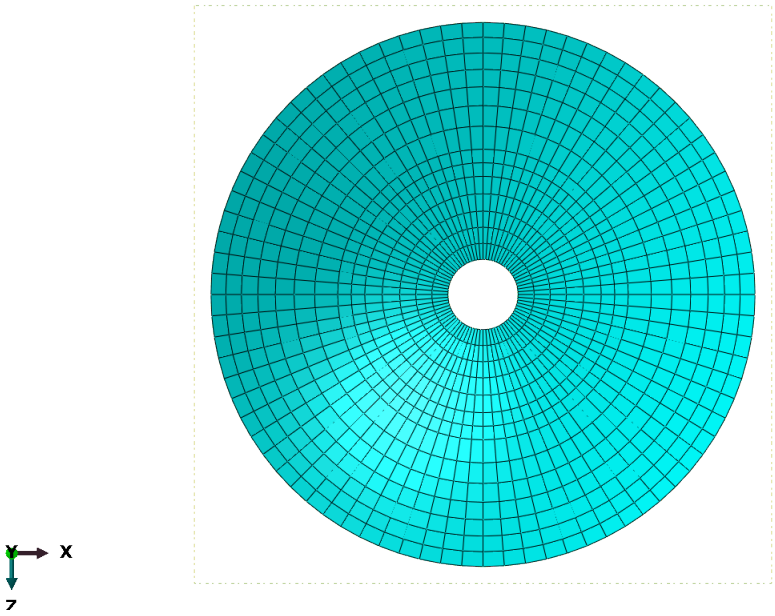

Figure 3.17: Reflector Mesh

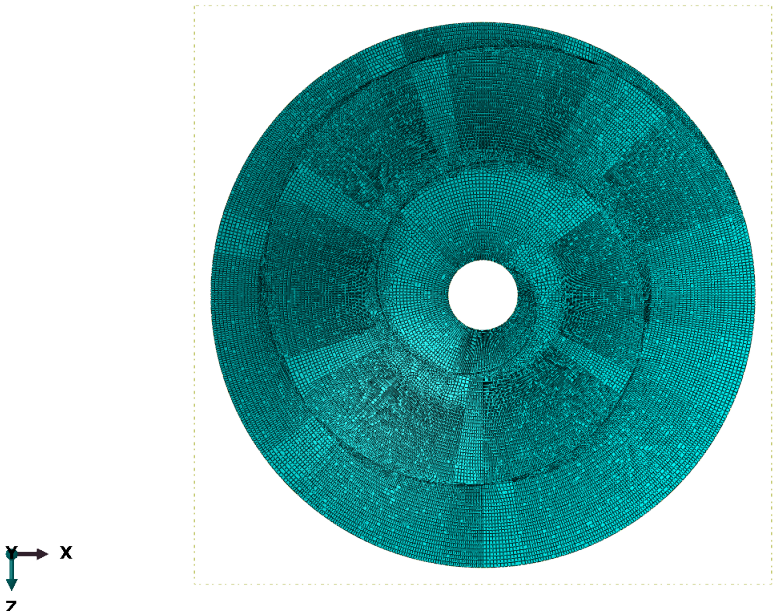

Figure 3.18: SDA Mesh

of different sizes at different angles to be created. As much as the Abaqus mesh generators can often deal with that for simpler sections of the reflector, sections as shown in Figure 3.20 lead to long thin triangular faces. As shown in Figure 3.19, these sections where the zipper intersect a radial and angular branch of the web at the same time, causes aspect ratio distortions [31], while the elements in the zipper experience parallelogram and angular distortions [31].

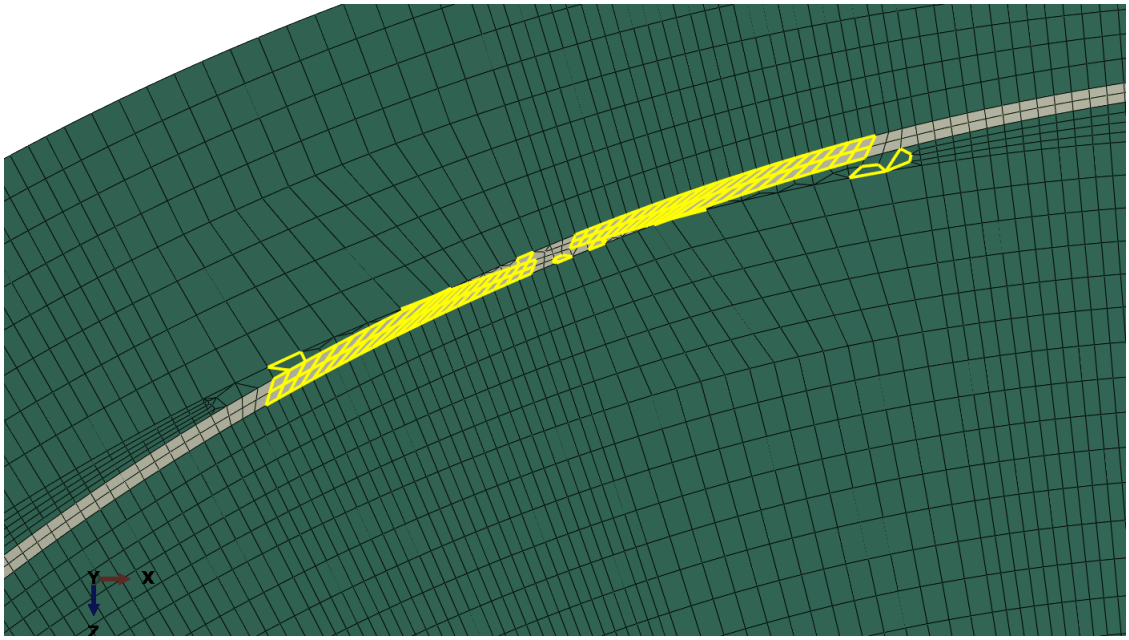

Figure 3.19: SDA Mesh Problems

In an attempt to minimize the number of distorted edges, a meshing study is performed. Table A.1, in the appendix, shows a few of the different attempts that are made to try and reduce the impact of distorted elements. One can see that the more elements are added, the overall percentage of warnings grew smaller. This made sense as the elements could be small enough to better fill the triangular regions previously mentioned. The main disadvantage of adding more elements is that the analysis time grows larger. Not only is the mesh sized changed but different approaches to meshing are created to try and favourably improve the mesh. Abaqus generates its own mesh patterns following seeding and region definitions. The default method is to just seed all edges with a general size and have Abaqus connect these seed point with elements of approximately the same size while trying to keep the elements in a certain shape.

It is important to note that ABAQUS makes a difference between a warning and an error when verifying the mesh. An error means the element will cause the analysis to terminate prematurely. A warning means the elements may cause questionable results and are outside the defined element shape parameters. As much as a warning signals a problem with the mesh it will still be able to complete the analysis.

Another approach to solving the meshing problems is to mesh different regions in different orders. The first order involved meshing the band first and then meshing the zipper. The second order is to do the opposite and mesh the zipper first and then the band. The third order is to mesh from the smallest region to the largest. The forth and last order, involved manually selecting the problem areas and meshing each separately before meshing the entire reflector. Of the four methods, the three first are included in the automation process and are tested with different parameters to see if a favourable mesh could be found. The last method could not be automated as there no way of parametrically selecting the problem areas. Because of this, this method is only tested once with a tight mesh but did not seem to improve overall mesh.

When looking back at Table A.1 the mesh that ended up having the lowest amount of warnings, not too many elements, and better elements, ended up being an automated meshing with the band edges seeded to

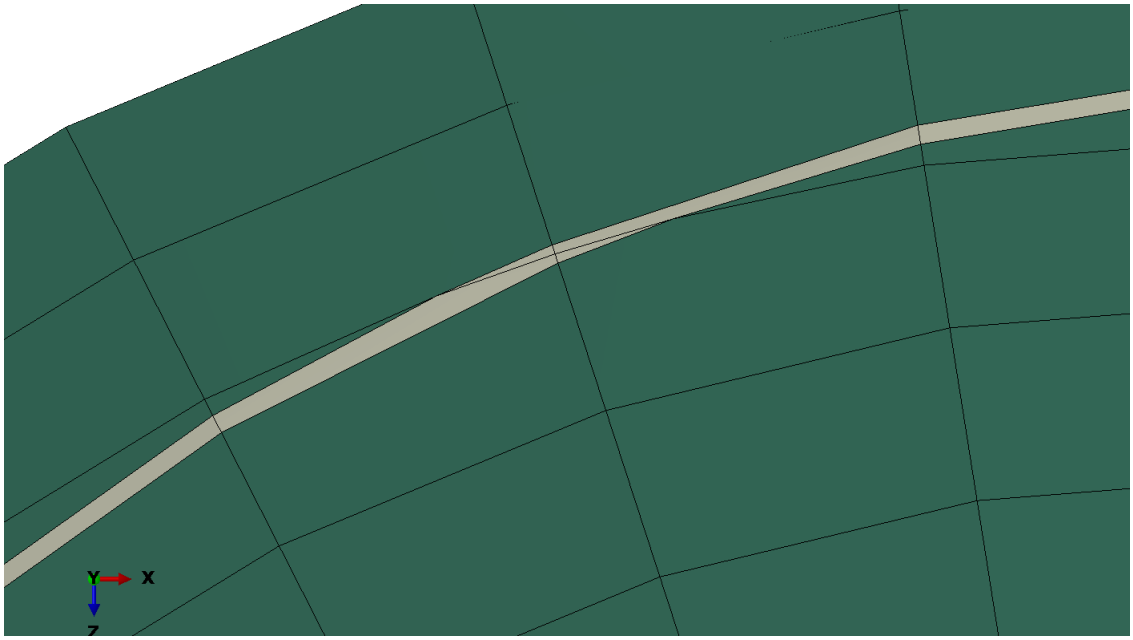

Figure 3.20: SDA Mesh Problems Partition

0.02, the zipper edges to 0.01 and the interior zipper edges to 0.005. This is selected as the best mesh for the analysis while keeping in mind that distortions may be caused by the faulty elements.

3.4.4. Abaqus Thermal Results

Looking at the Abaqus thermal results needs to be done in three different phases. The first phases, consists in comparing the results between ESATAN and Abaqus. This is a verification that the transfer of the ESATAN results is properly done and that the thermal analysis in Abaqus gives the same results. The second phase consists of comparing the Reflector and SDA CFRP model. This helps in confirming that the different meshing does not seriously impact the thermal analysis and that the base SDA model can be analysed. The last phase is the analysis of the base SDA model to see how the spiral affects the temperature map of the reflector compared to a normal reflector.

Data Transfer Validation

General Overview

Due to the chaining of software, it is important to make sure that the thermal result from ESATAN are not distorted when transferred to the Abaqus models. One must remember that ESATAN allows for a thermal analysis in orbit resulting in heat fluxes that are functions of the orbital position. These heat fluxes then allow for the calculation of temperatures on the reflector in ESATAN. The data being transferred from ESATAN to Abaqus corresponds to the heat fluxes and not the temperatures. The temperature field, in Abaqus, is calculated using a different solver and different approach than ESATAN, so it is important that the temperature fields are compared.

The first approach to comparing temperature fields between ESATAN and ABAQUS is to look at the minimum, mean, and maximum temperatures the reflector experiences. Figure 3.21a shows an overlay of the minimum, mean, and maximum temperatures of the ESATAN, Abaqus Reflector, and Abaqus SDA models. Looking at the LEO case, it is clear that the temperature extremes and mean match and that the temperature ranges are proberly propagating from the ESATAN data into Abaqus. By having nearly perfect overlapping results, one can say that the method of transferring the heat fluxes overall gives similar temperature profiles and temperature extremes.

Even though Figure 3.21a shows similar profiles, there are mainly 2 areas that differ. The first difference is at the start of the profile which shows a quick rise for both ABAQUS models. This is actually to be expected

as the ABAQUS models use a fixed initial temperature value of 350 K. Without this initial temperature there would see a sharp rise from 0 to 370 K. This anomaly could be fixed by just having ABAQUS calculated the mean temperature of the reflector or have ESATAN output the mean values of the reflector. This way the ABAQUS python script could auto set an initial temperature. Due to timing this is not implemented.

The second region is found at eclipse, when the temperature drops and then tends towards a cold steady state. What can be seen is that the trend in temperature is slightly off between the ESATAN and Abaqus results. In the LEO case, this slight difference is seen between 2000 and 3000s. This is mostly explained due to the difference in solver used between ESATAN and Abaqus. Even though this difference is present, it is only minor and deemed to not really impact the overall result of the LEO case. This difference is similarly seen in the Summer case and deemed to not highly impact the results. This can be seen in Figure 3.21b which depicts the minimum, mean, and maximum temperature for the Summer Case. Lastly, Figure 3.21c shows the same data for the Winter case. In this case the difference in temperature is higher at the time of eclipse, with the ESATAN trending down much faster than the Abaqus models. The difference in the mean temperature at 4000s is up to 70K. Several attempts were made to minimize this difference int he the trend of temperature but no solution was found. This discrepancy in the results seems to point it a difficulty for ESATAN to give the proper temperature when dealing with very fact changes in the loading cases. Overall, this problem for the Winter case was noted but deemed not enough of a problem to continue with this method of transferring thermal data between ESATAN and Abaqus. The main reason for this is that the most extreme case of expansion of the SDA, which will theoretically correspond to the moment of poorest performance of the reflector, will happen at the highest temperature. At that moment, the temperature profiles for the winter case, of all three models, overlap.

Three Dimensional Overview

As useful as it is to judge the transfer by looking at the maximum, minimum, and average temperatures, the models being studied are three dimensional. This means that to be able to properly judge the transfer of data between ESATAN and Abaqus, one needs to compare the reflector temperature fields three dimensionally. Figure 3.22 and Figure 3.23 show a comparison of the Abaqus Reflector model and the ESATAN model for the LEO case.

As previously mentioned, the LEO case is used as a base, as the temperature delta across the reflector is higher and therefore help to show the details of the change in temperature across the reflector. Not only is it a stress case for the analysis of the reflector, but it also allows to point to any problems in the analysis process. In Figure 3.22 and Figure 3.23, the ESATAN model is shown on the right, while the Abaqus Reflector model is shown on the left. The figures depict the change in the temperature field at 229.5, 803.1, 1606.0, 2180.0, 3786.0, 4704.0, and 5737.0. These time are chosen as they represent the different points of interest in the temperature of the profile. The first and last time steps both represent the start and end of the orbit. The second time step of 803.1, represents the moment of large temperature drop from hot to cold. The time steps of 1606.1 and 4704.4, represent the two spikes in temperature. The last two time steps of 2180.0 and 3786.0 represent the moment where the temperature is sloping to the cold case and the cold case itself.

It is important to mention the difference in the three dimensional description of the two models. As mentioned in the model description section, the ESATAN model uses the lumped capacitance approach, which means that each square represents a an isothermal node. This means that there is no interpolation process being made between each square. Abaqus on the other hand has its nodes at the intersection of the different lines and makes complex interpolation calculations to create isothermal lines across the reflector. It is for this reason that the ESATAN model has a jagged temeprature map, while the Abaqus model has smoother temperature patterns. It is also important to point out that the scaling of the temperature for both models changes througout Figure 3.22 and Figure 3.23. For a view of the Reflector model temperature field over time with a constant scaling, an animation can be found here[1].

Keeping in mind the discretization process, it is clear that the temperature fields between the two models are very similar. Throughout the orbit the temperature field has similar strength at similar locations of the reflector and shift in the same direction as the reflector orbits. The difference in temperature between the two

[1] https://imgur.com/a/hvC145j

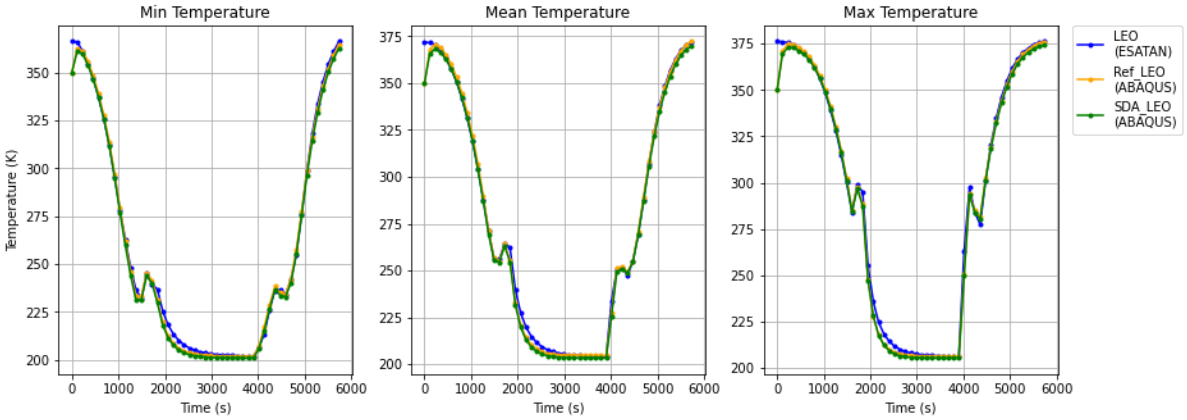

(a) LEO Orbit

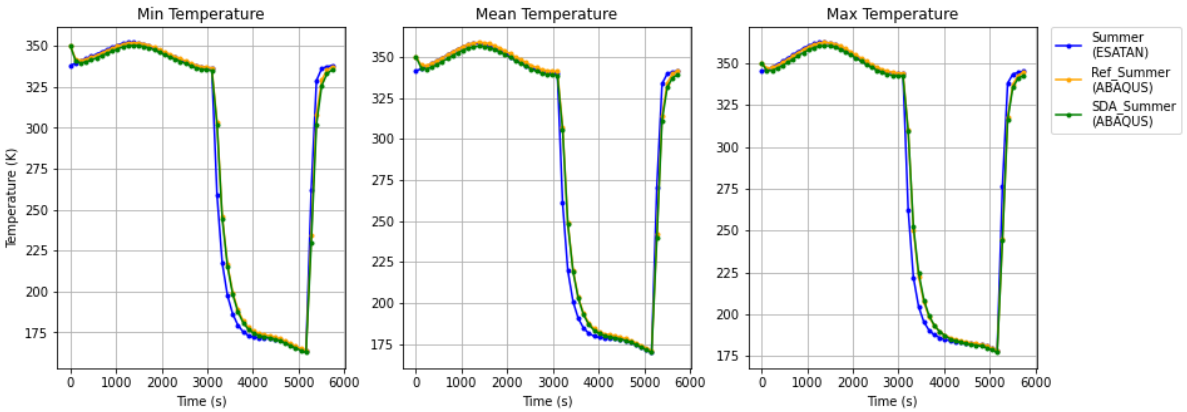

(b) Summer Orbit

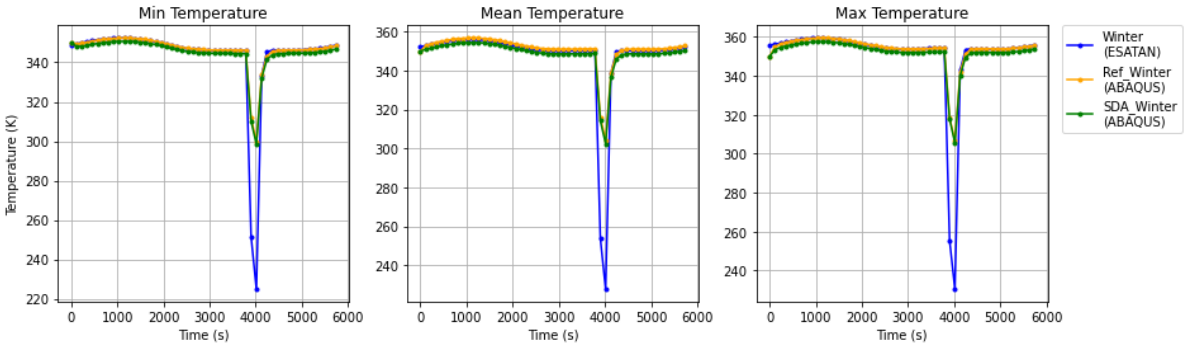

(c) Winter Orbit

Figure 3.21: Temperature Study between different software

reflectors is never more than 7K. Interestingly, when recalling Figure 3.9d, the temperature pattern reflects it's position in orbit. With the solar flux being the largest source of heat, it makes sense that as the reflector starts on the line connecting the earth and the sun, the highest temperature on the reflector should be located in the center of the reflector as the solar flux is incident to the back of the reflector. As the reflector orbit counter clockwise, the hot spot representing the solar flux shits to the right. As the reflector makes it to the eclipse, the overall temperature drop and a new hot spot, representing the IR heat flux comes from the left and shifts towards the center. As the reflector leaves the eclipse the IR heat flux moves to the right and the solar heat flux appears back from the left. With these results, one can conclude that the Abaqus results properly reflect the ESATAN results and that from a three dimensional aspect, the method of transfer of data is appropriate.

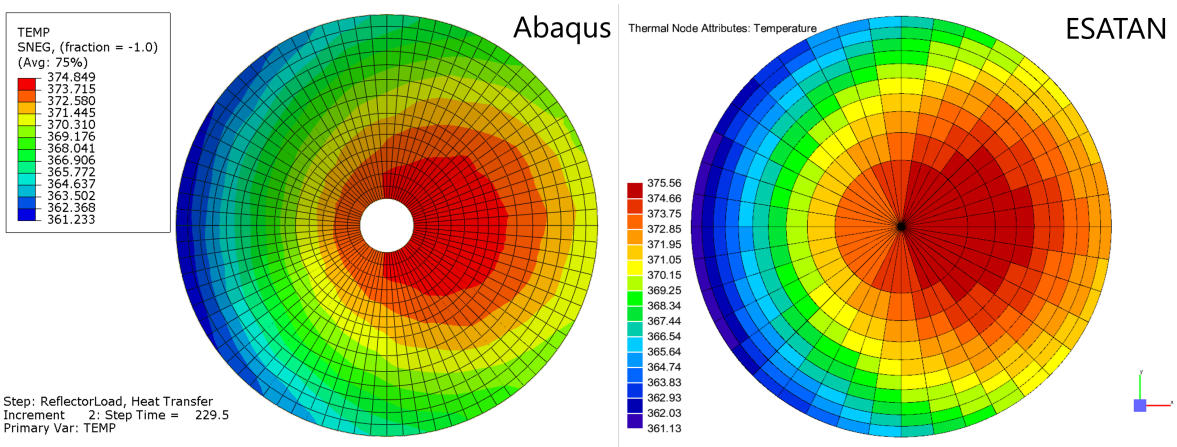

(a) t = 229.5

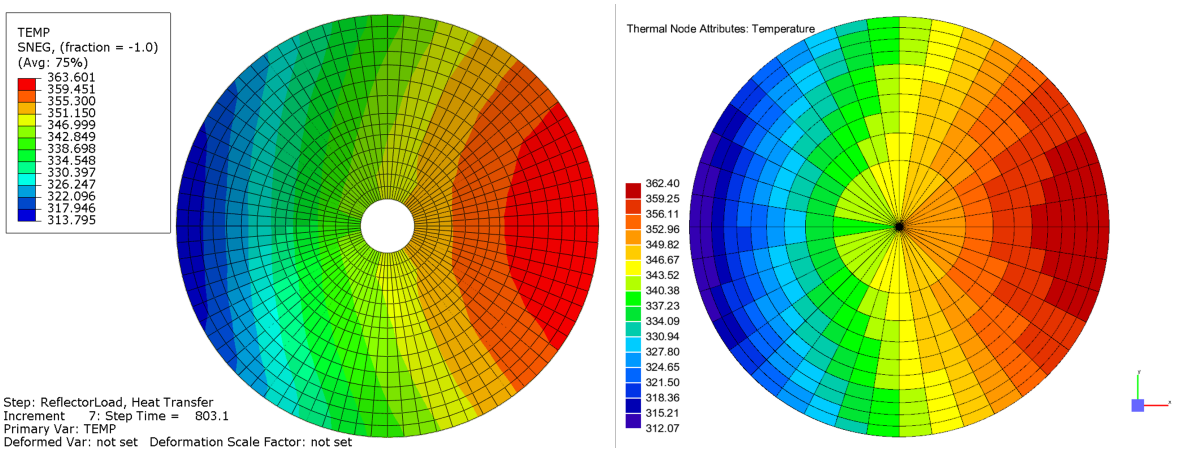

(b) t = 803.1

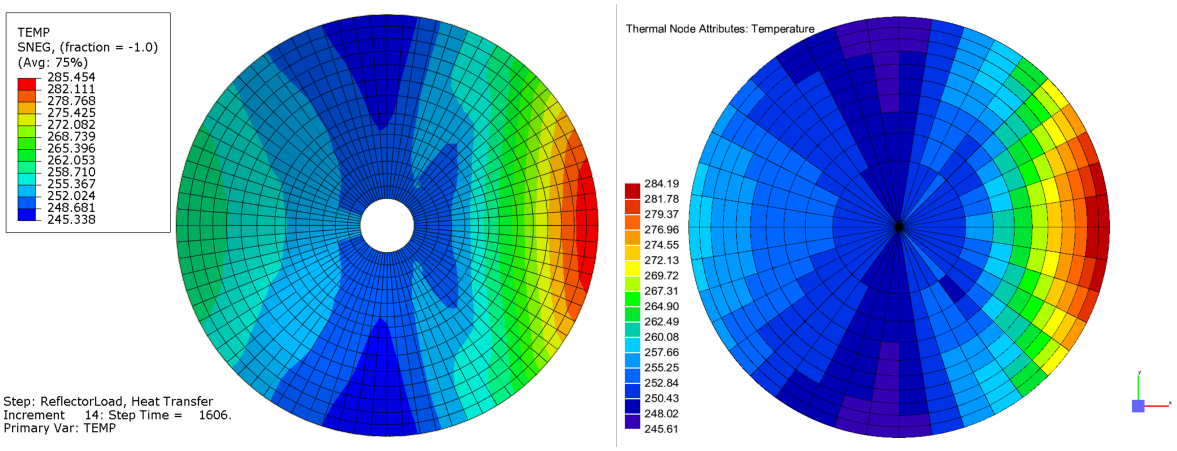

(c) t = 1606.0

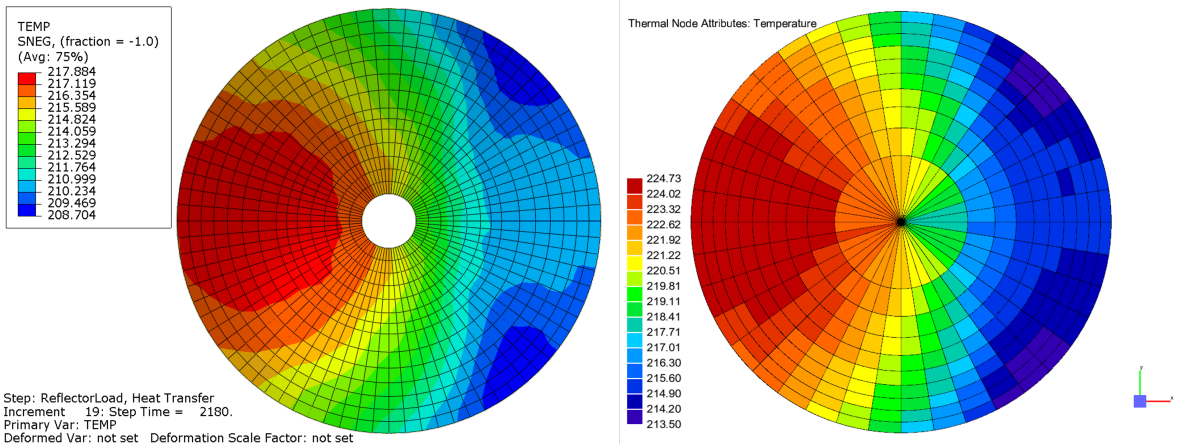

(d) t = 2180.0

Figure 3.22: Transfer Study

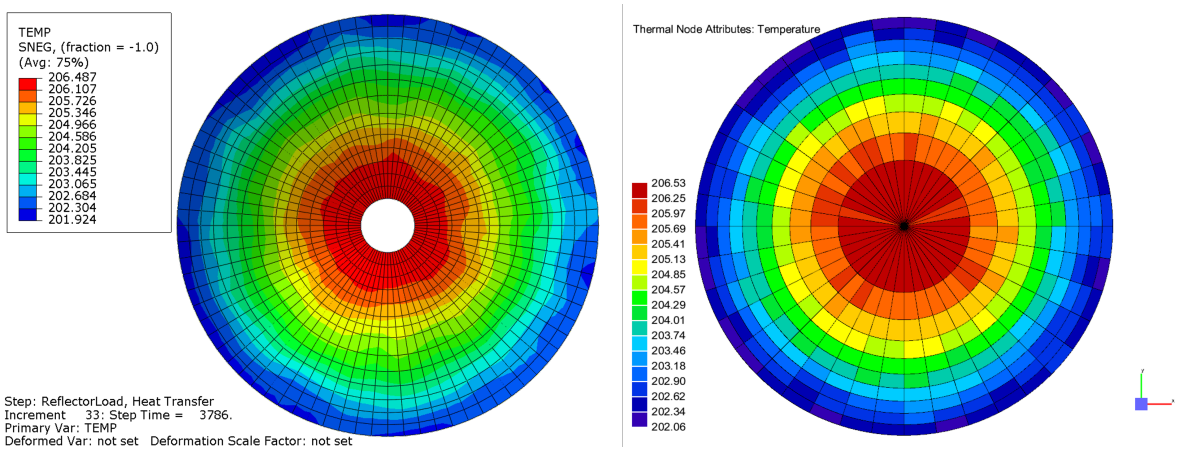

(a) t = 3786.0

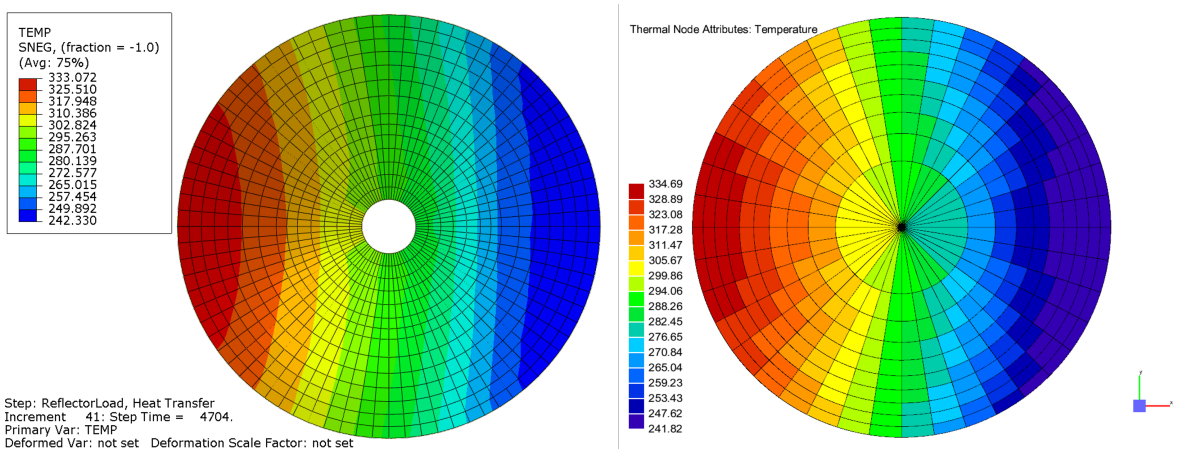

(b) t = 4704.0

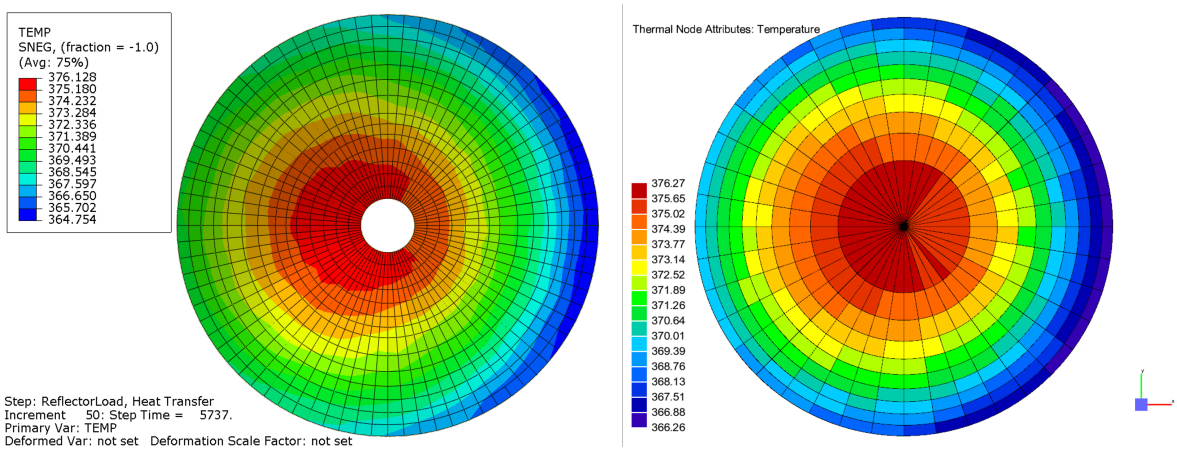

(c) t = 5737.0

Figure 3.23: Transfer Study Continued

Abaqus Mesh Validation

General Overview

With the method of transfer deemed appropriate, the next phase looks to compare the two different models used in Abaqus. As a reminder, to be able to analyse the SDA, a basic model of a reflector (Reflector) is modelled. This model has all the same parameters of the SDA, except that the spiral interface is omitted. This allows to better understand the effects of the spiral interband as all other parameters will match except for the spiral. This leads to one problem though as the meshing of the two models will be different. As shown in the model definition sections, the Reflector has a very clean and simple web like pattern, while the SDA has a much more complex mesh. Before making any jump to studying the SDA with its Aluminum spiral zipper, it is important to understand how the mesh may affect the results. This is even more important due to the fact that the analysis of the SDA meshing has resulted in some warnings that could not be corrected. To be able to study the effects of the mesh, and therefore the error in the SDA model, the SDA CFRP model was created. This model consists of defining the strip of material, representing the spiral interband, with the same material as the band. This in term looks to try and reproduce the Reflector model but with a different mesh. In both cases, CFRP (M55J) is used as material definition (as shown in Table 3.2) for the entire reflector.

Comparing the models quantitatively is not simple due to the meshing of the Reflector and SDA model being different. Figure 3.24a shows the mean temperature, with the range of minimum and maximum temperature, for the Reflector and SDA CFRP model. Both models represent the LEO orbit case. Both cases have nearly identical profiles with matching maximum and minimum ranges. Overall the mean temperature of the Reflector model is slightly higher over the entire orbit by approximately 1-2K. This difference is not necessarily consistent throughout the analysis and seems to grow large at locations of a more steady state kind of analysis. These regions can be found at the two hot cases (start and end of orbit), and at the cold case (eclipse). These differences are very small and go to show that the mesh overall does not impact the temperature profile and the temperature ranges experienced by the reflector.

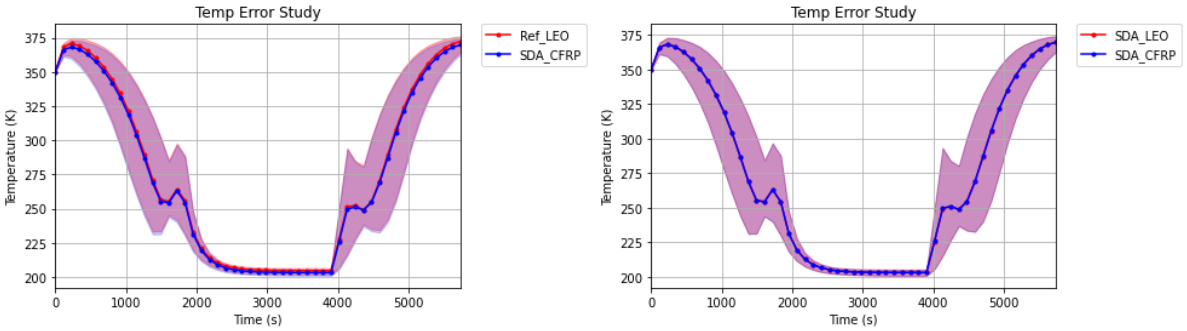

(a) Temperature Comparison between Reflector and SDA CFRP

(b) Temperature Comparison between SDA and SDA CFRP

Figure 3.24: Temperature comparisons

Three Dimensional Overview

As previously pointed out in the study of the data transfer between ESATAN and Abaqus, it is important to not just consider the overall results but also to compare the model with a 3 dimensional view. This is especially important when looking at the effects of the mesh as the mesh of the SDA is not uniform across the reflector, and the mesh analysis has show warnings only for elements at specific regions. These regions corresponded to the intersection of the spiral interface band and the circular sections of the web pattern partition. Figure 4.2 and Figure 4.3 show the temperature fields for the Reflector (left) and the SDA CFRP (right) at: 229, 688, 1606, 2180, 3786, and 4704s. An animation of the tow models side by side for a look at all time frames can be found here[2]. The spiral interface can be seen as the spiral region of smaller elements.

Similarly to the comparison between the ESATAN and the Reflector models, the meshes are different. Unlike previously, this time the method of solving the mesh is the same as they each use the Finite Element

[2]https://imgur.com/a/L6eJjCT

approach. Not only is the meshes different due to the presence of the spiral interface, but the size of the elements are also different. When testing out different meshes for the Reflector model, the following size for the elements were found to be enough for detailed results. Making the element size smaller did not show any serious improvement or changes to the results. In the case of the SDA, as pointed out in section 3.4.3, a battery of different methods and approaches were used to improve the meshing of the SDA, to limit the number and proportion of warnings on the mesh. This tighter mesh was found to be the best, and will of course slightly affect the interpolation calculations made between nodes. Therefore, any slight variation in the isolines between the Reflector and the SDA can be explained due to the interpolation calculations.

Looking at Figure 4.2, Figure 4.3 and the animation, it is clear that the temperature field pattern is globally the same throughout the orbit. The shift of the high temperature region towards the right happens at the same time and results in nearly identical thermal isolines. As depicted by the general overview, the overall temperature of the Reflector model seems to be higher by approximately 1-2K. This can be seen by the scaling differences. There are a three regions, depicted in the figures, where larger differences can be found. At 688.4s, the isoline depicting the 359.6-363.0K range on the SDA, seems to track a region of denser elements. Even though the same isoline on the Reflectir does seem to flatten out as it approaches the center of the reflector, the SDA model shows the isoline slightly heding back towards the exterior of the reflector. This shows just a slightly different bahivior of the isoline and seems to be present only for a short amount of time. At 1606, there is a noticeable difference bewteen the isolines just to the left of the center hole. Lastly, at 2180s, noticeable differences to the isolines depicting the 208.3-209.1K range, can be found. For each of these difference, the change in the isolines are slight and only happen for a single frame. In addtion, these changes are not a regions of the spiral interface. This goes to show that the change in the mesh does not seriously impact the temperature fields over the entire orbit and in addition, the distorted elements do not seriously affect the results of the thermal analysis.

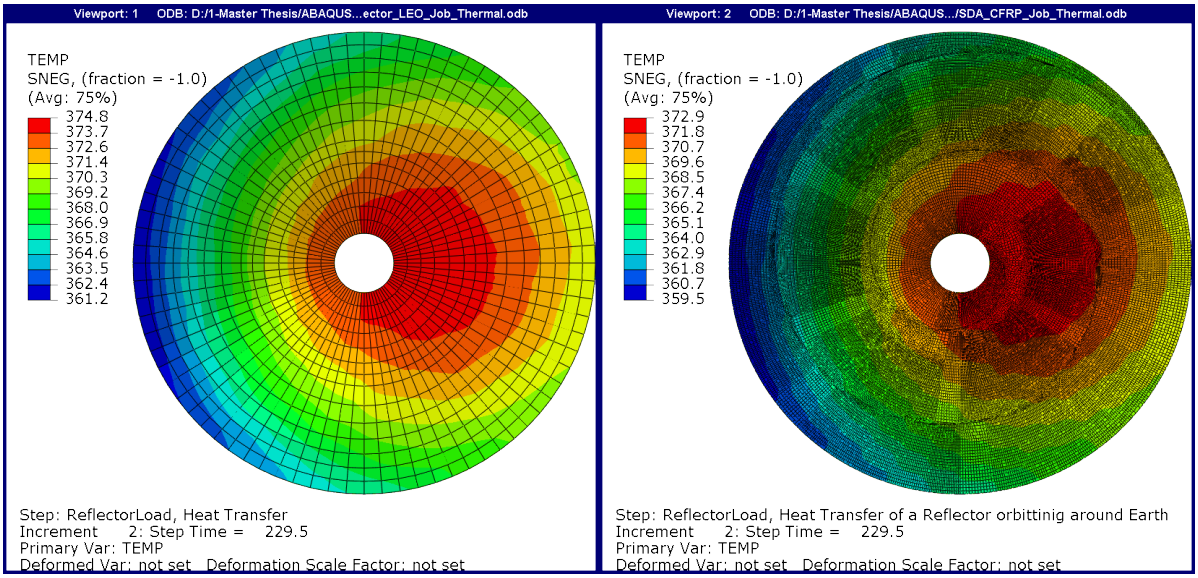

(a) t = 229.5

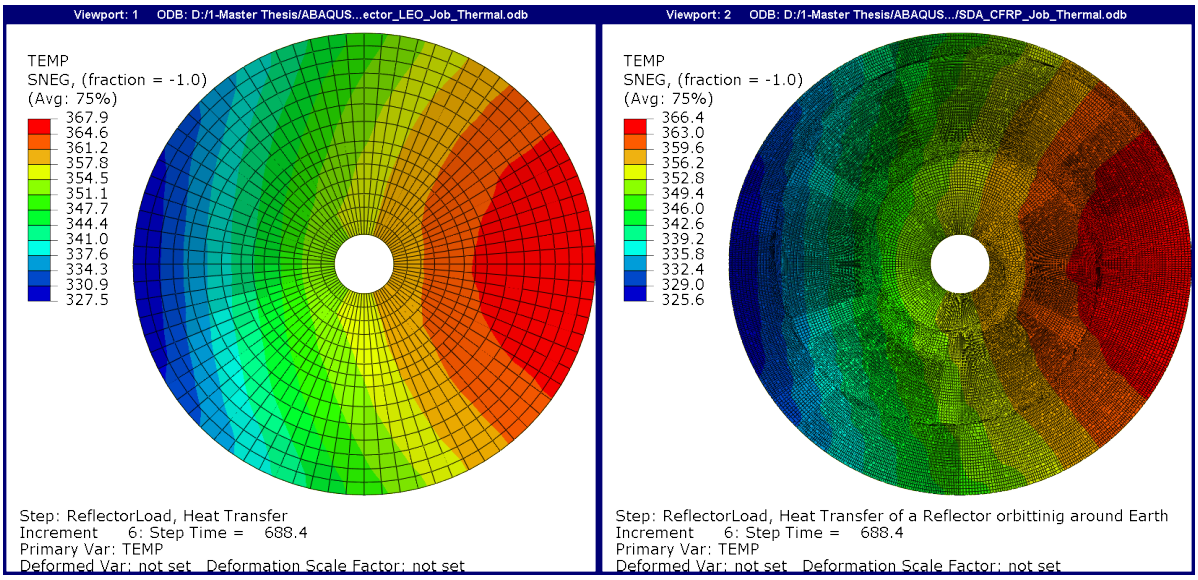

(b) t = 688.5

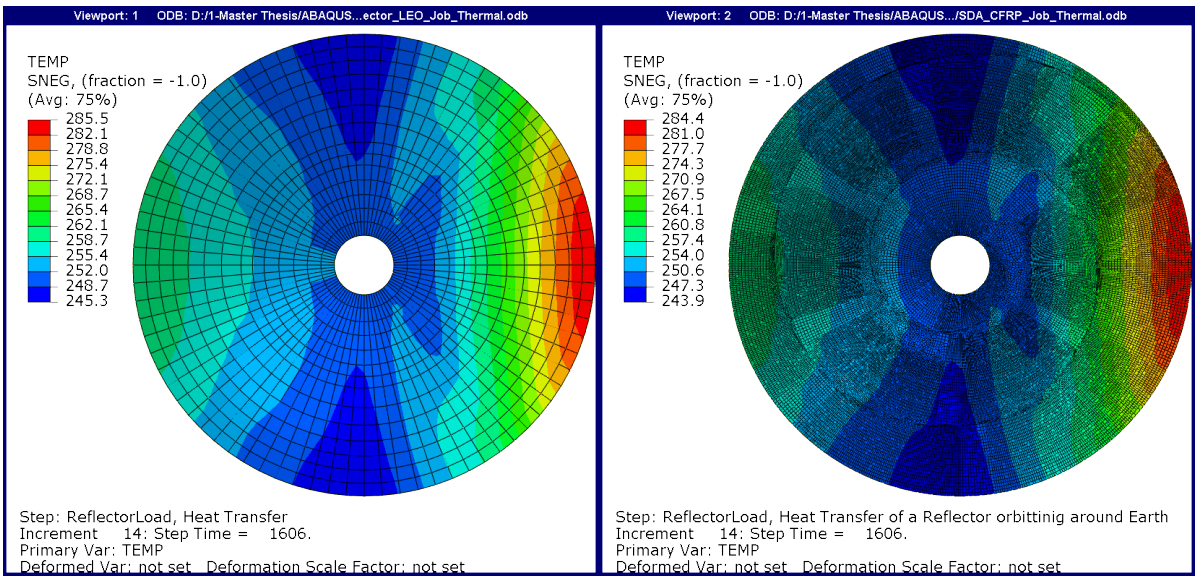

(c) t = 1606.0

Figure 3.25: Reflector and SDA CFRP comparison

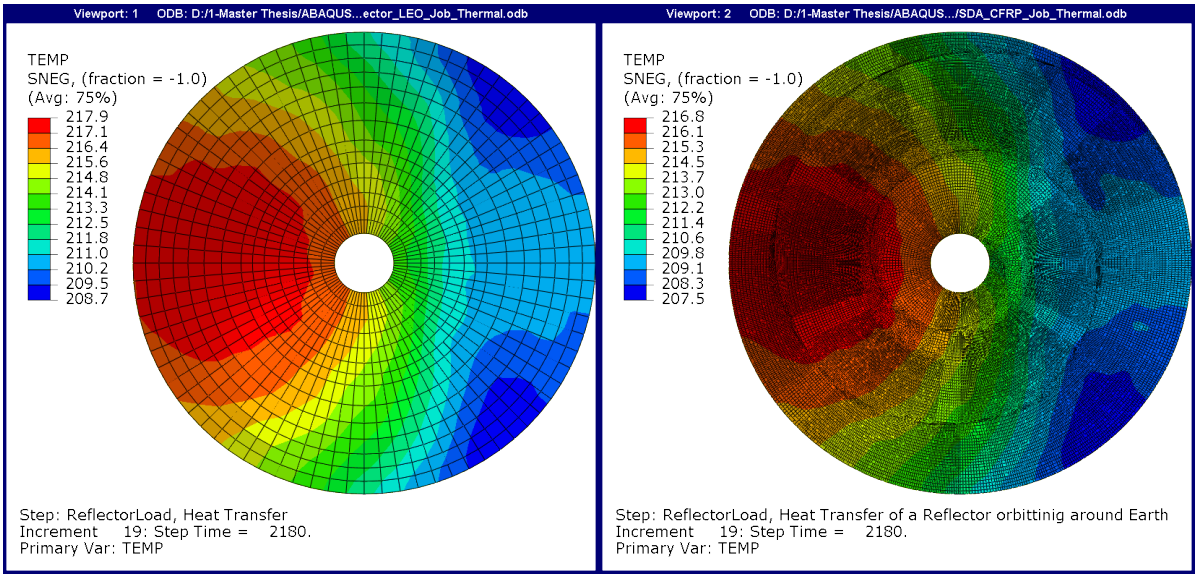

(a) t = 2180.0

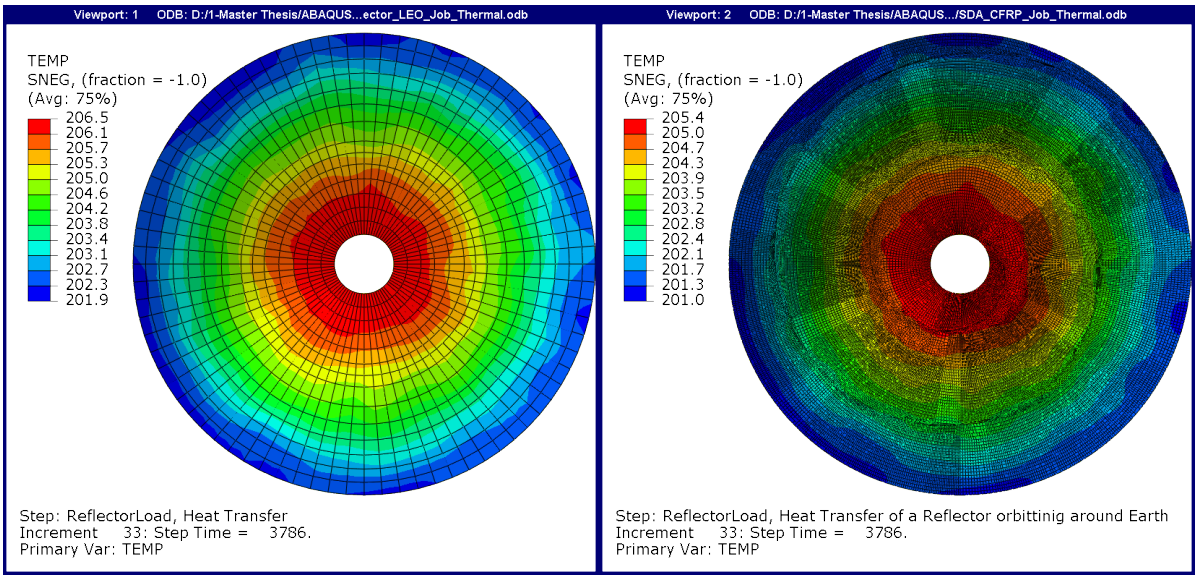

(b) t = 3786.0

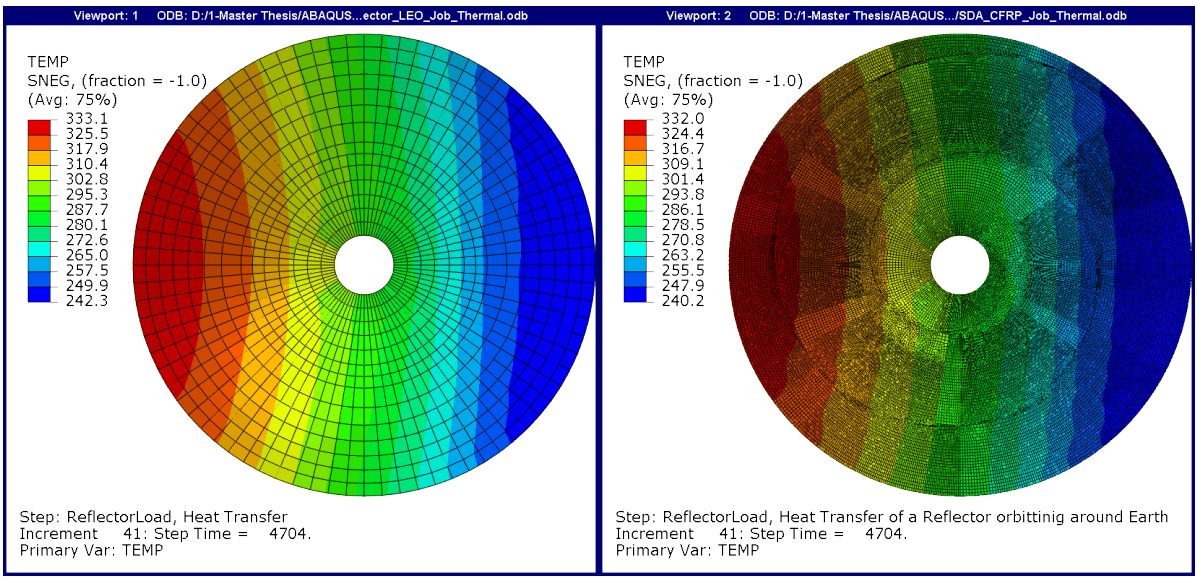

(c) t = 4704.0

Figure 3.26: Reflector and SDA CFRP comparison Continued

SDA Thermal Results

General Overview

With the effects of the mesh found in the previous section, the final phase of the thermal analysis can be performed. This phase consists of changing the material definition of the spiral interface from CFRP(M55J) to Aluminum 6063-T6. By doing this, the material of the zipper interface now has a higher density, conductivity, and specific heat. This allows to see the effects of a spiral interface on the temperature field of the reflector as the thermal capacitance and conductive couplings, form Equation 3.13, will be affected.

Looking at Figure 3.24b, the maximum, minumum, and mean temperatures of the SDA and SDA CFRP models are given. This helps to show how reflectors with similar meshed but different material definitions are affected. As shown in the Figure the mean temperature profiles match, and the temperature ranges at all times in orbit overlap perfectly. This goes to show, that overall the SDA temperature profile and temperature ranges are not affected by the presence of a spiral aluminum interface.

Three Dimensional Overview

With the overall temperature profile of the SDA studied, it is now important to look at the temperature field from a three dimensional aspect. Figure 3.29 shows the temperature field of the SDA for a LEO orbital case at 229.5, 688.5, 1606.0, 2180.0, 3786.0, and 4704.0s. An animation of the SDA in LEO for the entire orbit can be found here[3]. Even though the overall results point to there being no difference between the SDA with an alumimum spiral interface and the SDA CFRP, this does not mean that there is not a difference of temperatures at the interface.

As seen in Figure 3.29, when compared to Figure 4.2 and Figure 4.3, the overall temperature field is very similar at the different time frames. The temperature field has the hot spot start in the center with the solar flux driving the temperature. As the reflector orbits, the hot spot shifts to the right. A new hot spot driven by the IR flux appears from the right and traverses the reflector until the reflector leaves orbit. A new solar flux then appears on the left. With these behaviours, similar isolines can be seen with the circular and centred hot spot seen around 229.5 and 3786s. Similar saddle isolines are seen during the moments of large temperature change with the isolines traversing the reflector from top to bottom. As explained in the general overview, this is to be expected as the energy entering and leaving the reflector is the same as before. In addition the reflector modeled is very thin so the material is prone to fast temperature change as there is not a lot of mass to store energy.

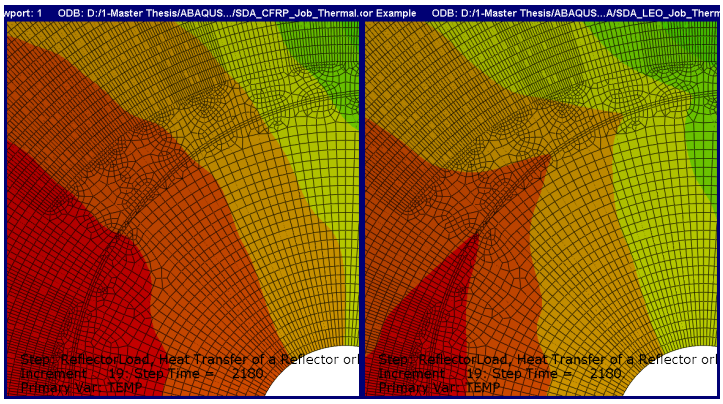

Figure 3.27: SDA CFRP and SDA Closup of the change in Isolines

Even though, the patterns are very similar, there is still a slight difference that can be found at the spiral interface. During times of large and fast temperature change, the isolines at the spiral interface shift abruptly. This makes sense due to the change in the conductive couplings and the thermal capacitance of these nodes. As a result, one can see that at the intersection of the spiral interface, the temperature field of these specific regions compared to that of the SDA CFRP are different. To better see this, Figure 3.27 shows a close up

[3]https://imgur.com/a/y0B17ak

of a spiral interface region at 2180s. This time corresponds to a drop in temperature after the first spike in temperature just before eclipse. In this Figure it is easier to see how the isolines are pulled in the direction of the spiral interface. As this corresponds to a time of loss of temperature, one can see how the aluminum, which has a higher thermal capacity and conducts heat easier, creates a path for the heat. The changes in the isolines are very localised and quickly disappear to have a similar shape as those of the SDA CFRP when the temperature stabilises.

With the effects of the spiral interface noted for the SDA, a similar approach can be made for the Summern and Winter case. An animation of the SDA in the Summer case can be found here[4], while an SDA in the Winter case can be found here[5].

Interestingly, due to the orbit having an inclination of 45°, the hot spot on the reflector in both cases does not simply traverse across the center of the reflector. In both cases, the hot spot arc across the top of the reflector. Due to these cases being pointed away from the sun at all times and not having the spikes in temperature before orbit, the drops in temperature is done more uniformly across the reflector. This leads to some interesting results due to the higher thermal capacitance of the aluminum. Figure 3.28 shows the temperature fields at the end of temperature drops for the Summer (left) and Winter (right) cases. Here the temperature difference between the band and the spiral interface can be seen to be dragged out across the spiral band for longer. One can see that as the temperature drops, the spiral band sections of the reflector drop in temperature slower than the band. This causes the spiral interface to have a slightly higher temperature than the band across the entire reflector. This process is similar for the exiting of the eclipse, except that this time, the spiral interface have lower temperature than the band. Even though the difference in temperature are not large, this does go to show that the spiral can cause the reflector to experiences localised temperature differences during moments of temperature change (entering and exiting eclipse).

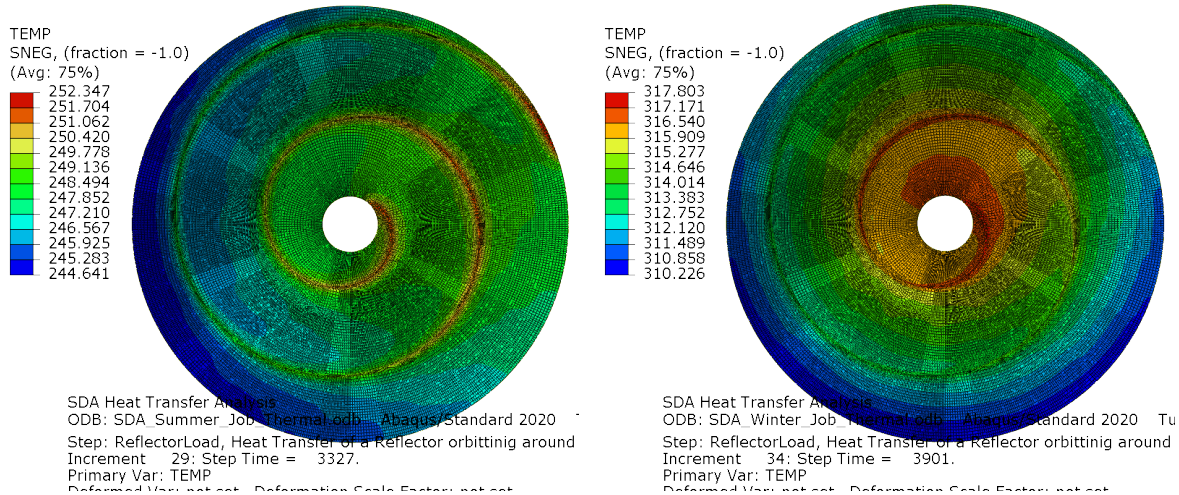

(a) Summer at t=3327s

(b) Winter at t=3901s

Figure 3.28: SDA Summer and Winter

[4]https://imgur.com/a/a26JLYz
[5]https://imgur.com/a/ePeSK7e

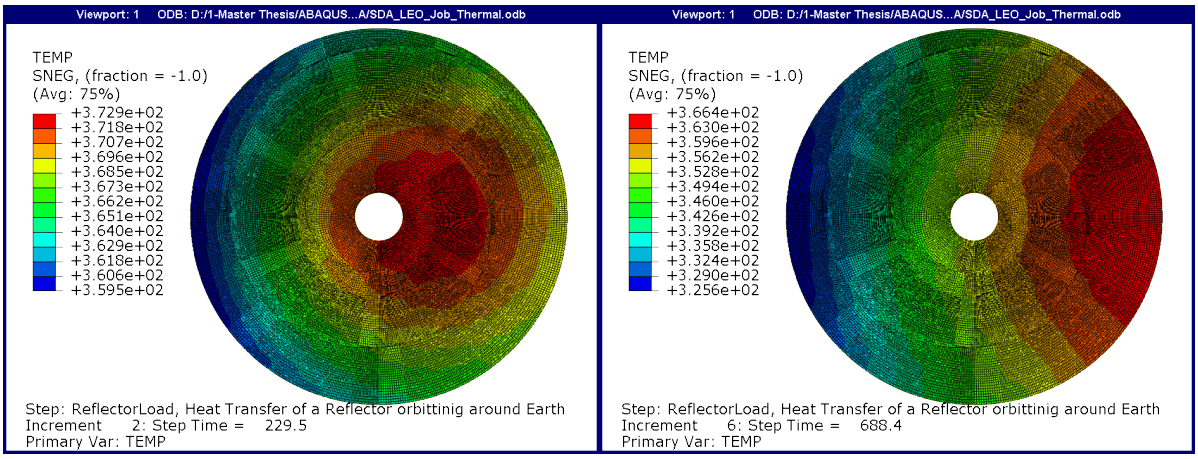

(a) t = 229.5 (b) t = 688.5

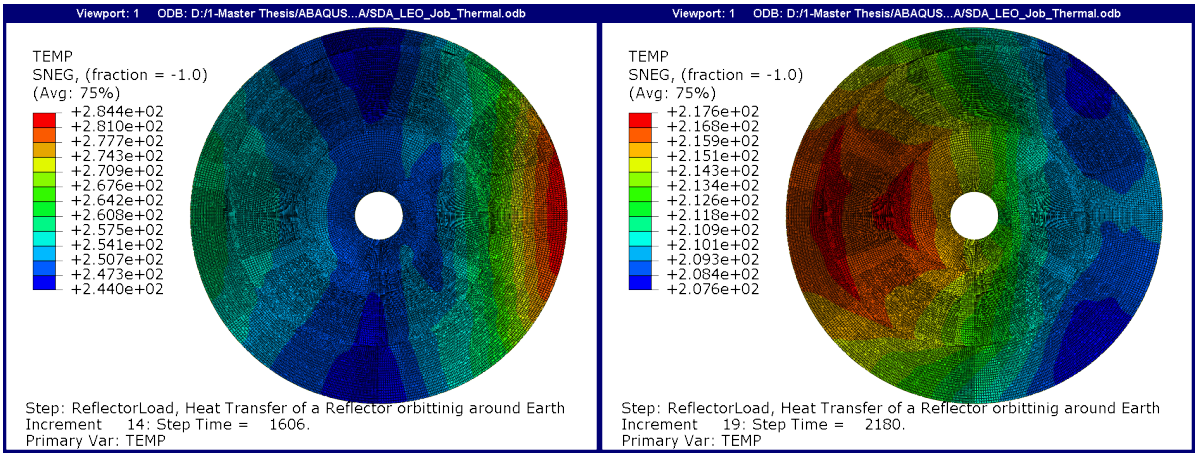

(c) t = 1606.0 (d) t = 2180.0

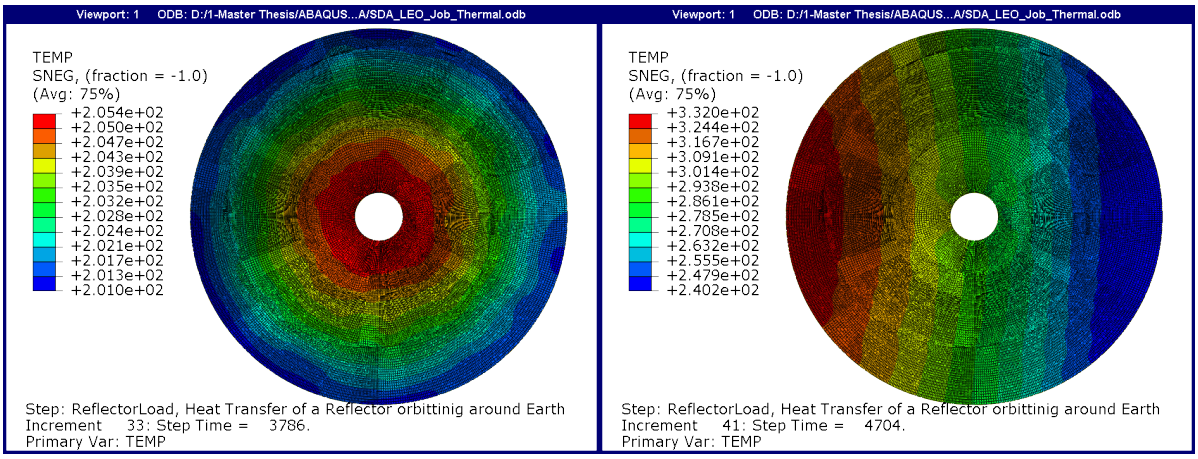

(e) t = 3786.0 (f) t = 4704.0

Figure 3.29: SDA Temperature Distribution

4

Thermo-Elastic Analysis

In this chapter a thermo-elastic analysis is performed for the Reflector and SDA model. Section 4.4.1 explains shortly the theory used to perform the thermo-elastic analysis. Section 4.4.2 describes shortly the reasoning behind the method selected to perform the thermo-elastic analysis. Lastly, section 4.4.3 presents the setting up of the model used to perform the thermo-elastic model, and shows the results obtained for different models.

4.1. Thermo-Elastic Analysis-An Explanation

With a spatially varying temperature on the reflector taking place, the materials on the reflector will expand and contract causing thermal strain to take place across the reflector. This thermal strain is inherent to the material selected and is defined be the thermal coefficient of expansion property. The thermal strain can be calculated using the following Equation[29]:

$$\epsilon^{th} = \alpha(\theta, f_\beta)(\theta - \theta^0) - (\alpha(\theta^I, f_\beta^I)(\theta^I - \theta^0) \tag{4.1}$$

where $\alpha(\theta, f_\beta)$ is the thermal expansion coefficient, θ is the current temperature, θ^I is the initial temperature f_β are the current values of the predefined field variables, f_β^I are the initial values of the field variables, and θ^0 is the reference temperature for the thermal expansion coefficient.

4.2. Method Selection

As previously discussed, the method of performing the thermo-elastic analysis is to be done using software. As a continuation of the thermal analysis, Abaqus is deemed the best way to perform the analysis. This is one of the reasons Abaqus is chosen as it had a defined process for performing a thermo-elastic analysis. In addition to this reason, it made building the thermo-elastic model much faster due to only needing to copy the thermal model and changing a few parameters. No reason could be found to stop using Abaqus for the thermo-elastic analysis.

4.3. Abaqus Thermo-Elastic

4.3.1. Model Definition

Assumptions

For the model being analysed, the following assumptions had to be made:

AE1 - No backing structure exists on the SDA due to its need to unroll from its stowed position.

AE2 - CFRP will be modelled as an isotropic material.

AE3 - The base of the SDA will be encastered to the bus of the satellite and therefore will no allow for transverse or rotational movement.

AE4 - Gravitational effects on the reflector will be omitted.

AE5 - The zipper will be modelled as a simple band consisting of a singular material property.

AE6 - The interband region will be modelled in a way where there will be no creation of empty space during the thermo-elastic analysis.

Abaqus Model

Building the Abaqus model is facilitated by the existence of the thermal model. Geometrically both model are the same and therefore just need to be copied from one model to the other. From a point of loading, the thermo-elastic model has no need for the surface heat fluxes used in the thermal model. The best way of placing temperature boundary conditions are through the means of the predefined field tool. This allows for the model to access the temperature fields resulting from the thermal analysis model and placing these temperature fields on the thermo-elastic model. This allows for an incrementation of 50 time steps to show the spatially varying temperature field. In addition, to changing the load definition, the step has to be changed to take into account the thermo-elastic analysis. As per the Abaqus sequentially coupled thermal-stress analysis procedure, the step is changed to "General, Static". Due to the change in analysis, the elements also have to be changed to accommodate the general, static analysis. For this analysis, the S4R and S3R elements are used. Luckily, due to copying the geometry from the thermal model, the mesh are the same between the thermal and thermo-elastic models. Lastly, a boundary condition is placed on the base of the reflector to show that the reflector is connected to the spacecraft bus. The boundary condition is set to encaster the base of the reflector.

Material Properties

The last addition needed to perform the thermo-elastic analysis is to add the last material properties required in this kind of analysis. These properties are listed out in Table 4.1.

Table 4.1: Thermo-Elastic material properties

Material	Coefficient of thermal Expansion	Young's Modulus	Poisson's Ratio
CFRP (M55J)	-1.1E-6	3.38E11	0.33
Aluminum 6063-T6	2.31E-5	6.89E10	0.33

4.3.2. Abaqus Thermo-elastic Results

The analysis of the thermo elastic result is done in two different phase. The first phase consists in comparing the thermo elastic results of the Reflector model and that of the SDA CFRP. Even thought the error in the mesh was deemed appropriate for the thermal analysis of the SDA, it is important to see how they may affect the thermo-elastic analysis. This is needed as the elements used in this analysis are different. Due to this, it is not possible to make the assumption that the thermo-elastic analysis is good just because the because the thermal analysis model shows no problem. The second phase consists of looking at the SDA and understanding how the spiral interface impacts the displacement of the reflector.

Abaqus Meshing Error

General Overview

For the first phase of the analysis, displacement will be primarily used as a means of comparing the different models. Figure 4.1a shows the transient result of the mean and max displacement for the Reflector and SDA CFRP model in a LEO case. There is no minimum displacement given as the encaster boundary condition keeps the center hole in place and therefore results in a minimum of no displacement.

Looking at Figure 4.1a, one can see how the displacement of the reflector has a similar shape as the temperature plots. The displacement starts high, before tending downwards as the reflector starts orbiting. Looking at the Reflector model, the mean displacement is 0.94mm at 229.5s with a maximum displacement of 1.24mm. This displacement then drops to a mean of 0.63mm at 1606s with a maximum of 0.99mm. The displacement then reacts to the spike in temperature with the mean displacement rising to 0.65mm at 1721s with a maximum of 1.17mm. Lastly the displacement lowers as the reflector tends to a cold case. Here the mean displacement is shown to be 0.48mm with the maximum displacement being 0.737mm. Similar deflections can be seen as the reflector exits eclipse and heats again. This includes the spike in temperature at eclipse exit resulting in a spike in the deflection.

Figure 4.1b, shows the absolute difference between the mean and maximum displacement value of the Reflector and SDA CFRP models. In addition of Figure 4.1a, this helps to show the error caused by the meshing. One can see that when comparing the mean temperatures, the SDA CFRP has a slightly higher displacement than the Reflector model. The difference in the displacement never exceeds 0.08mm across the entire, and drops to only having a difference of 0.04mm during the eclipse. The difference grows when looking at the difference in the maximum displacement where the maximum difference is 0.16mm. For total displacements of approximately 1.2mm at that time, this shows that the SDA mesh can lead to potentially large errors. Luckily, this large difference only last for the short moment of the spike in temperature. The average displacement error during the orbit is 0.08mm, which is more acceptable. Studying these plots helps to show the error in the displacement values of the SDA mesh relative to the Reflector model. One can see that there is a larger difference in the displacement values than those previously obtained for the temperature. Even though the difference in the values of the SDA CFRP with respect to the Reflector are high at the temperature spikes, due to the similar profile between the two models, it was deemed enough to continue with the analysis of the SDA.

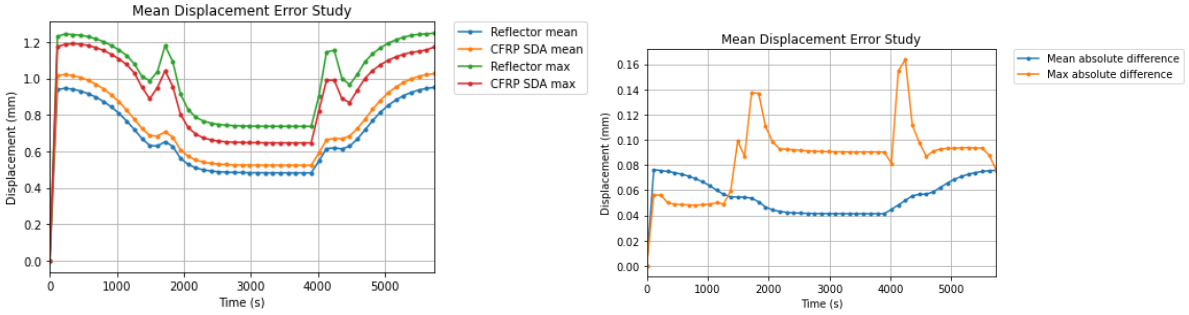

(a) Mean and Max Error Study

(b) Mean and Max Difference Error Study

Figure 4.1: Reflector and SDA CFRP overall displacement comparison

Three Dimensional Overview

Having studied the general displacement, the two models need to be compared three dimensionally. Figure 4.3 and Figure 4.3 show the displacement fields on the SDA CFRP (left) and the Reflector (right) at 229.5, 688.5, 1606.0, 2180.0, 3786.0, 4704.0s. An animation of the comparison of the displacement files with constant scaling can be found here[1]

Similarly to the temperature comparison, the meshes of the two models do not match. This is a continuation of the temperature models, as to perform the sequential thermo-elastic analysis, it is preferred to have the same mesh between the thermal and thermo-elastic models. This means the interpolation between the nodes will cause slight difference in the appearance of some of the displacements across the reflector.

Comparing the Reflector and SDA CFRP model across time, one can see that the displacement regions behaviour similarly to the temperature field in the fact that the high displacement regions move across the reflector to the left. This makes senses as the displacement will be higher at the regions of higher temperature and these are shifting towards the left as the reflector orbits. Other similar behaviours can be found between the two models. At 1606s one can see how, as the temperature shifts off to the side of the reflector and causes a higher displacement on the right of the reflector, two regions on the left are in turn displaced is response to the arrival of the IR hear flux and due to the shift on the right of the reflector.

As much as the movement and the overall displacements match, one can see differences between the SDA CFRP and Reflectors. This reflects what could be seen in general analysis with the maximum and mean displacements. The first major difference lies in the high displacement found just before the edge of the reflector. A similar ring can be found on the SDA CFRP, but it is not as pronounced as the Reflector model. This mostly goes to explain why the max displacement of the Reflector model is higher than the SDA CFRP. In addition,

[1] https://imgur.com/a/PlrOkh4

the SDA CFRP seems to have a axis of higher displacement that seems to go from the top left to the bottom right. This can be seen easily at time 229.5. No concrete explanation has been validated for the reason of this shift but it is most likely due to the meshing issue previously explained. Seeing that no solution could be found for the mesh issues, the 0.1mm difference caused by this problem could only be noted for further analysis of the SDA.

Overall, the SDA CFRP and the Reflector show similar behaviour in displacement over the orbit. The errors caused by the mesh are more visible for the displacement than for the temperature field but are still not large enough to show a major fault in the process of analysis. Therefore, this process is used in the study of the SDA.

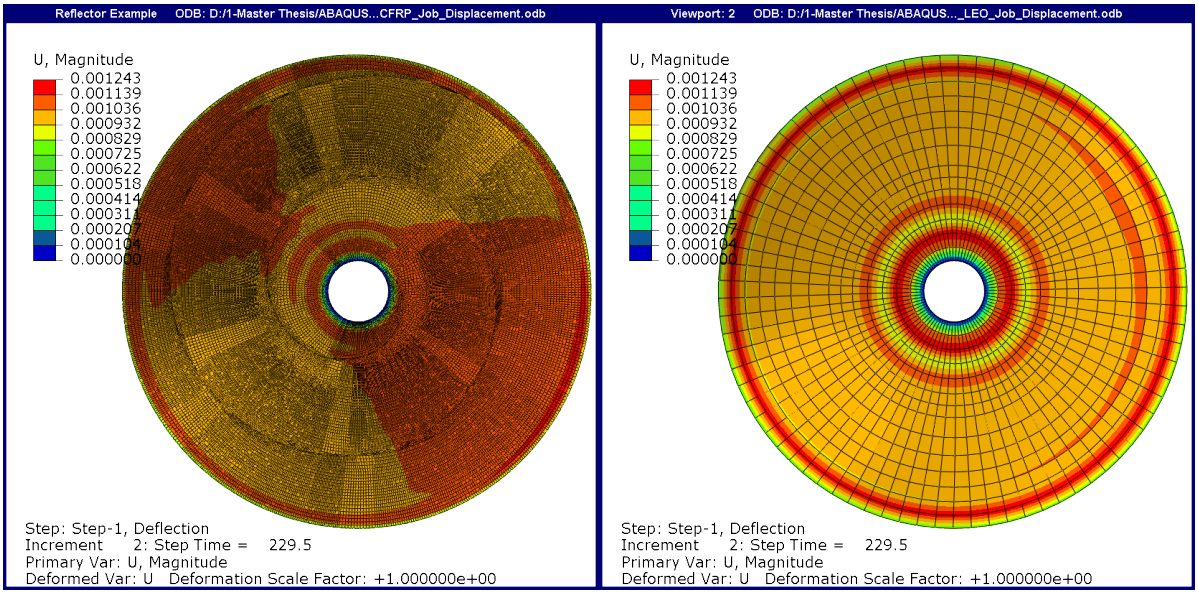

(a) t = 229.5

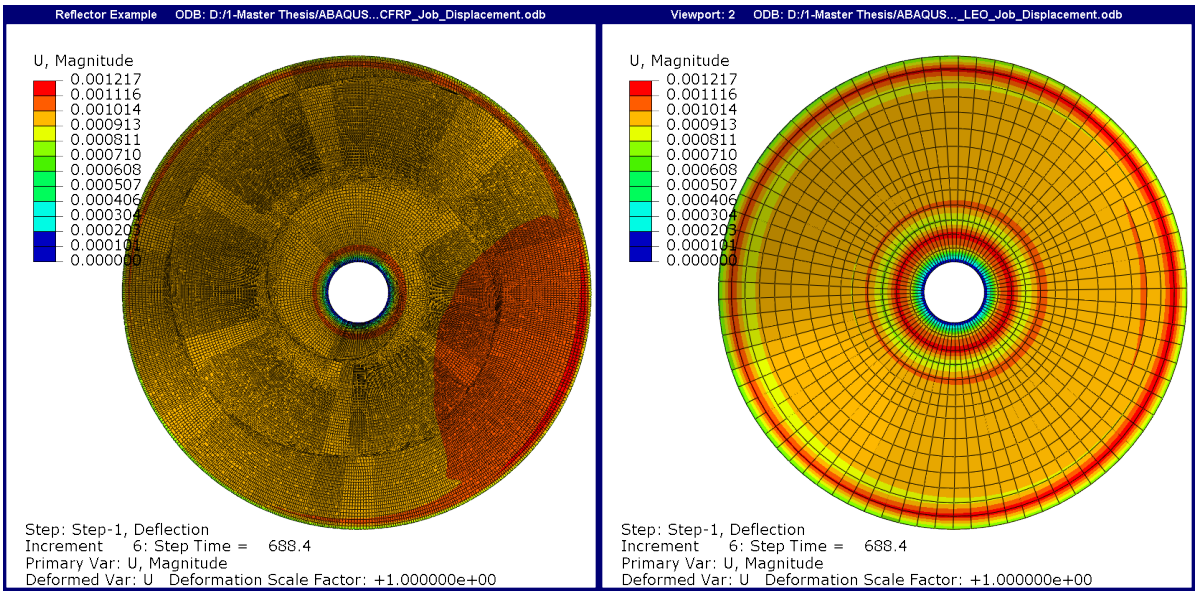

(b) t = 688.5

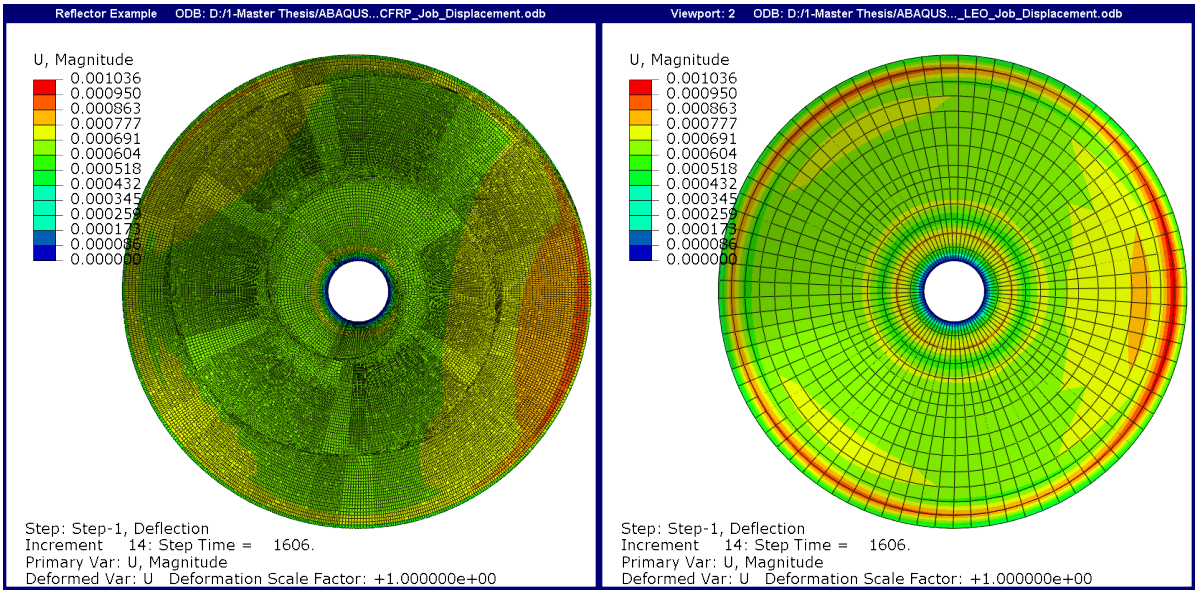

(c) t = 1606.0

Figure 4.2: Reflector and SDA CFRP displacement comparison

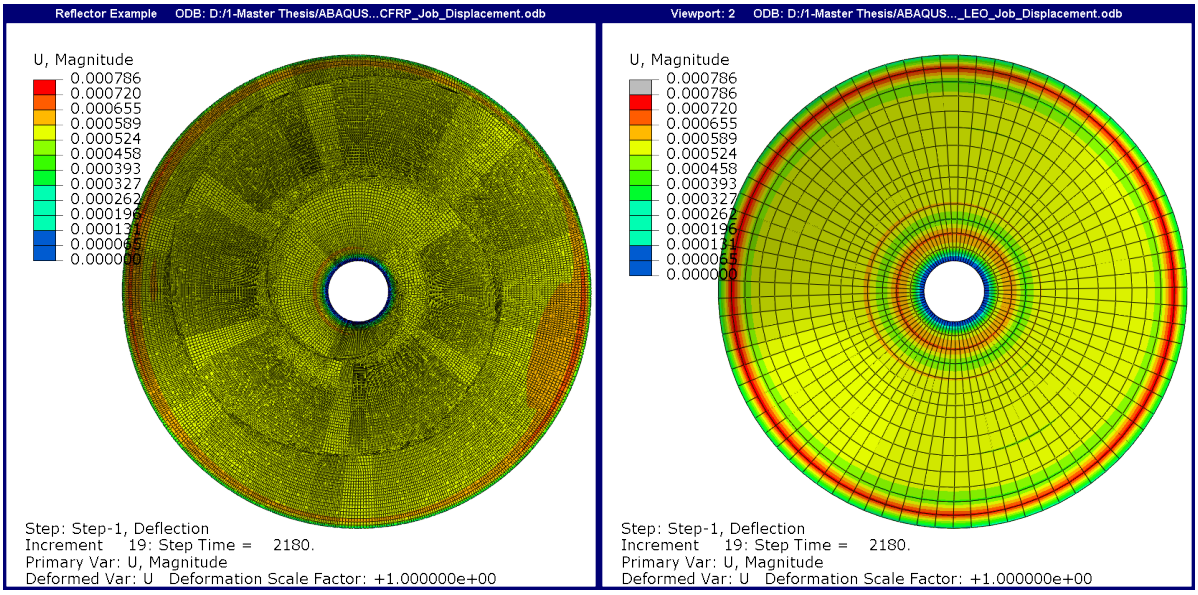

(a) t = 2180.0

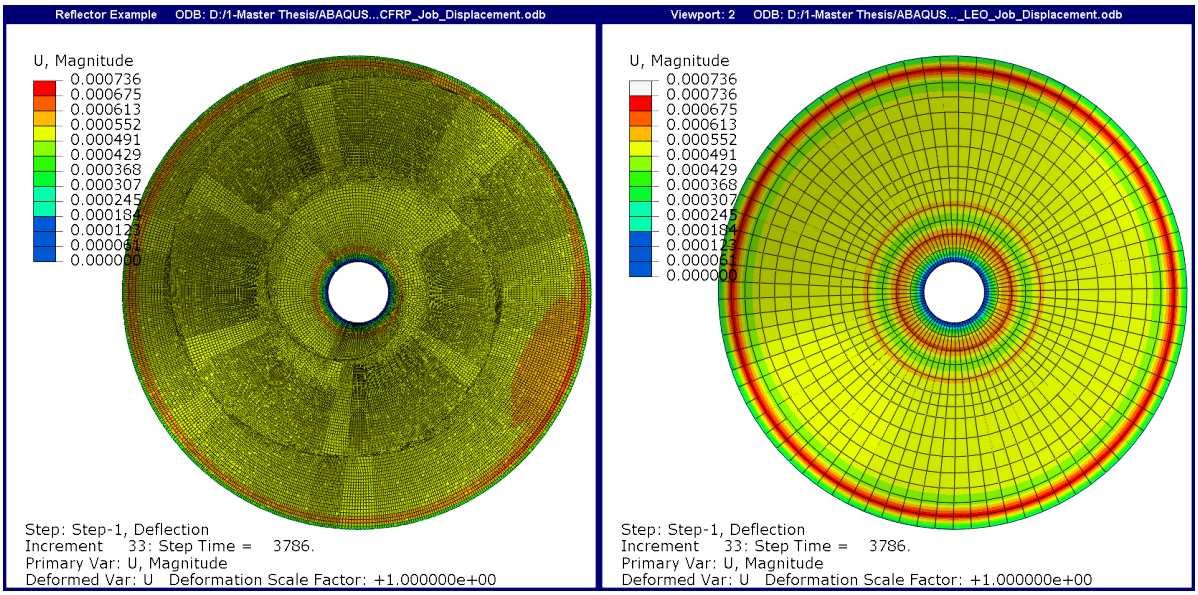

(b) t = 3786.0

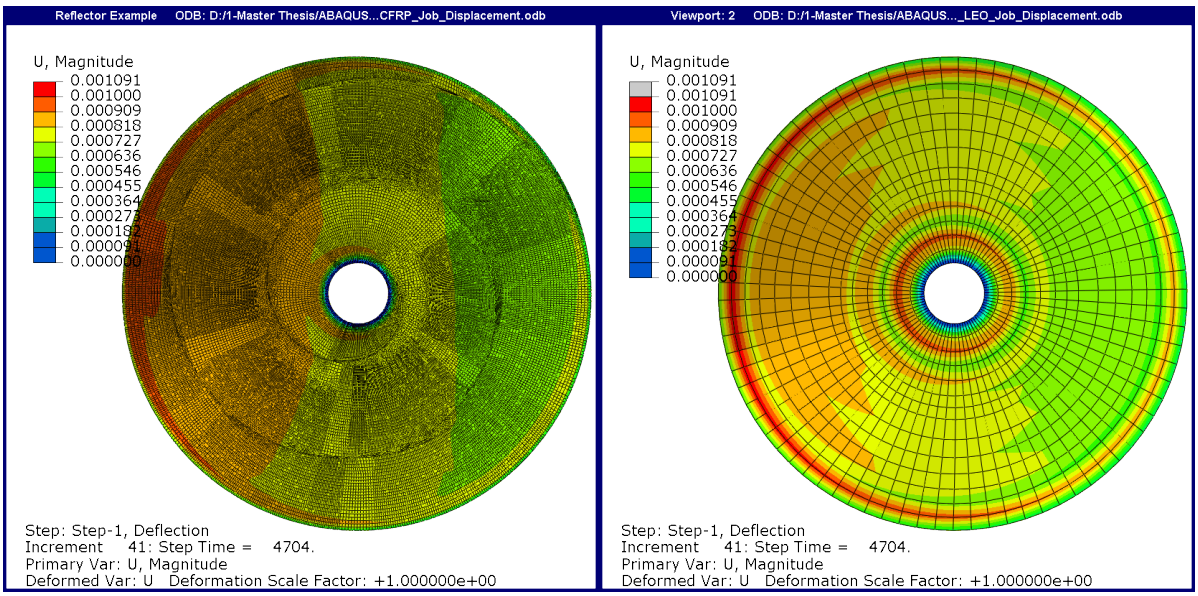

(c) t = 4704.0

Figure 4.3: Reflector and SDA CFRP displacement comparison Continued

SDA Thermo-elastic Results

General Overview

With the error in mind, the SDA model is then studied for the LEO, Summer, and Winter Cases with the Aluminum spiral interface. Figure 4.4 show the mean and maximum displacement for the Reflector and the SDA model for the LEO,Summer, and Winter case. Minimum displacement is not shown due to it being zero, as the base doesn't allow for any movement. These plots allow for a general overview of the displacement comparison between a Reflector without a spiral interface and a reflector having an aluminum spiral interface of the same size.

Looking at the behaviour of the displacement in the three cases, the SDA shows that it still react to the temperature when it comes to magnitude of displacement versus temperature. This is expected as the aluminum and spiral interface should similarly react to temperature change. Interestingly, though the magnitude of the displacement is much higher for the SDA than the Refector model. Even with the error of the mesh being considered, the SDA has a displacement that is more than an order of magnitude larger. Looking at the LEO case in Figure 4.4a, the mean displacement goes from 4.5mm at 229.5, to 2.2mm in eclipse, compared to the Reflector going from 0.9mm to 0.48mm at the same times. The difference in the maximum displacement is even larger with the SDA experiencing displacements of 21.5 to 10mm while the Reflector only experiences displacements of 1.2 to 0.7mm. The main explanation for this behaviour, when looking at the general results, seems to be potentially explained by the joint thinness of the reflector and the aluminum spiral interface having a CTE that is an order of magnitude larger than that of the CFRP.

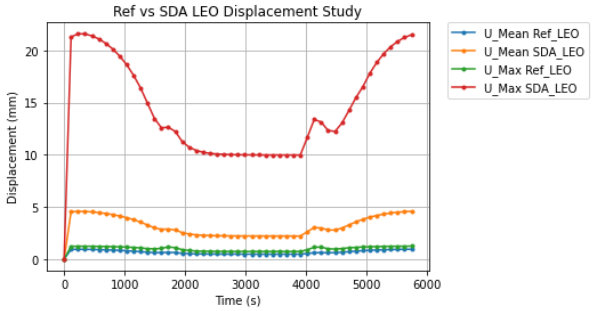

(a) LEO Displacement Study

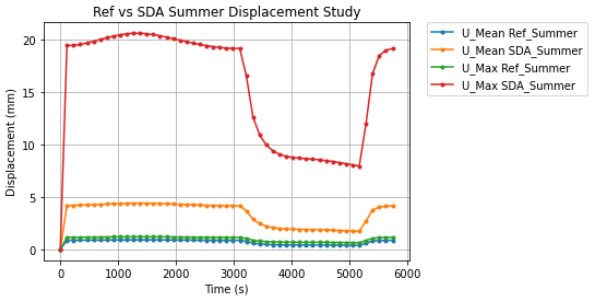

(b) Summer Displacement Study

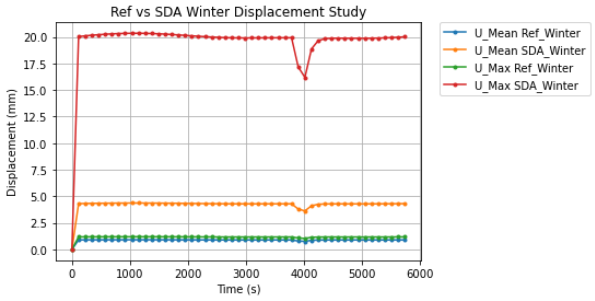

(c) Winter Displacement Study

Figure 4.4: Displacement Study

Three Dimensional Overview

Similarly to the analysis of the SDA, when looking at the temperatures, it is important to see if an explanation for the differences can be found when looking at the results for the entire reflector.

Figure 4.5, shows the displacement field at 1492s. An animation of the displacement for the SDA in LEO can be found here[2]. The reason only a single frame is shown is because the displacement pattern has a similar shape during the entire orbit. A slight shift in the pattern can be seen during the eclipse phase. The

[2]https://imgur.com/a/1QEJyRC

magnitude of the displacement across the reflectors follows the temperature profiles, but the overall shape of the displacement remains the same. A similar reaction can be seem in the Summer and Winter case. An animation of the displacement for the Summer case can be found here[3], while an animation for the Winter case can be found here[4]. For future reference, this displacement pattern seen on the SDA is referred to as the "cross pattern".

At this stage of the analysis, the cross pattern only appeared with the change in the material definition of the spiral interface. It goes to show how having a spiral interface can affect the displacement of a reflector when experiencing temperature changes in orbit. As dictated by Equation 4.1 the displacement is directly related to the temperature change and the CTE of the material used. With the CTE of Alumminum and CFRP being different, the difference in the CTE is most likely the cause of the cross pattern. The first major difference, as seen in the general overview, is that the order of magnitude of the CTE of the aluminum is higher than the CFRP causing the larger displacements. The second difference, is that the CTE's of both materials have different directions. This means that the aluminum and CFRP are looking to expand in different directions. This CTE mismatch causes the SDA to warp and get locked into this shape. It is important to note that the direction of the cross pattern is dictated by the geometry of the sprial interface as adding more or less of the spiral interface, structurally impacts the reflector, and causes it to warp differently.

In addition, by looking at Figure 4.5 the maximum deflection seems to be mostly happening in 2 specific areas: just past the tip of the spiral and the top of the SDA. At these points the displacement is almost double than that of the mean displacement and causes the high displacement in Figure 4.4a. It is not quite well understood why these two regions seem to show so much more displacement than the rest of the reflector. The temperature field does not point to such a large displacement at these places, so the only other possibility is in the geometry or design of the SDA with an aluminum zipper.

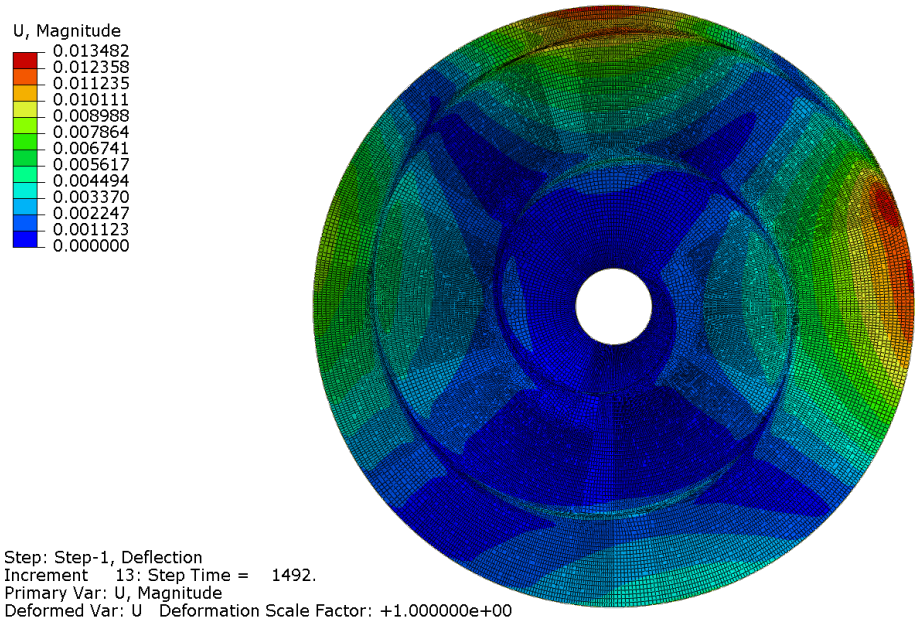

Figure 4.5: SDA LEO U at 1492

Lastly, Figure 4.6 shows the rotational displacement (UR), the stress (S), and the strain (E) at 1492s. When looking at the stresses and rotational displacement, one can see that the aluminum spiral interface experiences high stress and is also experiencing much higher rotational displacement than the band of the SDA.

[3] https://imgur.com/a/EjXWkvD
[4] https://imgur.com/a/GlOFQWW

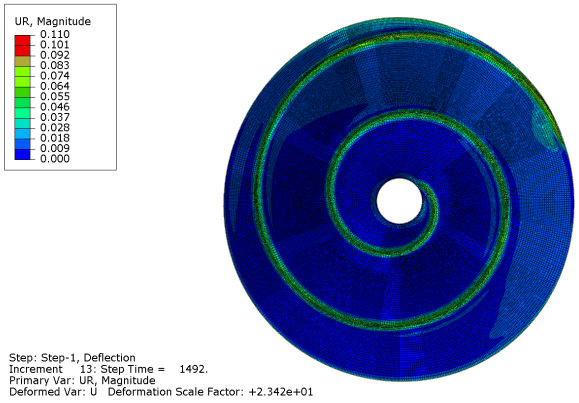

(a) SDA LEO UR at 1492

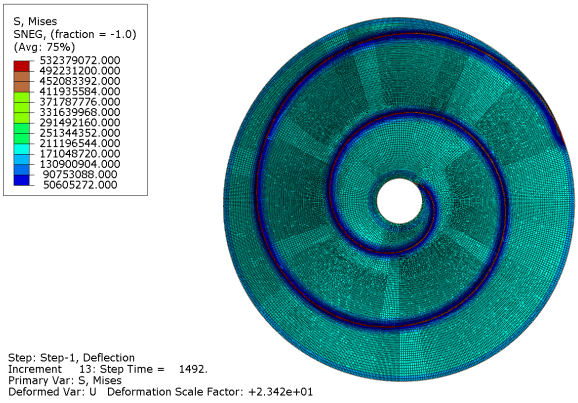

(b) SDA LEO S at 1492

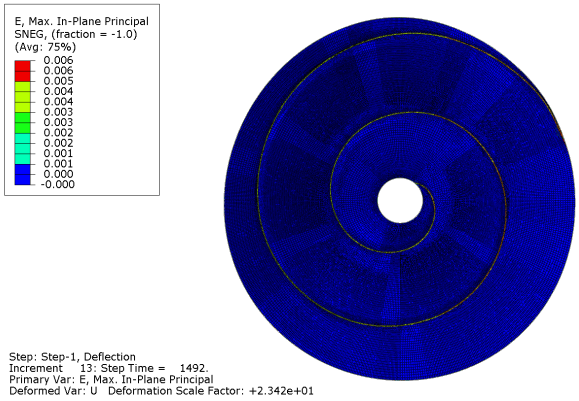

(c) SDA LEO E at 1492

Figure 4.6: SDA LEO Study

5

Initial Parametrization

To try and understand what may be happening with the SDA, a few parameters are changed to see their effect on the temperature field and on the displacements.

Spiral Coefficient of Thermal Expansion Study

The first parameter that is looked at is changing the CTE of the zipper material. To do this, the CFRP of the zipper is changed to see if the cross pattern could be recreated and see if it made displacement worst, as previously hypothesized. Figure 5.1 shows the maximum, minimum, and mean values for the temperature and displacement of the SDA CFRP model over the entire orbit. As can be seen looking at Figure 5.1a, the change in CTE of the zipper does not seem to have any effect on the overall temperature field of the SDA. This is coherent due to the CTE normally only impacting the displacement of the SDA. Figure 5.1b, shows that the maximum displacement goes up as the CTE value grows away from the normal CTE value of CFRP (M55J). With the mean value of the displacement not rising, this shows how the change in CTE causes the SDA to warp into the cross pattern previously mentioned. An animation of the CTE Study can be found here[1].

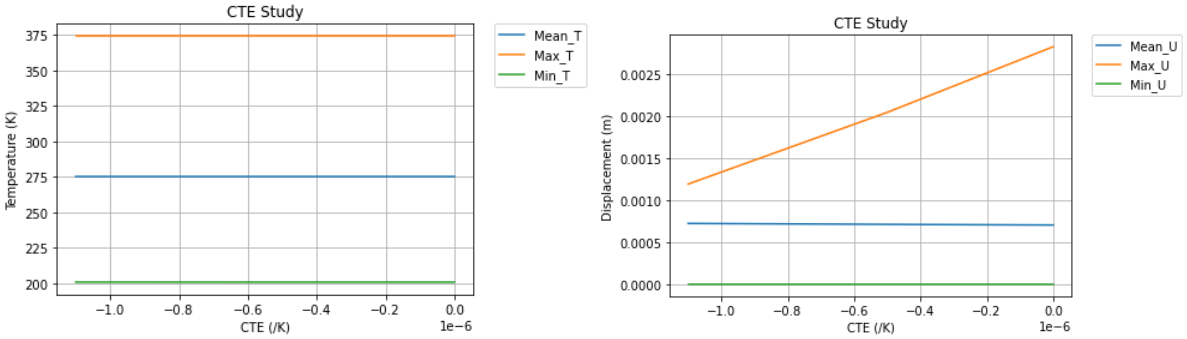

(a) CTE Temperature

(b) CTE Displacement

Figure 5.1: CTE Study

Reflector Thickness Study

The next change in parameter involved changing the thickness of the reflector. This is done because the original 0.4 mm thickness is first selected to match the similar CFRP sheets in the unfurlable petal reflector[8]. The problem is that even Park's reflector has ribs to support the sheets, as 0.4mm is very thin, and therefore might not support themselves. Figure 5.2 shows the maximum, minimum, and mean values for the temperature and displacement of a Aluminum zipper SDA. As expected, the thicker the sheets are, the stiffer they will be, and therefore allow for less displacement. They will also have a larger thermal capacity making the change in temperature slower and therefore shortening the range of temperature the reflector will endure. It

[1] https://imgur.com/a/3sIeVOW

is still important to keep in mind that the sheet of the SDA is meant to be able to role up and therefore cannot be made thicker as a solution of limiting the displacement. An animation of the thickness study with regards to temperature can be found here[2], and with regards to displacement can be found here[3].

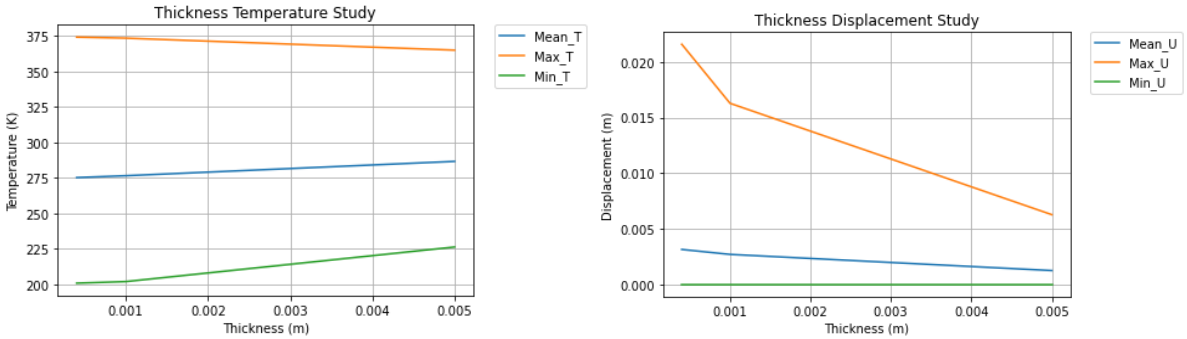

(a) TH Temperature

(b) TH Displacement

Figure 5.2: TH Study

Spiral Parameter Study

The next parameter that is varied is the spiral parameter. This parameter defines how tight of a spiral the SDA has. This in terms will define how wide the SDA strips are. By raising the spiral parameter the spiral width grows larger and therefore the length of the zipper grows smaller. Figure 5.3 show the maximum, minimum, and mean values of the temperature and displacement for the SDA with an Aluminum zipper. What can be seen from Figure 5.3a, is that the temperature ranges do not seem to be affected by the spiral parameter. In Figure 5.3b the mean displacement seems to grow as the spiral parameter grows, while there seems to be a fluctuation in the maximum displacement. Looking at Figure 5.4, one can see how the spiral parameter affects the cross pattern. An animation of the spiral parameter study with regards to the temperature can be found here[4], and with regards to displacement can be found here[5].

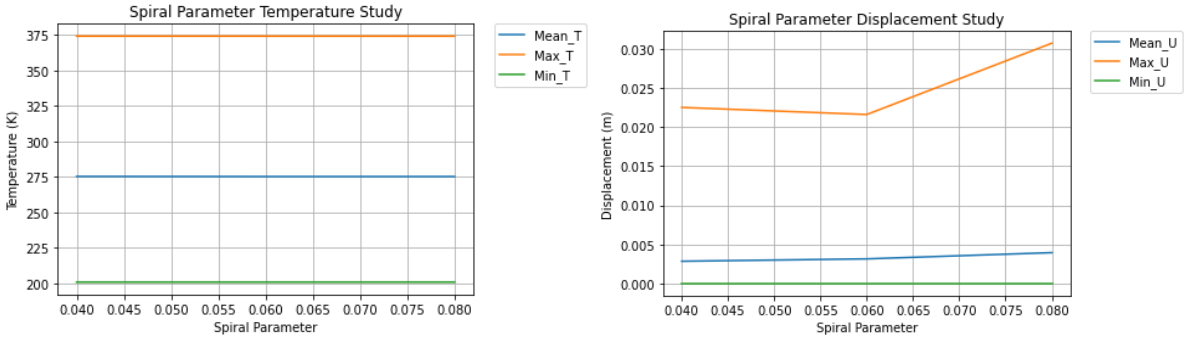

(a) SP Temperature

(b) SP Displacement

Figure 5.3: SP Study

Spiral Width Study

The next parameter changed is the width of the zipper. Because no design has been completed, it is important to see the effect the width of the zipper may pose. Figure 5.5 shows the maximum, minimum, and mean temperature and displacement of SDA with an Aluminum zipper. Here it is more obvious how the Aluminum zipper affects the maximum displacement of the reflector as the wider the zipper is, the higher is the max

[2]https://imgur.com/a/SFrHSdF
[3]https://imgur.com/a/02xoz1U
[4]https://imgur.com/a/XJHzW2K
[5]https://imgur.com/a/OKJLWL7

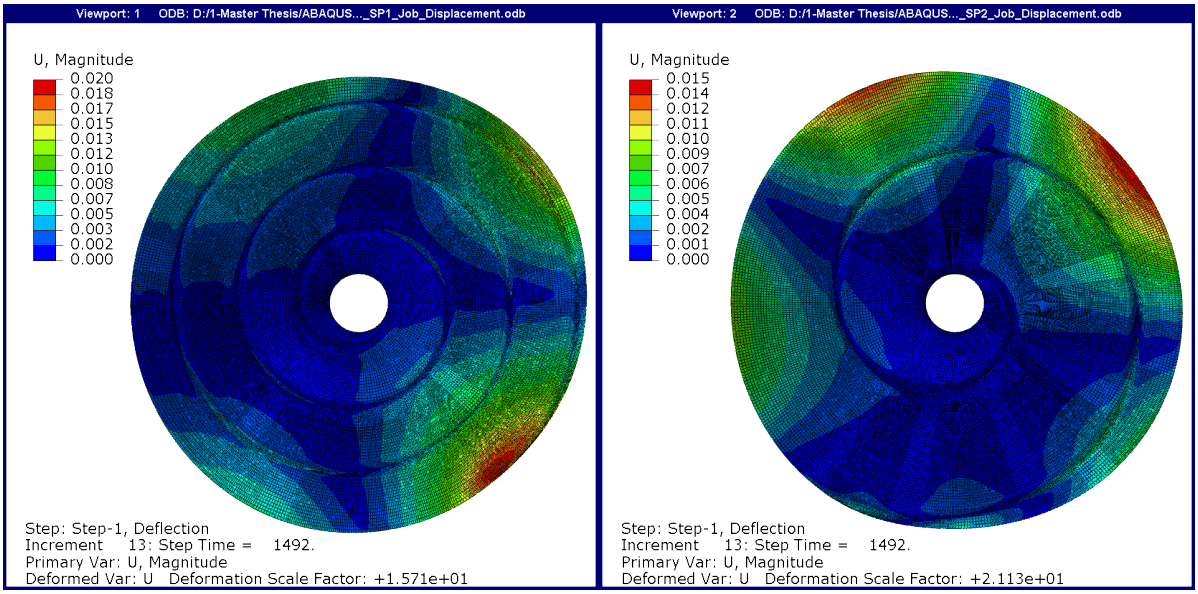

Figure 5.4: SDA with a Spiral Parameter of 0.04 (left) and 0.08 (right)

displacement. An animation of the spiral width study with regards to the temperature can be found here[6], and with regards to displacement can be found here[7].

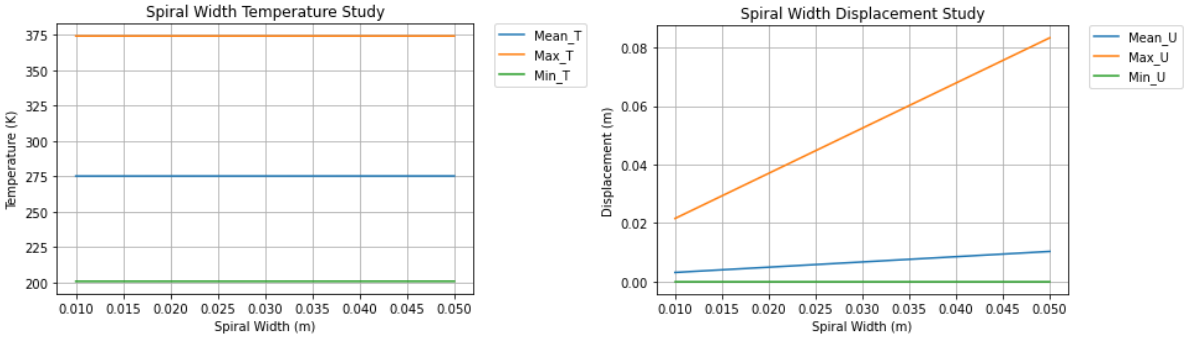

(a) SW Temperature

(b) SW Displacement

Figure 5.5: SW Study

Spiral Conductivity Study

The last parameter that is studied is the conductivity of the zipper. As seen from previous simulations, the Aluminum zipper largely affects the displacement of the reflector. An assumption had been made that to model the SDA, the zipper is going to be made using Aluminum 6063-T6. This zipper is going to be simulated as a band of material that would act as a resistance to the heat flows within the reflector. Another option is quickly looked at where the zipper is defined as CFRP but the conductivity is lowered to act as a contact conductance drop. Figure 5.6 shows the maximum, minimum, and mean values for the temperature and displacement of the CFRP SDA. As the figure shows, the temperature and displacements overall don't seem to vary depending on the conductivity drop at the zipper. This doesn't mean that there is not an effect at the region of the zipper. As shown in Figure 5.7 shows how a step can be seen where the isolines break at the zipper. An animation of the spiral conductivity study with regards to the temperature can be found here[8], and with regards to displacement can be found here[9].

[6]https://imgur.com/a/ozkGqmV
[7]https://imgur.com/a/pq0Hjgr
[8]https://imgur.com/a/m8du2HG
[9]https://imgur.com/a/YY4DOa0

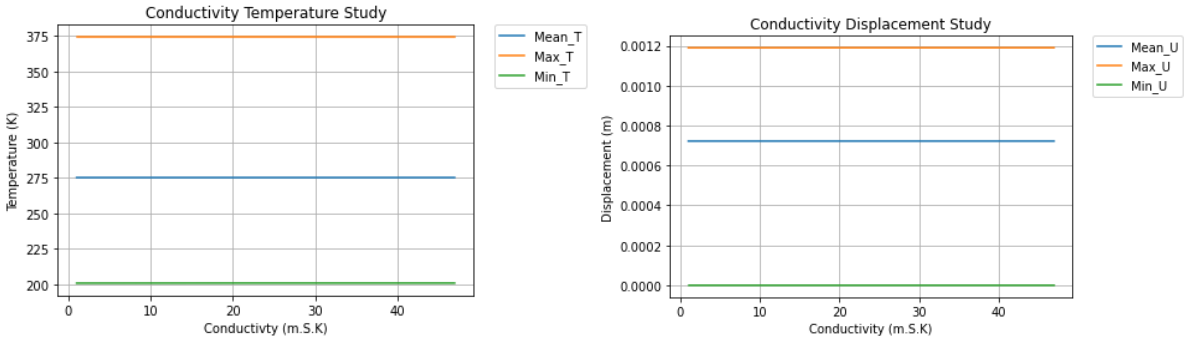

(a) K Temperature

(b) K Displacement

Figure 5.6: Conductivity Study

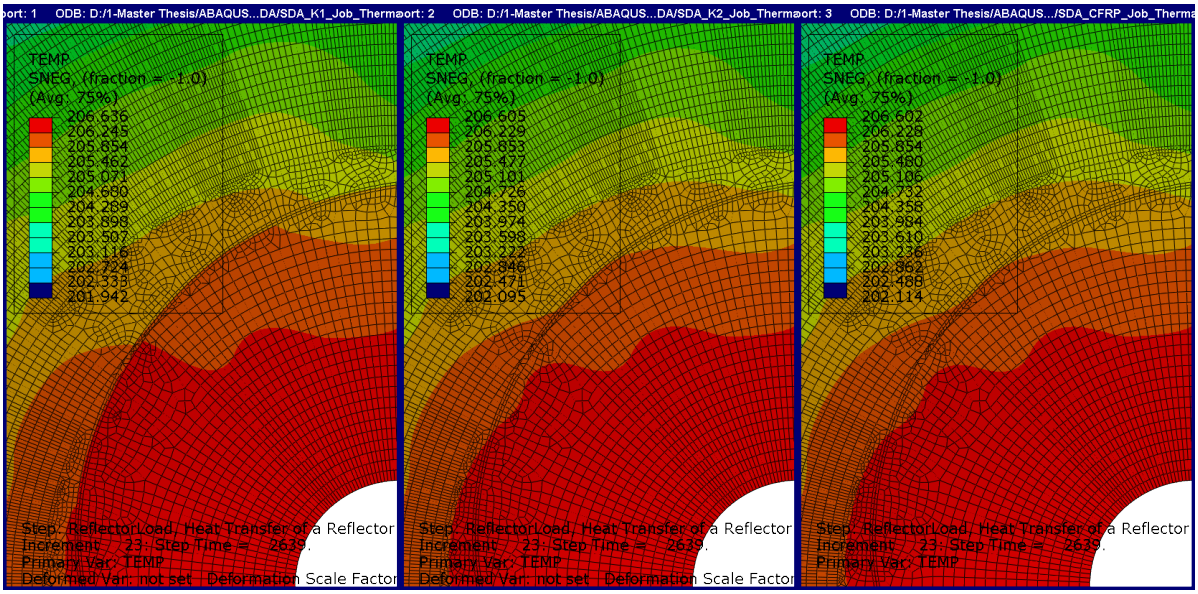

Figure 5.7: CFRP conductivity comparison

6

Radio Frequency Analysis

In this chapter, the effect of the displacement of the SDA on the radio frequency will be studied. Section 6.6.1 introduces some of the theory and equations used to compare the performance of the SDA with regards to Radio Frequency. Section 6.6.2 discusses the different methods that are used to perform the Radio Frequency analysis and the simplifications that are made to come up with a result. Lastly, section 6.6.3 displays the different results obtained for the base SDA model and discusses the results of a slight more performant design as dictated by the results found the in the thermal and thermo-elatsic chapters.

6.1. Radio Frequency Analysis - An Explanation

Due to the complexity of measuring the efficiency of a reflector, and due to the conceptual nature of the SDA, a technique involving predicting the gain of a reflector with regards to reflector surface tolerance is used. This method, created by John Ruze [7], makes a correlation between the surface root mean square (RMS) of the reflector and the gain of the antenna. This correlation is described by Equation6.1:

$$G(\epsilon) = G_0 e^{-(\frac{4\pi\epsilon}{\lambda})^2} \tag{6.1}$$

where ϵ is the surface RMS, λ is the wavelength, and G_0 is the gain of the antenna in the absence of surface error. The surface RMS is defined as the square root of the mean square. As stated by Ruze, this is an allowable approach for a shallow reflector. The RMS can be found using Equation 6.2:

$$x_{RMS} = \sqrt{\frac{1}{n}(x_1^2 + x_2^2 + ... + x_n^2)} \tag{6.2}$$

By using Ruze's Equation, Rochblatt [32] states that a typical spaceborn parabolic antenna reflector is required to have an RMS error of less than $\frac{\lambda}{20}$. This sets a goal to which the SDA can be compared.

6.2. Method Selection

As for the method used to study the impact of the displacement on the reflector, two methods are studied. The first method involved another transfer of the model to a third software called CST Microwave Studio. By being able to model the three dimensional software into a software specifically meant to calculate all the different aspect of the antenna reflector, there is hope that a detailed analysis of the SDA could be done with regards to the Radio Frequency field. Sadly, after many attempts, no successful way is found to properly transfer the model to CST and the method is abandoned. To simplify things, Ruze's approach is used just like had been done in Park's analysis [8]. This meant taking all the displacements for each node and using Equation 6.1 to calculate the RMS values. These RMS values can then be compared to the limit set by Rochblatt to see how the SDA performs.

6.3. Results

Just like in the previous sections, the RMS of the Reflector is compared to a CFRP SDA to study the error caused by the meshing. Figure 6.1 shows the RMS values for the entire orbit of a SDA with aluminum zipper

compared to the Reflector model. In Figure 6.1, similarly to previous comparisons between the Reflector and the SDA, the SDA RMS values are slightly higher than the Reflectors. This is most likely due to the slightly higher displacements that are seen in the thermo-elastic analysis. This is just a continuation of the SDA mesh causing slight error is the SDA model. This error is to be expected and it is a good sign that the RMS values are not excessively higher for the SDA than the Reflector.

Figure 6.1: RMS error

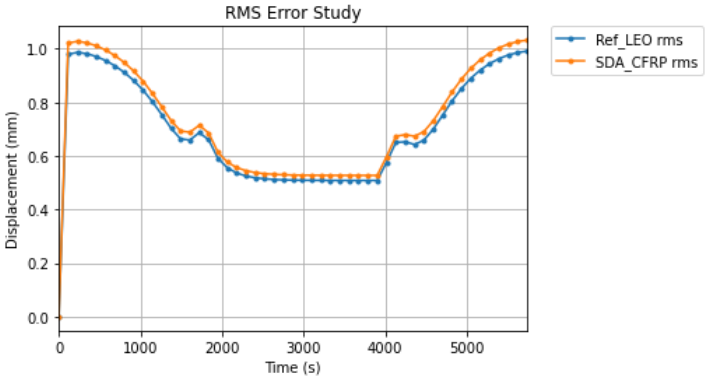

The next step is to take the RMS values and use them as an indicator of the reflectors ability to perform. This is possible because from Equation 6.1, where minimizing the Surface RMS error is the best way of improving the gain of the reflector. This process is similar to that taken by Park. Figure 6.2 shows the maximum RMS values found over an entire orbit for the LEO, Summer, and Winter Cases of the SDA compared to the Reflector LEO case. The maximum RMS over the entire orbit is used as it represented the worst case for the reflector and therefore would be a defining parameter in deciding if the reflector fulfilled any gain requirement. Due to not having any requirement yet for the reflector, the Rochblatt limit of $\frac{\lambda}{20}$ is used as the parameter to judge the Reflector. Just like in Park's analysis, a few points are added to the RMS plot to show the $\frac{\lambda}{20}$ limit. To also visualize the performance of the reflector, other limits are placed to show different ranges of performance. These point are then calculated for the mean frequency of the frequency bands (L, S, C, Ku, Ka) and are set to be: $\frac{\lambda}{15}$, $\frac{\lambda}{30}$, $\frac{\lambda}{50}$. The lower the $\frac{\lambda}{NUMBER}$ the better the performance of the reflector.

Looking at Figure 6.2 it is clear that the SDA with an Aluminum zipper would not be able to perform in space due to the displacements it would experience. There is a clear jump from the max RMS of the Reflector compared to the SDA value, with the Aluminum zipper SDA having an RMS value of 6mm while the Reflector's max RMS is around 1mm. One can also see that the max RMS for the LEO, Summer, and Winter case for the SDA are very similar. This is explained due to the fact that our current model has always pointed to maximum displacement taking place at the locations of maximum temperature as is consistent with the equations used. Each of these cases experience similar maximum temperatures with the maximum temperatures of the LEO, Summer, and Winter cases being respectively 376.2, 362.3, and 359.4K. Looking at the max RMS of the Reflector model, it shows that it is capable of performing under the $\frac{\lambda}{20}$ limit up until the Ku band at which point it is just above the limit. For a reflector modelled without any ribs or thermal control methods, this is already fairly impressive performance, and a good comparison between the SDA and a model without any zipper. It also does show the impact of the high displacement caused by the CTE mismatch impacts the reflector greatly.

In an attempt to look at the SDA without the cross pattern, a separate case is created to try and show a better case for the SDA. In this case, called SDA Improved, results from chapter 5 are used at the researchers discretion to try and improve the SDA model's design and find a way to mitigate the CTE mismatch effects. The first main difference is that the zipper is switched to a CFRP with a very low conductivity to still simulate the interface. A Silicon Dioxide coating is then used due to its capacity of lowering the rate of change in temperature, and the spiral parameter is lowered to 0.04 which showed better displacement performance. Lastly, the thickness is raised to 1mm to give more stiffness to the band. Note, that even though the model is named SDA Improved, no optimization process is performed to find the best design for the SDA.

Figure 6.2: RMS Study

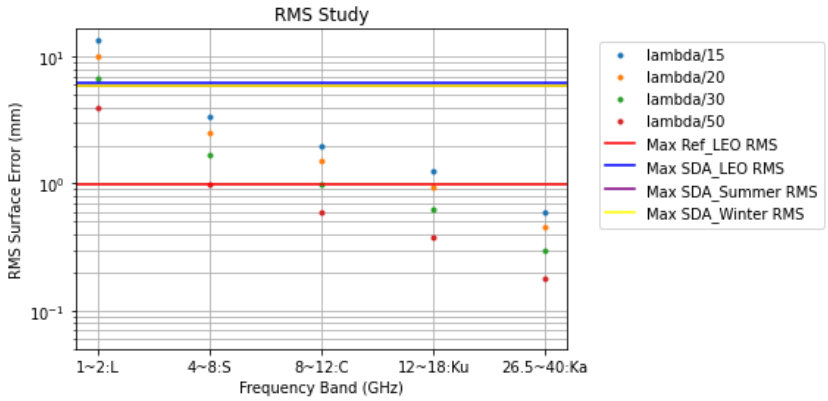

Figure 6.3 shows the results of the maximum RMS of the SDA improved. Even with this case, the SDA is only able to perform within the $\frac{\lambda}{20}$ in the Ku range. This is similar to the Reflector model and shows that with proper design considerations, the SDA's performance can be seriously improved to match a normal reflectors performance. What is also shown in Figure 6.3 is the results of the Reflector in T.Park's analysis. It can be shown how the T.Park petal reflector's performance has a much better performance than the SDA and the SDA improved. This goes to show that the design of the SDA still has improvements to be made for it to be able to perform similarly to reflectors that have gone through many more design iterations than the SDA.

Figure 6.3: RMS1 Study

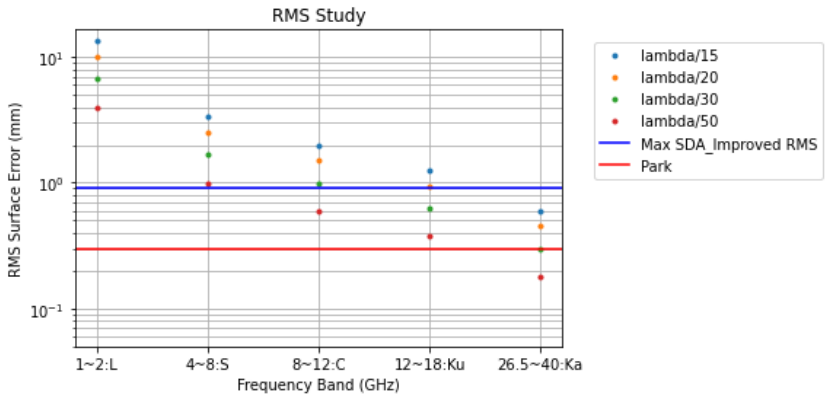

7

Discussion and Conclusion

In this chapter an overall discussion of the SDA and its performance in the thermal environment of space is discussed.

7.1. Overall Performance of the SDA

Reflectors are affected by many different parameters in space but also need to be able to properly perform to reflect the incoming signal to the desired location. This thesis looked to study the effects of the thermal environment on the reflectors performance and has been able to consistently set up a thermal and thermo-elastic model to find the temperature and following displacement field on the reflector. Different low earth orbits have been considered and shown how a reflector can experience large changes of temperature with a change of temperature of 100K in less than 100s for a reflector with a CFRP coating. A silicon dioxide and white paint coatings are also studied to compare the performance of a reflector and confirmed that the white paint coating lowered the temperature range experienced by the reflector, while the silicon dioxide coating caused the reflector to be less reactive to temperature changed.

To perform the thermo-elastic analysis a transfer of the thermal results to a FEM software had to be done. Using a python script [10] to transfer and build the models, the results have shown that similar results as those obtained in the thermal anlysis can be obtained in the new process. Problems did arise when building the SDA model. Meshing of the SDA model is found to be difficult and even after many different attempts to mesh the reflector has shown to have distorted elements. To be able to judge the error that is caused by the mesh, the SDA CFRP model is used and then compared to a Reflector model. It is shown that the SDA model had slightly higher temperatures than the Reflector model. This error in temperature never exceeded more than 2.9K and therefore the SDA model is still deemed appropriate enough from a thermal stand point.

Using the same python script, a thermo-elastic model is created to see the displacement across the reflector. Once again the SDA model is compared to a Reflector model and showed a similar shift in the results due to meshing and the continuation of the error from the thermal model. This error is never more than 0.08mm in the deflection and therefore is deemed to be insignificant enough to which a conclusion could not be made. The main issue observed with the SDA is the presence of a cross pattern that would appear due to the CTE mismatch between the zipper and the bands. This is tested by having a full CFRP model and changing the CTE of the zipper. The further the CTE of the zipper is from that of the band, the more pronounced the cross pattern became. In addition, several other parameters are changed to test different design parameters. The spiral parameter of the SDA is shown to not heavily affect the overall mean displacement and is shown to even limit the high displacements area that seemed to be caused by the geometry of the SDA. Thickness of the SDA is also changed and showed for obvious reasons less displacement for a thicker reflector.

Using surface RMS as a means to judge the performance of the SDA, it is shown that for a SDA with Aluminum zipper, the displacements caused for this size of a reflector are much higher than a same reflector without the spiral zipper (6mm vs 1mm rms). This is once again due to the cross pattern and the high displacement areas caused by the presence of the zipper and the CTE mismatch. A last model is then performed

with a low conductivity CFRP zipper to still simulate the thermal contact conduction between the bands, which showed a already much better performance of 0.85mm. Comparing this surface rms to that obtained in Parks analysis for his petal reflector, the current model of the SDA seems to still have much more displacement and therefore a large loss in gain.

It is important to note that this thesis is an initial dive into the thermal performance of the SDA for space. As the SDA is still a concept no real design has been issued and therefore many other aspect of the SDA still have to be studied. Currently, what has been shown is the serious effects caused by CTE mismatching of the zipper and the bands, and how the geometry of the zipper may cause very high displacement regions which seriously impact the performance of the reflector. As easy as it might be to just use the same material for the zipper and the band, a material will have to be found that is flexible enough for the band to be able to role up but also stiff enough to be able to survive the stress caused by thermal deformation at the zipper region.

7.2. Creation of a Tool

It is hard to state currently that the SDA technology cannot perform in the thermal environment of space due to the many parameters that can affect its performance. The analysis shown throughout this thesis has given pointers in which the SDA design can be improved to survive thermal loading. Because of the possibility of change to the SDA and in the eventuality of a mission design being provided, the process outlined in this thesis can be used to judge the performance of the SDA in space. The python scripts [10] used to transfer ESATAN data to ABAQUS, and then build the ABAQUS models, can be used as a base to build more intricate thermal analyses for the SDA and its use in space. Currently the model that is being simulated is a good model to judge the concept of the SDA in the thermal environment of space but not that for a detailed design.

Over the course of this thesis, over 3000 lines of python code [10] have been written to transfer data between ESATAN and ABAQUS, build a Reflector and SDA models, run and output results for both models, and finally take the displacement and temperature data and output a number of plots and results for each model created. Overall, these lines of code have been split in 3 different files: SDA, Reflector, and Output Script. Even though there are similitude between the Reflector and SDA code [10], each has been created to be able to run separately with variable user input. Each of these 2 scripts are capable of retrieving different ESATAN models, build the thermal and thermo-elastic models at the discretion of the user, run the models, and output report files. The Output Script uses a class structure to be able to read both ESATAN and ABAQUS results and output a variety of different plots showing the effects of the temperature field on the displacement of the reflector and the corresponding surface RMS.

7.3. Limitations of the Analysis

A few limitations are found to performing a detailed analysis for the SDA with regard to the space thermal environment.

The first limitation is the conceptual nature of the SDA. As discussed in section 3.1.2 the thermal analysis process is iterative and last during the entire design phase of the satellite. The stage at which the current SDA technology is, leaves many options for parameters that can be changed and makes it very difficult to give an initial direction to the analysis. To remedy this, this thesis decided to use similar materials and coatings as described in previous literature and used an Aluminum zipper and CFRP band. Throughout this analysis, the effect of choosing these materials has heavily impacted results and has made analysis of results less certain. To try and remedy this, a simple parametric analysis is performed but did not encompass the entire domain of different variables that can be changed for the SDA. This also means that the conclusion that have been made for this design of the SDA do not point to an optimized model but to that of the model selected at the researchers discretion.

A second limitation of the analysis is the detail in which each field of research is tackled. As has been shown for this thesis, to properly analyse the impact of the thermal environment, thermal, structural, and radio frequency engineering is required. These are large fields of research that all bring their own intricacies to the analysis. Many simplifications had to be made to be able to be able to come up with the results obtained in

this thesis and each may be affected by deepening the level of research in each field. Overall, the results obtained are still a good indicator of what would happen for the SDA but do not necessarily catch the intricacies a zipper type of inter-band connector might have on the displacements of the reflector.

7.4. Answering Research Questions

The following research questions are posed at the start of this thesis. Here are shortened answers for each following question:

SQ1: What temperature fields may be expected on a reflector orbiting Earth?

Throughout the analysis, the temperatures experienced by the reflector are heavily reliant on the coating, material property, and orbital parameters chosen for the reflector. For the SDA analysed with an Aluminum zipper, the reflector experienced temperatures ranging from 175K to 375K with temperature changes of almost 100K in less than 100s. It has also been shown how the reflector if always pointing to Earth can also have differences of 93K on the reflector at a single time.

SQ2: How does the zipper interface impact the temperature field on the reflector?

To simplify the modelling of the SDA, the zipper interface is simplified to a band of material on the reflector. The impact of the zipper interface on the reflector are found to be minimal to the overall temperature ranges experienced by the reflector. Due to there being no internal energy generated on the reflector, the zipper acted, as expected, as a resistance to the flow of heat within the reflector. The impact of the zipper to the thermal field is also highly driven by the choice of material used for the zipper and the band. It is found that the lower the conductivity the zipper had, the more the thermal isolines are broken at the location of the zipper and therefore caused localised areas of higher temperature gradient. It is also shown how the impact of this step in temperature is mostly found in regions of large temperature change throughout the orbit of the satellite. The specific heat of the material is also shown to be able to affect the temperature field. As per the definition of the specific heat, the higher the specific heat, the longer it took for the zipper to change temperature. This is mostly observed during times in the orbit with large temperature on the reflector.

SQ3: How does the temperature field experienced by a reflector affect the deformation of the SDA?

Looking at the displacement fields of the different reflector, it can be shown how the reflector's shape experiences a small saddling effect as described in literature[9]. This means that one side of the reflector will experience bending across a certain axis as the thermal loading across the reflector grows. It has also been shown how this saddling effect is limited if the reflector is pointing consistently at or away from the reflector at all times. When comparing the base reflector model to that seen in the literature, the displacements are relatively high with displacement of 1.2mm. It has to be noted though that the model of the Reflector has no backing structure or other means of forcing shape and therefore is expected to be high. It has to be noted that the literature has also shown similar results of 1.1mm displacement[9] for a complex solid reflector. Displacement is , as expected, limited by changing material and by also making the cross section of the reflector thicker. lastly, as expected, the maximum displacement value are found to be during maximum temperature moments of the reflector in orbit.

SQ4: How does the zipper interface impact the deformation of the reflector?

The base SDA model that is designed with an Aluminum zipper and CFRP band shows signs of much higher deflection with max displacements of 20mm. What is interesting to see though is that these high displacement areas are localized to 2 regions. No explanation has been found for these localized regions of high displacement but can maybe be explained by the geometry of the spiral zipper impacting the deformation of the reflector or by the CTE mismatch. It has also been shown how a cross pattern appears on the reflector that has also been explained by CTE mismatch between the band and the zipper. This cross pattern has been shown to be present throughout the entire orbit of the reflector and has displacement values change with accordance to the temperature change on the reflector. This has mostly shown how sensitive the parabolic reflector shape can be to the presence of the spiral zipper with a different CTE than the band. Interestingly,

the comparison between mean and max displacement of the SDA and Reflector are found to be less big for the mean displacement than the max displacement. This goes to show that the mean displacement is largely driven by these high displacement regions. When looking at a full CFRP with a low conductivity zipper, the cross pattern and the high displacement regions disappeared and caused the maximum displacement of the reflector to match that of the SDA CFRP (which has matching conductivity between band and zipper). This doesn't mean though that the stresses on the zipper do not differ as it has been shown how with lower conductivity, the temperature profile does change a specific regions of the zipper. In conclusion, the zipper highly impacts the reflector if made out of a different material and also leads to higher localised stress regions at certain zipper locations as shown in Figure 5.7.

SQ5: How does the deformation of the SDA impact its performance?

It has been shown using the Ruze equation how the gain is affected by surface RMS. Using the limits set by Rochblatt of $\frac{\lambda}{20}$, the RMS values of the Reflector and SDA model are compared for different frequency bands and is shown that the SDA had a much higher RMS than the Reflector model. The low conductivity CFRP SDA is also compared and shown to have a lower surface RMS of 1mm. This would make the SDA be able to perform for a Ku band incoming frequency signal. This shows how the SDA has very poor performance when CTE mismatch is involved but can have similar performance as the Reflector model.

RQ: Would an asymmetric spiral band parabolic reflector with a inter-band zipper interface properly perform with regards to the space thermal environment?

The current base model of the SDA (aluminum spiral interface) would not, under the limits set by Rochblatt, properly perform as a reflector due to the 20mm max displacement regions seen throughout the orbital period. It has been shown that by matching the CTE of the spiral interface and reflector band, the small effects caused by the spiral interface are not large enough to impact the deformations more than those seen on the normal reflector.

7.5. Recommendations for Further Analysis

There are many step that can be taken to further improve the analysis of the SDA with regards to the space thermal environments.

The first aspect to consider is a more detailed analysis of the zipper interface region. This would mean modelling different zipper designs and checking how stresses caused by thermal strain impact the zipper. It would also be interesting to model it with regards to contact conductivity. As contact conductivity is pressure driven in space, it would be interesting to see how when the thermal changes causes the strain at the zipper to try and separate, it might also impact the conductivity and therefore make the change in thermal strain less linear. Lastly, by having a better design if the zipper, more lateral displacement can be analysed to show if there could be uncoupling of the zipper because of high thermal strain. Overall, getting a more detailed analysis of the zipper region may lead to better material choice decisions, as the SDA still needs to be able to roll up while being rigid enough to keep it shape, and also have the zipper maintain its hold.

The second aspect to be considered is to improve the parametrization scheme that is started in the thermoelastic chapter. Currently, 2 other points are often used to see the trend in temperature and displacement when changing different variables. Improving the scripts [10] may allow for more in depth parametrizations scheme to be done and give a better image of ways of improving the design of the SDA. This could also lead to optimization schemes pointing to the best way to design the SDA with regards to different user inputs.

The third aspect to improve on, would be to find a way of improving the meshing of the SDA. As discussed, the current model still shows distorted elements which have shown to impact the overall results slightly. By maybe using meshing software, a better model could be created for the SDA.

The fourth step that could be taken would be to have a more detailed modelling of the material properties for the different parts of the reflector. Currently, all materials are isotropically defined but seeing as a CFRP material is used for the band, a model could be made to show the impact of the way fibre layering direction

scheme has on the displacement of the reflector. This could also be done for the way the CTE is defined as most materials do not have constant CTEs over temperature ranges. These could be added to the model to improve the accuracy of the model.

Fifthly, different designs of the band could be studied to see if honeycomb structures or other stiffening methods could be incorporated to the SDA. This would allow for an interesting design problem as each method tested out would have to be fold-able and would most likely have to use origami engineering techniques. By looking to incorporate these techniques, it would be interesting to see how folds and origami techniques affect the heat flow through the materials.

Sixthly, a model of the SDA could be tested in real life to see how it compares to the results obtained through out this thesis. By testing the SDA in thermal chambers, the effect of the zipper could be better defined and then modelled in the python scripts. This would also serve as a validation of the work performed through this thesis and could also point to an errors made with assumptions.

The last and probably most important aspect to improve on would be to perform a pre tensioning analysis on the reflector to be able to model the tensioning of the SDA caused during deployment. As discussed by Yellowhorse, the SDA would be tensioned into its shape when deployed. The stress in the reflector would then have to be added to the current model and show how it impacts the overall analysis. With the addition of the stress caused during deployment, the SDA may be able to show better performance as the current model starts from an un-tensioned state. The pre tensioning of the SDA could counteract the thermal strain, but would cause higher stresses within the zipper region. To be able to take full advantage of this analysis, the first step ,of improving the zipper analysis, must be performed to show how the material chosen for the band deals with the high stress.

7.6. Conclusion

This thesis looked to study the effect of the thermal environment on the SDA reflector that was conceptualised in "SELF-ASSEMBLING KIRIGAMI STRUCTURES" by Yellowhorse [2]. After an extensive literature review [5], the following research question was asked: Would an asymmetric spiral band parabolic reflector with a spiral inter-band interface properly perform with regards to the space thermal environment?

Throughout this thesis report, a methodology is described which allowed for the successful study of an SDA over different orbits by using ESATAN-TMS, ABAQUS, and python scripting. This methodology allowed for the temperature mapping of an SDA for a summer, winter, and equatorial LEO orbits. This resulted in finding temperature ranging from 175K to 375K with temperature changes of 100K in less than 100s. The reflector was also shown to, at its worst, have a 93K temperature delta on the reflector at a single time. The effect of the spiral interface was found to be minimal with regards to overall temperature experienced by the reflector and only created slightly higher temperature deltas at the spiral interface during moment of rapid temperature change. This effect was exacerbated as the gap of the spiral interface grew.

When studying the displacement of the reflector with regards to temperature, the basic Reflector model was found to experience maximum displacements of 1.2mm while the SDA experienced displacements of 20mm. This maximum displacement was found at moments of maximum temperature on the reflectors but did not necessarily coincide with location of maximum temperature. The spiral interface cause the SDA reflector to displace in a cross pattern and would often stay locked in that position with the magnitude of displacement still varying during orbit. The maximum displacement regions of the SDA often coincided near the end of the band but no direct correlation could be found in predicting the exact region of the maximum displacement when the geometry of the reflector and the spiral interface were changed. The forming of the cross pattern was found to be caused by the CTE mismatch caused by the researchers decsion to have the base SDA model have an Aluminium spiral interface and a CFRP band. A parametrization study has shown that by matching the CTE, there is a minima difference between the SDA and Reflector models.

The effects of the high displacement region are propagated through the RMS study of the reflector. Using surface RMS as a comparison parameters to judge the reflector performance, it is shown that the SDA does not meet the $\frac{\lambda}{20}$ limit set by Rochblatt [32]. The SDA is shown the have a maximum surface RMS of 6mm

while the Reflector model has a maximum surface RMS of 1mm. Similarly to the displacement study, it has been shown that the RMS of the SDA lowers to 1mm when the CTE of the spiral interface and the band match. This shows that the spiral interface effects can be limited to the point where it performs similarly to a basic reflector. It is important to still note that the 1mm displacement shows that the reflector still does not perform as well as reflector seem in literature.

The answer to the research question is that the base model of the SDA studied throughout this thesis would not properly perform with regards to the thermal environment as a cross pattern displacement region would form and a high displacement would distort incoming signals. This answer does not conclude on the overal judgement of the SDA with regards to the thermal environemtn as it has been shown that the SDA's performance can be significantly improved just be means of matching the CTE of the materials across the reflector. Finally, it is important to still note the assumptions made through this analysis as many points listed out in section 7.7.5 could still lead to further improvement of the SDA's performance.

Bibliography

[1] P. Salvador. Europe Cities. July 11, 2022. URL: https://europe-cities.com/2022/07/11/james-webb-telescope-the-most-distant-image-of-the-universe-unveiled-at-the-cite-de-lespace-in-toulouse/.

[2] A. Yellowhorse. "SELF-ASSEMBLING KIRIGAMI STRUCTURES". In: (), p. 7.

[3] S. Satter. *PASS Spacecraft Antenna Technology Study*. Aug. 1, 1991.

[4] J. Meseguer. *Spacecraft Thermal Control*. Woodhead Publishing in Mechanical Engineering. Oxford ; Philadelphia: Woodhead Pub, 2012. 382 pp. ISBN: 978-1-84569-996-3.

[5] N. van der Wielen. *Thermal Robustness of a Spiral Dish Antenna Reflector*.

[6] W. Boyer. "Large Space Antenna Systems Technology, 1984". In: NASA Langley Research Center Hampton, VA, United States: NASA, Apr. 1, 1985. URL: https://ntrs.nasa.gov/citations/19850015502 (visited on 06/23/2021).

[7] J. Ruze. "Antenna Tolerance Theory—A Review". In: *Proceedings of the IEEE* 54.4 (1966), pp. 633–640. ISSN: 0018-9219. DOI: 10.1109/PROC.1966.4784. URL: http://ieeexplore.ieee.org/document/1446714/ (visited on 05/25/2022).

[8] T. Park. "Thermal Design and Analysis of Unfurlable CFRP Skin-Based Parabolic Reflector for Spaceborne SAR Antenna". In: *International Journal of Aeronautical and Space Sciences* 22.2 (Apr. 2021), pp. 433–444. ISSN: 2093-274X, 2093-2480. DOI: 10.1007/s42405-020-00301-7. URL: https://link.springer.com/10.1007/s42405-020-00301-7 (visited on 03/14/2022).

[9] R. Sharp. *Thermal Distortion Analysis of Antennas in Space*. 1989.

[10] N. van der Wielen. *Python Scripts for Themoelastic Analysis of SDA*. Delft, Netherlands: TU Delft, 2022. URL: https://doi.org/10.4121/20398698.

[11] *Compliant Mechanism Research*. compliantmechanism.byu. URL: https://www.compliantmechanisms.byu.edu/ (visited on 01/06/2021).

[12] D. Hilbert. *Geometry and the Imagination*. New York: Chelsa Publishing Company, 1990. ISBN: 978-0-8284-1087-8.

[13] Y. Lu. "A Review of the Space Environment Effects on Spacecraft in Different Orbits". In: *IEEE Access* 7 (2019), pp. 93473–93488. ISSN: 2169-3536. DOI: 10.1109/ACCESS.2019.2927811. URL: https://ieeexplore.ieee.org/document/8758870/ (visited on 06/08/2021).

[14] K. Chang-sung. "Fast Intra-Prediction Model Selection for H.264 Codec". In: ITCom 2003. Orlando, FL, Nov. 19, 2003, p. 99. DOI: 10.1117/12.511393. URL: http://proceedings.spiedigitallibrary.org/proceeding.aspx?doi=10.1117/12.511393 (visited on 06/10/2021).

[15] D. Bhanderi. "Modeling Earth Albedo for Satellites in Earth Orbit". In: *AIAA Guidance, Navigation, and Control Conference and Exhibit*. AIAA Guidance, Navigation, and Control Conference and Exhibit. San Francisco, California: American Institute of Aeronautics and Astronautics, Aug. 15, 2005. ISBN: 978-1-62410-056-7. DOI: 10.2514/6.2005-6465. URL: https://arc.aiaa.org/doi/10.2514/6.2005-6465 (visited on 06/10/2021).

[16] X. Wu. "Surface Temperature and Infrared Feature of a Satellite". In: 40 (May 2011).

[17] M. Finckenor. *A Researcher' Guide to: International Space Station*. URL: https://www.nasa.gov/sites/default/files/files/NP-2015-03-015-JSC_Space_Environment-ISS-Mini-Book-2015-508.pdf (visited on 07/06/2021).

[18] C. Liu. "Distributed State Estimation for Networked Spacecraft Thermal Experiments Over Sensor Networks With Randomly Varying Transmission Delays". In: *IEEE Access* 6 (2018), pp. 56658–56665. ISSN: 2169-3536. DOI: 10.1109/ACCESS.2018.2872780. URL: https://ieeexplore.ieee.org/document/8476559/ (visited on 06/10/2021).

[19] A. Phoenix. "Adaptive Thermal Conductivity Metamaterials: Enabling Active and Passive Thermal Control". In: *Journal of Thermal Science and Engineering Applications* 10.5 (Oct. 1, 2018), p. 051020. ISSN: 1948-5085, 1948-5093. DOI: 10.1115/1.4040280. URL: https://asmedigitalcollection.asme.org/thermalscienceapplication/article/doi/10.1115/1.4040280/448132/Adaptive-Thermal-Conductivity-Metamaterials (visited on 06/10/2021).

[20] J. Liu. "Modeling and Analysis of MEMS-based Cooling System for Nano-Satellite Active Thermal Control". In: *2008 2nd International Symposium on Systems and Control in Aerospace and Astronautics*. 2008 2nd International Symposium on Systems and Control in Aerospace and Astronautics (ISSCAA). Shenzhen, China: IEEE, Dec. 2008, pp. 1–6. ISBN: 978-1-4244-2385-9 978-1-4244-3908-9. DOI: 10.1109/ISSCAA.2008.4776207. URL: http://ieeexplore.ieee.org/document/4776207/ (visited on 06/10/2021).

[21] X. Xeng. "Thermal Analysis Of Space Inflatable Deployment Scelerosis Film Antenna Structures". Shanghai, China: Shanghai Jiao Tong Univ., 2011.

[22] C. Wiley. "Synthetic Aperture Radars". In: *IEEE Transactions on Aerospace and Electronic Systems* AES-21.3 (May 1985), pp. 440–443. ISSN: 0018-9251. DOI: 10.1109/TAES.1985.310578. URL: http://ieeexplore.ieee.org/document/4104077/ (visited on 05/25/2022).

[23] *AE1222-II: Aerospace Design & Systems Engineering Elements I*. 2018.

[24] G. Lu. "Studies of Thermal Deformation and Shape Control of a Space Planar Phased Array Antenna". In: *Aerospace Science and Technology* 93 (Oct. 2019), p. 105311. ISSN: 12709638. DOI: 10.1016/j.ast.2019.105311. URL: https://linkinghub.elsevier.com/retrieve/pii/S1270963818322557 (visited on 03/08/2021).

[25] G. Rogers. "Heat Transfer". In: *International Journal of Heat and Mass Transfer* 5.1-2 (Jan. 1962), p. 101. ISSN: 00179310. DOI: 10.1016/0017-9310(62)90114-X. URL: https://linkinghub.elsevier.com/retrieve/pii/001793106290114X (visited on 06/10/2022).

[26] R. Karam. *Satellite Thermal Control for Systems Engineers*. Reston ,VA: American Institute of Aeronautics and Astronautics, Jan. 1, 1998. ISBN: 978-1-56347-276-3 978-1-60086-652-4. DOI: 10.2514/4.866524. URL: https://arc.aiaa.org/doi/book/10.2514/4.866524 (visited on 05/22/2022).

[27] ITP Engines. *ESATAN-TMS Thermal User Manual*. 2017.

[28] ITP Engines. *ESATAN-TMS Thermal Engineering Manual*. 2015.

[29] M. Smith. *ABAQUS/Standard User's Manual, Version 6.9*. United States: Dassault Systèmes Simulia Corp, 2009.

[30] D. Fixsen. "THE TEMPERATURE OF THE COSMIC MICROWAVE BACKGROUND". In: *The Astrophysical Journal* 707.2 (Dec. 20, 2009), pp. 916–920. ISSN: 0004-637X, 1538-4357. DOI: 10.1088/0004-637X/707/2/916. URL: https://iopscience.iop.org/article/10.1088/0004-637X/707/2/916 (visited on 05/15/2022).

[31] N. Lee. "Effects of Element Distortions on the Performance of Isoparametric Elements". In: *International Journal for Numerical Methods in Engineering* 36.20 (Oct. 30, 1993), pp. 3553–3576. ISSN: 0029-5981, 1097-0207. DOI: 10.1002/nme.1620362009. URL: https://onlinelibrary.wiley.com/doi/10.1002/nme.1620362009 (visited on 03/09/2022).

[32] D. Rochblatt. "Microwave Antenna Holography". In: *IEEE Transactions on Microwave Theory and Techniques* 40.6 (June 1992), pp. 1294–1300. ISSN: 00189480. DOI: 10.1109/22.141363. URL: http://ieeexplore.ieee.org/document/141363/ (visited on 06/04/2022).

[33] *SFU - Space Flyer Unit - Achievements so Far - Japan Space Systems.Url*. J Space systems. URL: https://web.archive.org/web/20160801141025/http://www.jspacesystems.or.jp/en/project/past/sfu/.

[34] D. Martin. *Projects*. JPL Science. URL: https://science.jpl.nasa.gov/projects/Starshade/.

[35] N. Turner. "A Review of Origami Applications in Mechanical Engineering". In: *Proceedings of the Institution of Mechanical Engineers, Part C: Journal of Mechanical Engineering Science* 230.14 (Aug. 2016), pp. 2345–2362. ISSN: 0954-4062, 2041-2983. DOI: 10.1177/0954406215597713. URL: http://journals.sagepub.com/doi/10.1177/0954406215597713 (visited on 06/01/2021).

[36] N. Turner. “A Review of Origami Applications in Mechanical Engineering”. In: *Proceedings of the Institution of Mechanical Engineers, Part C: Journal of Mechanical Engineering Science* 230.14 (Aug. 2016), pp. 2345–2362. ISSN: 0954-4062, 2041-2983. DOI: 10.1177/0954406215597713. URL: http://journals.sagepub.com/doi/10.1177/0954406215597713 (visited on 03/08/2021).

[37] L. Burrows. *Designing a Pop-up Future*. seas.harvard.edu. URL: https://www.seas.harvard.edu/news/2016/01/designing-pop-future (visited on 05/28/2021).

[38] M. Morgan. “Towards Developing Product Applications of Thick Origami Using the Offset Panel Technique”. In: *Mechanical Sciences* 7.1 (Mar. 7, 2016), pp. 69–77. ISSN: 2191-916X. DOI: 10.5194/ms-7-69-2016. URL: https://ms.copernicus.org/articles/7/69/2016/ (visited on 05/26/2021).

[39] S. Perks. *Sleek*. Flat-pack physics. URL: http://live.iop-pp01.agh.sleek.net/2015/11/18/flat-pack-physics/.

[40] S. Zirbel. “Accommodating Thickness in Origami-Based Deployable Arrays1”. In: *Journal of Mechanical Design* 135.11 (Nov. 1, 2013), p. 111005. ISSN: 1050-0472, 1528-9001. DOI: 10.1115/1.4025372. URL: https://asmedigitalcollection.asme.org/mechanicaldesign/article/doi/10.1115/1.4025372/693901/Accommodating-Thickness-in-OrigamiBased-Deployable (visited on 05/26/2021).

[41] M. Yim, ed. *Origami 5: Fifth International Meeting of Origami Science, Mathematics, and Education*. A K Peters/CRC Press, June 21, 2011. ISBN: 978-1-56881-714-9 978-1-4398-7350-2. DOI: 10.1201/b10971. URL: http://www.crcnetbase.com/doi/book/10.1201/b10971 (visited on 05/26/2021).

[42] C. Hoberman. “REVERSIBLY EXPANDABLESTRUCTURES”. Pat.

[43] C. Hoberman. “Folding Structures Made of Thick Hinged Sheets”. U.S. pat. 7,794,019 B2. Sept. 14, 2010. URL: https://patents.google.com/patent/US7794019B2/en (visited on 02/06/2021).

[44] Z. Abel. “RIGID ORIGAMI VERTICES: CONDITIONS AND FORCING SETS”. In: (), p. 14.

[45] Y. Chen. “Origami of Thick Panels”. In: *Science* 349.6246 (July 24, 2015), pp. 396–400. ISSN: 0036-8075, 1095-9203. DOI: 10.1126/science.aab2870. URL: https://www.sciencemag.org/lookup/doi/10.1126/science.aab2870 (visited on 05/26/2021).

[46] R. Lang. “Rigidly Foldable Thick Origami Using Designed-Offset Linkages”. In: *Journal of Mechanisms and Robotics* 12.2 (Apr. 1, 2020), p. 021106. ISSN: 1942-4302, 1942-4310. DOI: 10.1115/1.4045940. URL: https://asmedigitalcollection.asme.org/mechanismsrobotics/article/doi/10.1115/1.4045940/1072472/Rigidly-Foldable-Thick-Origami-Using-Designed (visited on 05/26/2021).

[47] R. Lang. *Origami in Action: Paper Toys That Fly, Flap, Gobble, and Inflate!* 1st St. Martin’s Griffin ed. New York: St. Martin’s Griffin, 1997. 157 pp. ISBN: 978-0-312-15618-3.

[48] J. Shafer. *Origami to Astonish and Amuse*. 1st ed. New York: St. Martin’s Griffin, 2001. 251 pp. ISBN: 978-0-312-25404-9.

[49] J. Shafer. *Origami Ooh La La! Action Origami for Performance and Play*. Charleston, 2011. ISBN: 978-1-4564-3964-4.

[50] S. Guest. “INEXTENSIONAL WRAPPING OF FLAT MEMBRANES”. In: (1992), p. 12.

[51] R. Lang. “Single Degree-of-Freedom Rigidly Foldable Cut Origami Flashers”. In: *Journal of Mechanisms and Robotics* 8.3 (June 1, 2016), p. 031005. ISSN: 1942-4302, 1942-4310. DOI: 10.1115/1.4032102. URL: https://asmedigitalcollection.asme.org/mechanismsrobotics/article/doi/10.1115/1.4032102/441838/Single-DegreeofFreedom-Rigidly-Foldable-Cut (visited on 05/26/2021).

[52] *James Webb Space Telescope*. Jwst.nasa.gov. May 31, 2021. URL: https://jwst.nasa.gov/content/features/origami.html.

[53] T. Shyu. “A Kirigami Approach to Engineering Elasticity in Nanocomposites through Patterned Defects”. In: *Nature Materials* 14.8 (Aug. 2015), pp. 785–789. ISSN: 1476-1122, 1476-4660. DOI: 10.1038/nmat4327. URL: http://www.nature.com/articles/nmat4327 (visited on 03/08/2021).

[54] F. Collins. “Design of a Spherical Robot Arm with the Spiral Zipper Prismatic Joint”. In: *2016 IEEE International Conference on Robotics and Automation (ICRA)*. 2016 IEEE International Conference on Robotics and Automation (ICRA). Stockholm, Sweden: IEEE, May 2016, pp. 2137–2143. ISBN: 978-1-4673-8026-3. DOI: 10.1109/ICRA.2016.7487363. URL: http://ieeexplore.ieee.org/document/7487363/ (visited on 03/08/2021).

[55] B. Tibbalds. “Inextensional Packaging of Thin Shell Slit Reflectors”. In: (2004), p. 10.

[56] S. Guest. “A New Concept for Solid Surface Deployable Antennas”. In: *Acta Astronautica* 38.2 (Jan. 1996), pp. 103–113. ISSN: 00945765. DOI: 10.1016/0094-5765(96)00009-4. URL: https://linkinghub.elsevier.com/retrieve/pii/0094576596000094 (visited on 05/26/2021).

[57] L. Wilson. “Origami Sunshield Concepts for Space Telescopes”. In: *54th AIAA/ASME/ASCE/AHS/ASC Structures, Structural Dynamics, and Materials Conference*. 54th AIAA/ASME/ASCE/AHS/ASC Structures, Structural Dynamics, and Materials Conference. Boston, Massachusetts: American Institute of Aeronautics and Astronautics, Apr. 8, 2013. ISBN: 978-1-62410-223-3. DOI: 10.2514/6.2013-1594. URL: https://arc.aiaa.org/doi/10.2514/6.2013-1594 (visited on 05/27/2021).

[58] E. Gdoutos. “Ultralight Deployable Space Structure Prototype”. In: *AIAA Scitech 2020 Forum*. AIAA Scitech 2020 Forum. Orlando, FL: American Institute of Aeronautics and Astronautics, Jan. 6, 2020. ISBN: 978-1-62410-595-1. DOI: 10.2514/6.2020-0692. URL: https://arc.aiaa.org/doi/10.2514/6.2020-0692 (visited on 05/27/2021).

[59] E. Gdoutos. “Ultralight Spacecraft Structure Prototype”. In: *AIAA Scitech 2019 Forum*. AIAA Scitech 2019 Forum. San Diego, California: American Institute of Aeronautics and Astronautics, Jan. 7, 2019. ISBN: 978-1-62410-578-4. DOI: 10.2514/6.2019-1749. URL: https://arc.aiaa.org/doi/10.2514/6.2019-1749 (visited on 05/27/2021).

[60] M. Arya. “Ultralight Structures for Space Solar Power Satellites”. In: *3rd AIAA Spacecraft Structures Conference*. 3rd AIAA Spacecraft Structures Conference. San Diego, California, USA: American Institute of Aeronautics and Astronautics, Jan. 4, 2016. ISBN: 978-1-62410-394-0. DOI: 10.2514/6.2016-1950. URL: https://arc.aiaa.org/doi/10.2514/6.2016-1950 (visited on 05/27/2021).

[61] D. Williams. “Origami-Inspired Shape-Changing Phased Array”. In: *2020 50th European Microwave Conference (EuMC)*. 2020 50th European Microwave Conference (EuMC). Utrecht, Netherlands: IEEE, Jan. 12, 2021, pp. 344–347. ISBN: 978-2-87487-059-0. DOI: 10.23919/EuMC48046.2021.9338189. URL: https://ieeexplore.ieee.org/document/9338189/ (visited on 05/27/2021).

[62] H. Sawada. “Mission Report on The Solar Power Sail Deployment Demonstration of IKAROS”. In: *52nd AIAA/ASME/ASCE/AHS/ASC Structures, Structural Dynamics and Materials Conference*. 52nd AIAA/ASME/ASCE/AHS/ASC Structures, Structural Dynamics and Materials Conference. Denver, Colorado: American Institute of Aeronautics and Astronautics, Apr. 4, 2011. ISBN: 978-1-60086-951-8. DOI: 10.2514/6.2011-1887. URL: https://arc.aiaa.org/doi/10.2514/6.2011-1887 (visited on 05/31/2021).

[63] A. Yo. “From Origami to Ikaros”. Workshop. URL: https://edu.jaxa.jp/activities/SEEC/material/assets/SEEC27-yo.pdf (visited on 05/31/2021).

A

Meshing Attempts

Table A.1: Meshing Attempts

Description of Mesh Procedure	Global Seed Size	minSizeFactor	b_edges	z_edges	z_int_edges	Number of Elements	Analysis Warning (%)	Analysis Error (%)
Mesh Spiral and then Band	0.01	0.1	0.01	0.01	0.01	100844	0.0247908	0.00
Automated meshing	0.1	0.1	N/A	N/A	N/A	1327	0.979653	0.00
Automated meshing	0.05	0.1	N/A	N/A	N/A	4071	0.663228	0.00
Automated meshing	0.01	0.1	N/A	N/A	N/A	82350	0.0910747	0.00
Automated meshing	0.005	0.1	N/A	N/A	N/A	238388	0.0532745	0.00
Mesh Spiral and then Band	0.1	0.1	N/A	N/A	N/A	1166	1.45798	0.00
Mesh Spiral and then Band	0.05	0.1	N/A	N/A	N/A	3854	0.726518	0.00
Mesh Spiral and then Band	0.01	0.1	N/A	N/A	N/A	90798	0.0484592	0.00
Mesh Spiral and then Band	0.005	0.1	N/A	N/A	N/A	316181	0.0113859	0.00
Mesh Band and then Spiral	0.1	0.1	N/A	N/A	N/A	1208	0.496689	0.00
Mesh Band and then Spiral	0.05	0.1	N/A	N/A	N/A	4096	1.19629	0.00
Mesh Band and then Spiral	0.01	0.1	N/A	N/A	N/A	77924	0.178379	0.00
Mesh Band and then Spiral	0.005	0.1	N/A	N/A	N/A	268042	0.0720036	0.00
Mesh from the Smallest Area to the Largest	0.1	0.1	N/A	N/A	N/A	1327	0.979653	0.00
Mesh from the Smallest Area to the Largest	0.05	0.1	N/A	N/A	N/A	4071	0.663228	0.00
Mesh from the Smallest Area to the Largest	0.01	0.1	N/A	N/A	N/A	82350	0.0910747	0.00
Mesh from the Smallest Area to the Largest	0.005	0.1	N/A	N/A	N/A	238388	0.0532745	0.00
Automated meshing	0.05	0.5	N/A	N/A	N/A	4066	0.713232	0.00
Automated meshing	0.05	0.9	N/A	N/A	N/A	4066	0.713232	0.00
Automated meshing	0.1	0.1	0.02	0.01	0.005	49766	0.436041	0.00
Automated meshing	0.1	0.1	0.1	0.1	0.1	1666	0.720288	0.00
Automated meshing	0.01	0.1	0.1	0.05	0.1	2726	1.06383	0.07
Automated meshing	0.01	0.1	0.1	0.01	0.1	7701	2.84379	0.00
Automated meshing	0.01	0.1	0.05	0.1	0.1	6263	0.574804	0.26
Automated meshing	0.01	0.1	0.01	0.1	0.1	84652	0.164202	0.00
Automated meshing	0.01	0.1	0.1	0.1	0.05	1705	1.23167	0.00
Automated meshing	0.01	0.1	0.1	0.1	0.01	1919	0.833768	0.00
Automated meshing	0.01	0.1	0.1	0.01	0.01	7576	2.48152	0.00
Automated meshing	0.01	0.1	0.05	0.01	0.01	9714	1.72946	0.00
Mesh Spiral and then Band	0.01	0.1	0.05	0.01	0.01	9705	1.74137	0.00

B

Origami and Kirigami Engineering

The space industry has turned to the old art of paper folding to improve and design new mechanisms for space. In 1996, JAXA launched the Space Flying Unit (SFU)[33] that deployed a large 2D array, using an Origami Miura fold, as proof of concept that large structures could be deployed and used in space. More recently, JPL has been working on the Starshade project[34], represented in Figure B.1, which uses a custom Origami fold to deploy an incredibly large 50m structure to shield the light of the Sun to permit telescopes to take pictures of distant stars without getting blinded by the light of our solar system's Star.

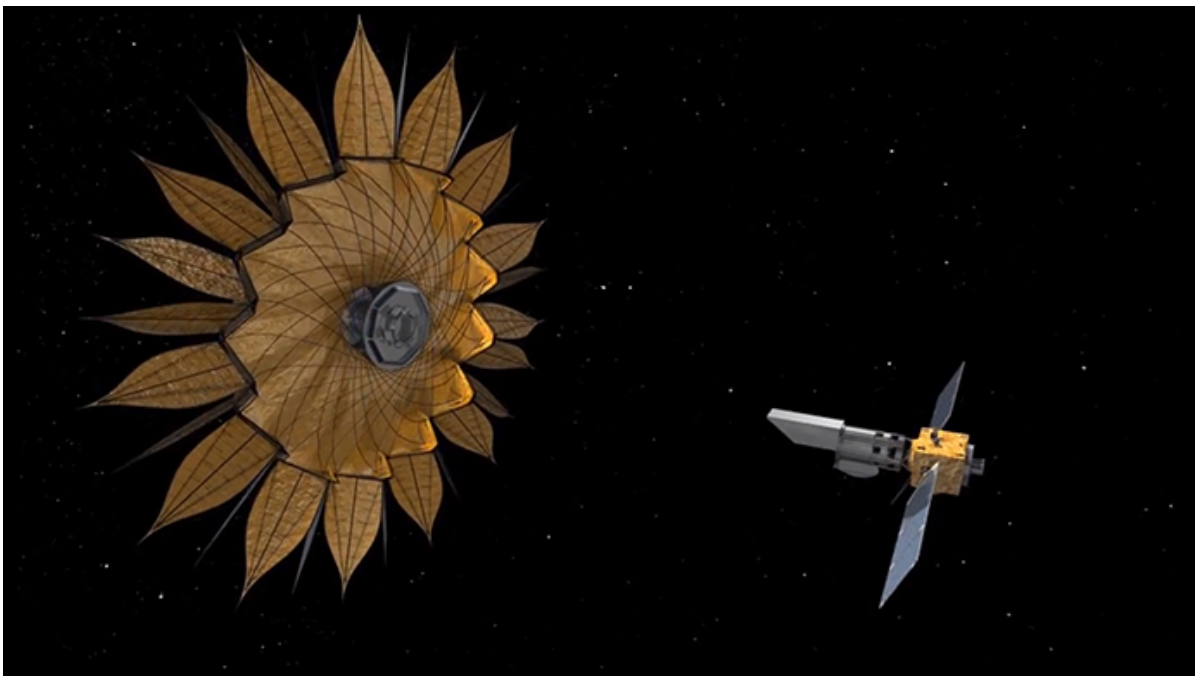

Figure B.1: Concept image of the Starshade [34]

What does Origami really bring to engineering that normal engineering techniques cannot? First, Origami is the art of folding paper; "ori" meaning folded and "kami" meaning paper. This basic technique involves using a flat sheet of paper and folding it into a desired three dimensional shape. Inversely, a bundled-up piece of paper, properly unfolded can become a larger flat surface. This shows how Origami brings a duality to every structure: folded and unfolded. Due to this duality, Origami makes every structure a dynamic one as it has to be able to transition from one form to the other. Even though the order in which each fold is made can be complicated, the mechanism used to transfer from each form is just through the simple actions of folding or unfolding[35][**sorgucORIGAMICSARCHITECTUREMEDIUM**]. As progress has been made to

mathematically predict the sequence and location of the folds, it has become much easier to create a mechanism using Origami to fulfil specific needs. This is one of the reasons why Origami has been seen as a possible engineering tool for space missions which require well rounded technologies.

One of the most important contributors in the field of Space Origami is Koryo Miura. Many attribute the rise in use of Origami, and similar art forms, in the space industry to Miura[36]. He invented the Miura fold that was used on the SFU. Miura proposed a pattern that revolutionized the large space structure industry as his pattern allowed for an optimized storage of a very large 2D plane that could be deployed through the simple mechanism of pulling a single corner. An example of this fold can be seen in Figure B.3. Moreover, Miura's fold has been a used as a starting point for many designs in other technical fields such as medicine and architecture[37].

Figure B.2: A comparison of thickness accommodation methods [38]

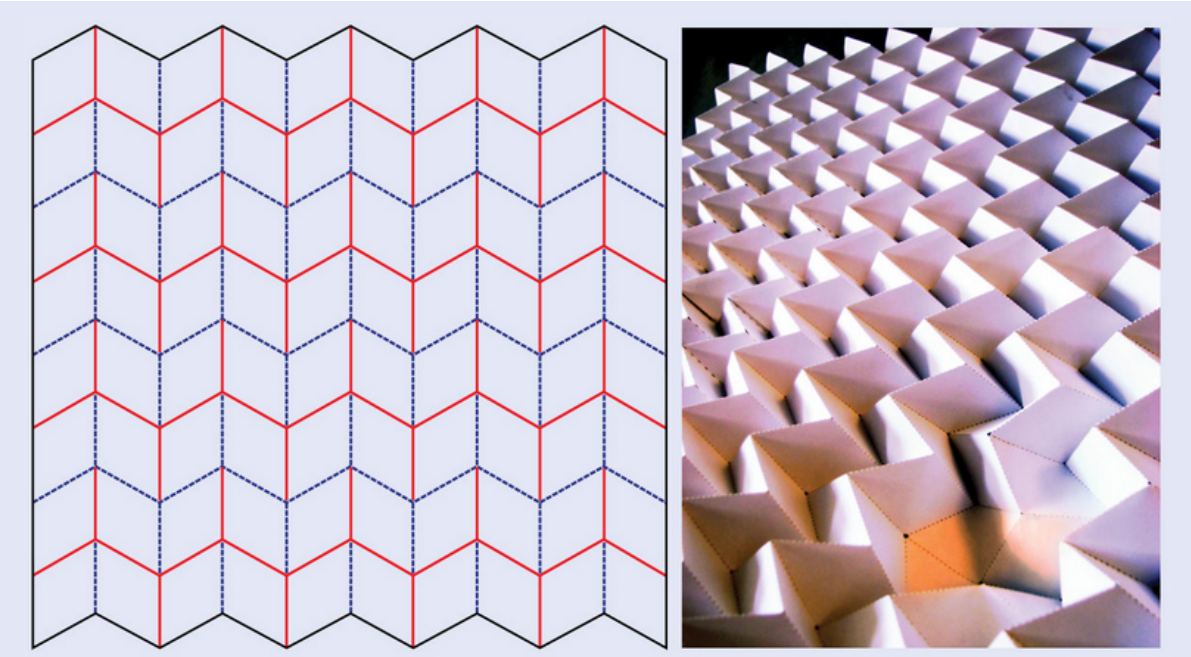

Figure B.3: Miura Pattern and fold [39]

Another big name in the field of Origami is Robert J. Lang. Lang is a master of Origami, who has pioneered the combination or western mathematical oriented Origami with eastern Origami's emphasis on line and form. Lang has helped bridge the gap between the mathematical concept and actually building mechanisms, by accommodating thickness within the design of Origami folds[40]. He has introduced and studied many different techniques and folds that help create flexible designs and models that have high deployed-to-stowed ratio.

Table B.1: A comparison of thickness accommodation methods [38]

Method	Kinematics preserved	ROM preserved	Single DOF	Unfolds flat	Application considerations
Axis-shift[41]	No	Yes	Yes	Yes	Limited to selected fold patterns
Offset joint[42][43]	No	Yes	Yes	Yes, varied thickness	Limited to selected fold patterns
Membrane folds[40]	No	Yes, if gaps between panels ≥ 2 x thickness	No, gaps allow movement	Yes	Deployed system requires tension at edges to keep membranes stretched
Tapered panels[41]	Yes	No	Yes	Yes	Required tapering of panels limits possible geometry and materials
Offset crease[44]	No	Yes	No	Yes	Panels required to be trimmed to avoid self-interference at vertices
Spatial linkages[45]	No	Yes	Yes	No	Fold angles and panel thicknesses limited by the spatial mechanism
Offset panel[46]	Yes	Yes	Yes	No	Cutouts in panels may be required to avoid self-intersection

As shown in Table B.1, by studying the different folds and method proposed by other researchers, Lang was able to accommodate a thickness to a flasher design (first conceptualized by Shafer and Palmer who in turn were inspired off of unpublished work from David Huffman)[47][48][49]. Lang has further built on work from Guest and Pelegrino who have shown a modeling technique for wrapping thin membranes around a central hub [50]. By combining these work, Lang and a team at Brigham Young University were able to design a flasher that could be used as a solar array for a satellite. As shown in Figure B.4, the array could be compactly stored by wrapping itself around the body of the satellite and then deployed into a large circular structure with an increased reliability of deployment.

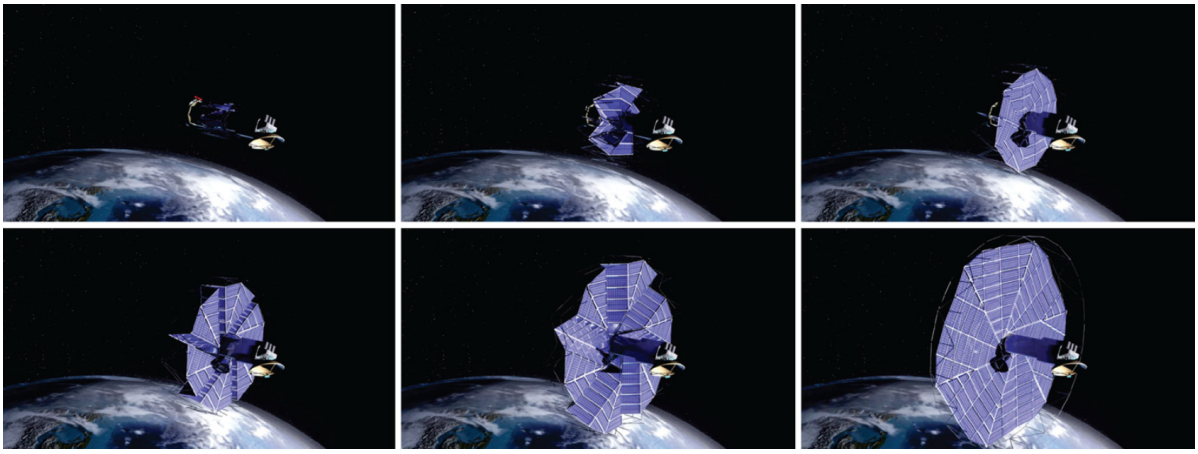

Figure B.4: A computer-generated model of the solar array as it might work on a spacecraft [40]

Lang has continued to work on the flasher concept and has designed a flasher in which by a appropriate choice of sector angle and with the introduction of a cut, forms a single degree-of-freedom mechanism[51]. Lang has worked with NASA in the development of the James Webb Telescope which used Origami to compactly store the 18 hexagonal beryllium mirrors for launch. This will allow NASA to upgrade from a 2.5m diameter mirror on the Hubble Telescope to a 6.5m diameter mirror on the Webb without needing a much bigger launcher[52].

By using a cut in his reflector Lang moves away from the pure form of Origami engineering into a new Kirigami Engineering. If Origami is the art of folding a single piece of paper to form an object, Kirigami is the art of folding, while also making cuts, to form a specific structure. Kirigami has shown to have certain different benefits over Origami. Terry C. Shyu has shown that, by specifically creating microscale Kirigami pattern, one can affect the elasticity of a nano-composite and increase its ultimate strain from 4 to 370% [53]. An example of these Microscale patterns can be seen in Figure B.5.

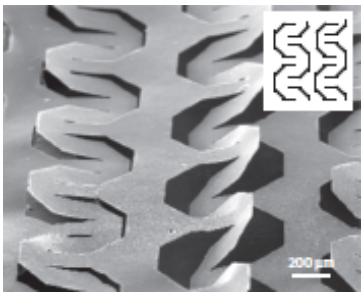

Figure B.5: Microscale Kirigami Patterns [53]

In addition, by specifically cutting a sheet of paper and meshing the paper together, engineers have been able to create unidirectional stiff structures that can extend and contract [54]. This has been used for creating drone cameras that can extend above walls, and has also been used to create long stiff robotic arms. An example of this can be seen in Figure B.6.

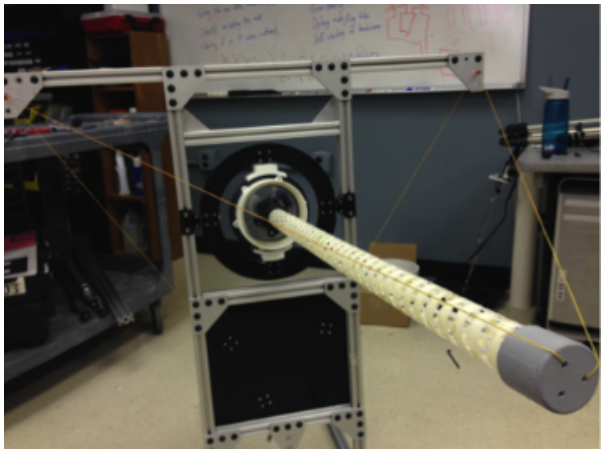

Figure B.6: Spiral Zipper Mechanism forming Extendable Arm [54]

As much as Lang has demonstrated the use of the flasher design for the construction of a satellite solar array, his work was based off of another important name in the field of space Origami structures, Pelegrino. In "Inextensional Wrapping of Flat Membranes" [50] Pelegrino and Guest propose a method for wrapping of a flat, thin membrane around a central hub. In this paper, one of the biggest assumptions is that they are working with a zero thickness surface. Pelegrino and Guest do acknowledge that the idea of folding patterns for space mechanisms does not start with them but is inspired by work proposed from Temple and Oswald, and work from Miura. It is important to point out that Pelegrino and Guest, and Temple and Oswald, see their folding patterns as a different branch of Origami than Miura as they introduce curvature and wrapping to their folding, while Miura stuck with the more linear aspect of Oriental Origami. Pelegrino and Guest did go on to design a thin shell reflector based off of their folding pattern where, as shown in Figure B.7, the reflector could fold onto a central hub thanks to it's 6 different flexible "petals"[55][56].

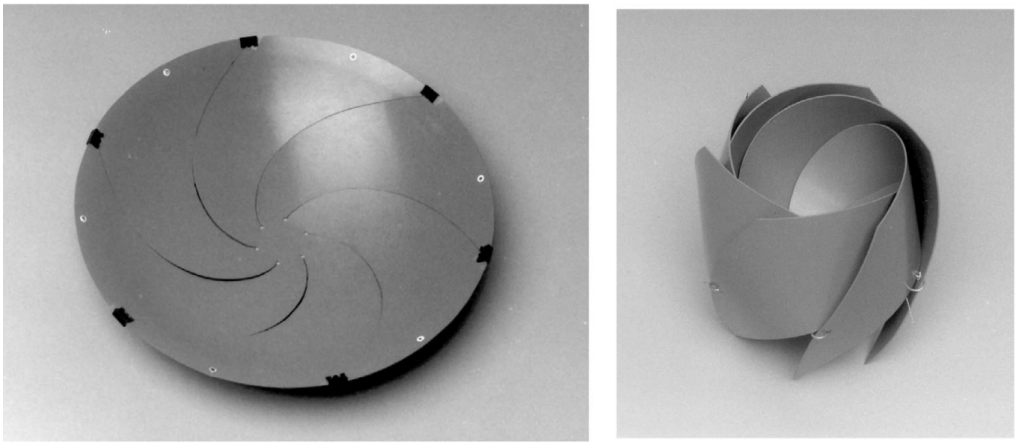

Figure B.7: Small scale model, deployed and packaged [55]

Pelegrino has continued to work with Origami to build new sunshields for space telescopes [57], ultralight satellites[58][59], solar arrays [60], and antennas. Lately, Pelegrino has combined Origami and Kirigami to work on a novel phase-change array that uses Origami an Kirigami's mobility to have an array switch between planar, spherical, and cylindrical configurations. This increases the diversity of radiation patterns that can be synthesized by the array[61].

In 2010, another step forward in the utility of Origami for space was made when IKAROS deployed a 14m square solar sail from a 1.6m spacecraft bus[62] [63]. Not only did IKAROS prove again that Origami was a great technique for the deployment of large structures in space, but it was also used as a proof of concept for a new technology, the solar sail (see Figure B.8).

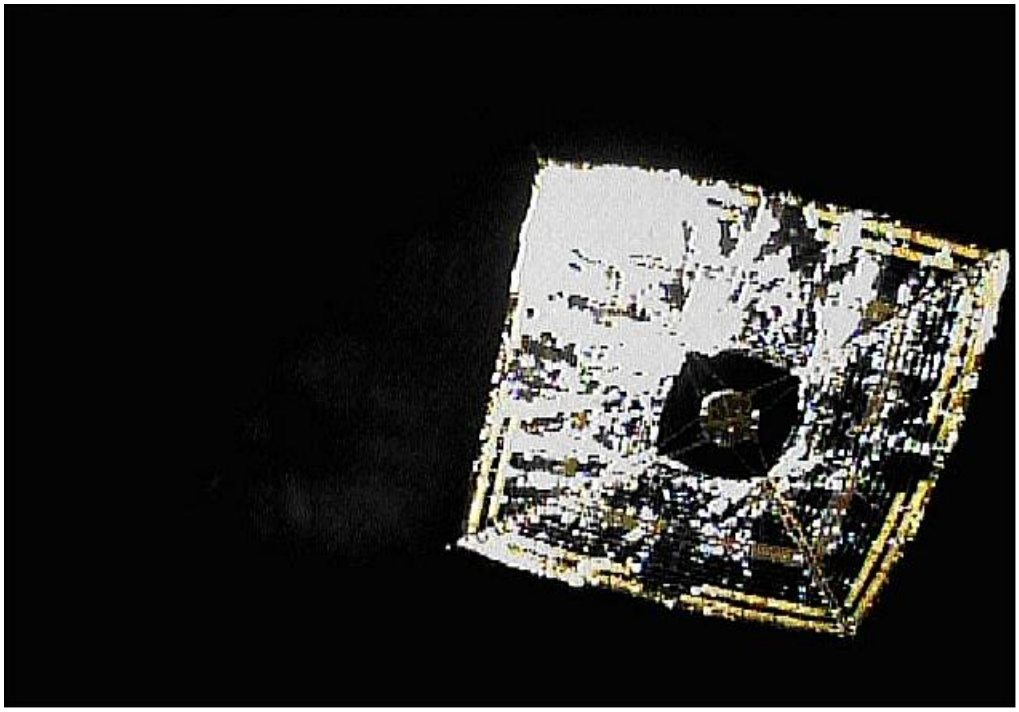

Figure B.8: Images of IKAROS with a deployed solar sail